The Use of the Multi-channel Analysis of Surface Waves (MASW) Method as an Initial Estimator of Liquefaction Susceptibility in Greymouth, New Zealand

---

A thesis submitted in partial fulfilment of the requirements for the degree of

Master of Science in Engineering Geology

at the

University of Canterbury

By

Clem Alexander Molloy Gibbens

2014

Looking east up Mawheranui (the Grey River) towards Greymouth. The world-renowned Greymouth Barber, a katabatic wind formation is pictured rolling over the Twelve Apostles Range (left) and Peter Ridge (right).

Acknowledgements

I wish to acknowledge the following people who have assisted me in writing this thesis:

To my supervisors Mr. David Bell and Dr. Brendan Duffy. Your guidance and support throughout the entire process was greatly appreciated. I know at times you were frustrated with me but you were always available to assist when I asked.

To the guys that assisted me in the field: Brendan, Cam Asher, my 'little' brother Reid and my dad Jim. Thanks for giving up your time to ensure I was able to collect the data efficiently. Also thank you to Southern Geophysical for lending me the gear.

To the technical team in the geology department, thanks for making the last minute rush jobs to get field equipment so much easier and less stressful.

To Karl at the Grey District Council and Elena and Mark at Opus Consultants in Greymouth, thanks for giving me access to the sites for testing, and also for providing me with useful information for use in my thesis.

To the people that helped keep me sane: Cam, Gina Vettoretti, Emma Rhodes, Mitch Green, Jono Mukhtar, Millie Gibbens, Andy Kelly, all the guys and girls in the office and everyone else who I have crossed paths with. Thanks for all the laughs over the last few years.

Lastly, and probably the biggest thanks, goes to my family. For all the love and support you have shown throughout the university studies. My parents, Therese and Jim, you have been there whenever I needed you. All the little talks and words of wisdom helped get me through (and the odd bit of financial support too). To my brothers, Jordie and Reid, and my sister Millie; thanks for being there when I needed a break or chat. My extended family, especially Brian and Diane Molloy, thanks for being there (and for all the fresh vegetables). And last to my grandmother, Maureen. She was one of my biggest fans throughout my thesis but unfortunately she isn't here to see me finish it, so this thesis is dedicated, in part, for her.

Abstract

Combined analysis of the geomorphic evolution of Greymouth with Multi-channel Analysis of Surface Waves (MASW) provides new insight into the geotechnical implications of reclamation work.

The MASW method utilises the frequency dependent velocity (dispersion) of planar Rayleigh waves created by a seismic source as a way of assessing the stiffness of the subsurface material. The surface wave is inverted to calculate a shear wave velocity (Park et al., 1999). Once corrected, these shear-wave (V_S) velocities can be used to obtain a factor of safety for liquefaction susceptibility based on a design earthquake.

The primary study site was the township of Greymouth, on the West Coast of New Zealand's South Island. Greymouth is built on geologically young (Holocene-age) deposits of beach and river sands and gravels, and estuarine and lagoonal silts (Dowrick et al., 2004). Greymouth is also in a tectonically active region, with the high seismic hazard imposed by the Alpine Fault and other nearby faults, along with the age and type of sediment, mean the probability of liquefaction occurring is high particularly for the low-lying areas around the estuary and coastline. Repeated mapping over 150 years shows that the geomorphology of the Greymouth Township has been heavily modified during that timeframe, with both anthropogenic and natural processes developing the land into its current form. Identification of changes in the landscape was based on historical maps for the area and interpreting them to be either anthropogenic or natural changes, such as reclamation work or removal of material through natural events.

This study focuses on the effect that anthropogenic and natural geomorphic processes have on the stiffness of subsurface material and its liquefaction susceptibility for three different design earthquake events. Areas of natural ground and areas of reclaimed land, with differing ages, were investigated through the use of the MASW method, allowing an initial estimation of the relationship between landscape modification and liquefaction susceptibility. The susceptibility to liquefaction of these different materials is important to critical infrastructure, such as the St. John Ambulance Building and Greymouth Aerodrome, which must remain

functional following an earthquake. Areas of early reclamation at the Greymouth Aerodrome site have factors of safety less than 1 and will liquefy in most plausible earthquake scenarios, although the majority of the runway has a high factor of safety and should resist liquefaction. The land west of the St. John's building has slightly to moderately positive factors of safety. Other areas have factors of safety that reflect the different geology and reclamation history.

Table of Contents

List of Figures

List of Tables

1 Introduction

This thesis examines the use of multichannel analysis of surface waves (MASW) for the initial assessment of liquefaction potential as a guide to a more detailed testing regime.

1.1 Background

The susceptibility of a soil material to liquefy during seismic loading is enhanced in young loose sediments. This is generally reflected in the low resistance to penetration (e.g. using CPT- and SPT-based testing), high pore-water content (saturation), and relatively low deformation values.

Techniques for emplacement of uncontrolled and controlled (engineered) fill, which is effectively young sediment, have evolved over the 20th century with implications for its rigidity, porosity and strength. However, it is presently unclear to what extent anthropogenic cut/fill processes over these long time periods affect the soil stability in urban environments.

In September 2010, Canterbury experienced the first of 4 large, severely-damaging earthquakes (Quigley et al., 2010; 2012). This earthquake initiated a sequence of thousands of aftershocks, including the lethal February 2011 earthquake that claimed 185 lives in New Zealand's second most populated city, Christchurch (Bannister and Gledhill, 2012). The subsurface geology in Christchurch and the surrounding area was extensively known (Brown and Weeber, 1992) as well as the potential for a proximal seismic hazard (Pettinga et al., 2001; Downes and Yetton, 2012). However, even with this knowledge the land on which Christchurch is constructed performed poorly during these events. As a result of these events, the focus of many city, district and regional councils has been shifted to developing ground models of the subsurface beneath the developed areas they have control over.

It is a widely accepted fact that natural soft, saturated sediments can fail during earthquakes with examples including the 1964 Niigata Earthquake (Ishihara and Koga, 1981), 2004 Chuetsu Earthquake (Wang et al., 2007), and February 2011 Christchurch Earthquake (Brackley, 2012). Also areas of emplaced fill can fail during seismic events, for example the 1994 Northridge Earthquake (Stewart et al., 1996)

and the 1995 Kobe Earthquake (Soga, 1998). During the Canterbury Earthquake Sequence (CES) areas of known fill in the city failed as a result of liquefaction, either due to failure of the fill itself, or of the underlying sediment. Fill emplacement has to be done correctly so that the land is safe under earthquake loading. If fill emplacement is not done correctly then the possibility of the sediments beneath the fill liquefying is increased, which can lead to failure of the material overlying the liquefiable material.

Liquefaction resistance can be estimated using several techniques, with Cone Penetration Tests (CPT's) and Standard Penetration Tests (SPT's) being the most common methods. The original procedure for assessment of liquefaction resistance was developed by Seed and Idriss (1971) using the SPT method and in the mid-1980's the procedure for using CPT was introduced by Robertson and Campanella (1985). These original procedures have both been revised and updated numerous times since their introduction. Idriss and Boulanger (2008) provides the framework for assessment of liquefaction resistance, though this will not be covered within the scope of this study.

Andrus and Stokoe (2000) provided a way for estimation of liquefaction resistance based on shear-wave velocity (Vs). This is a promising alternative, or supplement, to the penetration-based approaches. The use of Vs as an index for liquefaction resistance is soundly based because both Vs and liquefaction resistance are similarly influenced by many of the same factors (for example, age of deposit, water content and void ratio). Advantages of using Vs as an indication of liquefaction resistance include, but are not limited to the following: (1) measurements are possible in soils that are hard to sample where penetration tests may be unreliable; (2) Vs is a basic mechanical property of soil materials, directly related to small strain shear modulus; (3) Vs can be estimated by surface inversion techniques (e.g. Stokoe et al., 1994; Park et al., 1999). There are other advantages, and also disadvantages, covered later in this thesis.

Greymouth, located on the West Coast of New Zealand's South Island, is constructed on the delta of the Grey River. Modern European occupation of the area began in the mid-19th century due to the abundance of gold and coal in the region. The population has increased since the first settlement, with a population of

approximately 9940 currently residing within the Greymouth area (2013 estimate from Statistics New Zealand). This has meant that land requirements have increased, leading to widespread modification of the natural landscape. The sediments on which the town is constructed are geologically young, and therefore may be susceptible to liquefaction and other geotechnical issues following a seismic event (McCahon et al., 2007). Robinson and Davies (2013) reported that McCahon et al. (2007) found that liquefaction was likely to occur in a number of places. These included the swampy areas of large lakes and around the river estuary in Greymouth.

Greymouth is located close to multiple active fault sources, including the Alpine Fault, and the possibility of severe shaking being experienced during an earthquake is high; meaning liquefaction could be considered probable rather than a possibility. This study aims to make an initial estimate of liquefaction potential through: (1) documenting the anthro-geomorphic evolution of Greymouth; (2) Using MASW to evaluate Vs of selected sites where modification has occurred; and (3) discuss the implications for seismic hazard mitigation and resilience of key infrastructure.

1.2 Objectives

The primary objective of this study has been to make an initial determination of liquefaction resistance for low-lying areas in Greymouth and surrounding suburbs, and with some respect towards the impact of the estuary modification. Using the MASW method, shear-wave velocity (Vs) profiles were obtained to give initial estimates of liquefaction potential using the simplified procedure outlined by Andrus and Stokoe (2000).

This primary objective was achieved by the following:

- Determination of areas of natural and reclaimed land by studying historical maps of the township, allowing for the development of a geomorphological evolution timeline over the last 150 years; The area that this study concentrates on is the suburb of Blaketown and areas on the western side of the Greymouth Township, south of the Grey River, where the Erua Moana Lagoon and Karoro Lake, which make up the estuary, are located.
- Using the timeline, assessment of the feasibility for MASW testing for areas of natural soil and areas of reclamation of varying ages. Three areas were tested as part of this study: The Greymouth Aerodrome, the old Victoria Park Racecourse, and the Truck Stop, owned by Aratuna Freighters, located at the north-western end of Charles O'Connor Street. All of these areas were chosen due to the fact that they have, at some stage during the past two centuries, been influenced by the estuary located within the wider Greymouth area, and also due to them all having reclamation land within the site boundaries. More specific details for these sites are given in Chapter 5.
- Subsequent processing and analysis of the MASW shear-wave profiles to provide an initial estimate for liquefaction potential;
- Discussion of the implication of the results with regard to the seismic hazard for the Greymouth Township, with emphasis on key infrastructure (e.g. St John's Ambulance Building, Greymouth Aerodrome)

Greymouth was chosen due to its high seismic hazard, relatively young soft sediments, and my own personal connection to the area.

1.3 Regional Geological Setting

The West Coast region studied encompasses part of the tectonically active Alpine Fault on the South Island of New Zealand. This fault separates the Indo-Australian and Pacific plates.

Much of the ground on which the town of Greymouth, and much of the other West Coast towns, is founded on is geologically young ground. Greymouth, along with Westport, Hokitika and Karamea are located at river mouths and in a lagoonal or estuarine environment which formed in postglacial times when sea level reached its present day levels approximately 6,000-7,000 years ago, and as such are especially susceptible to liquefaction effects.

The locations of these towns are shown in Figure 1.1.

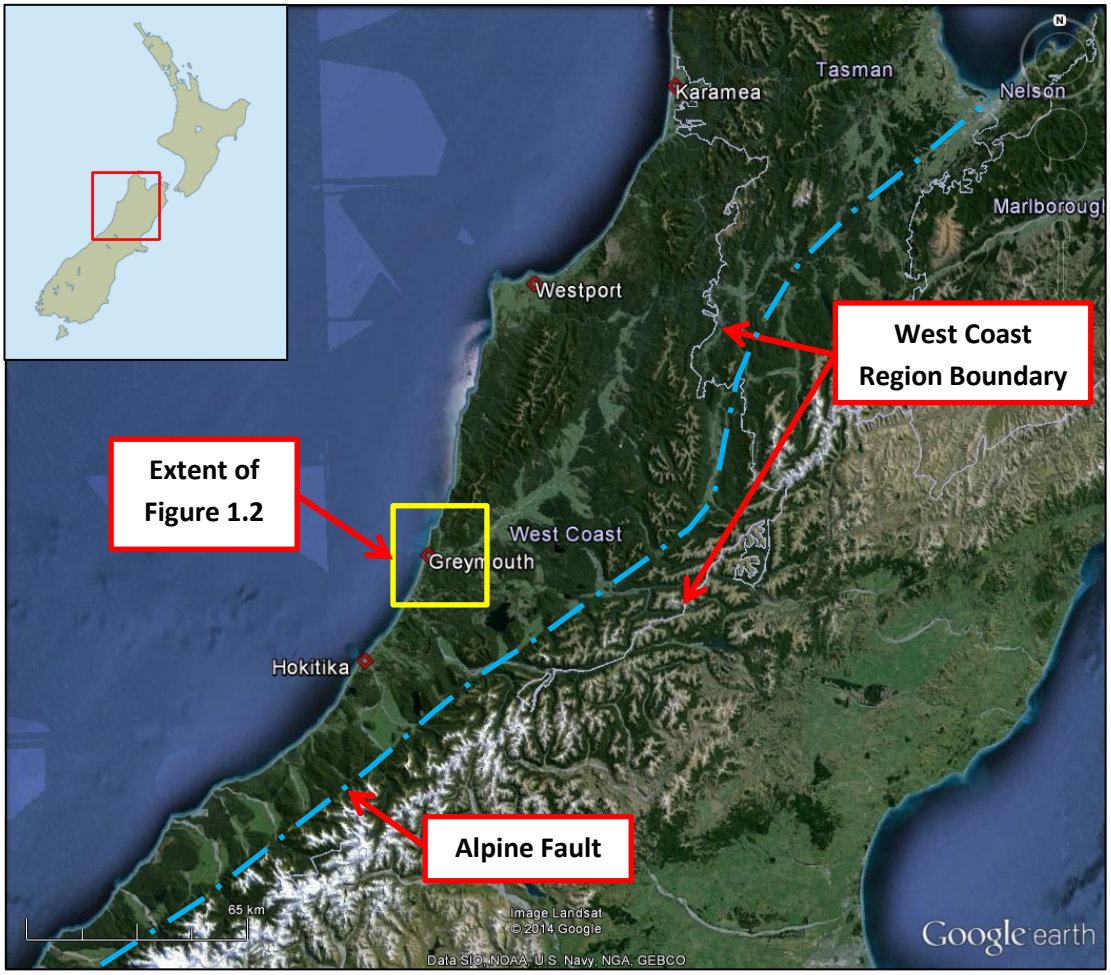

Figure 1.1 - Locations of Key West Coast Town Locations (with Alpine Fault lineated)

The geological evolution of the West Coast has occurred all throughout the Paleozoic, Mesozoic and Cenozoic (Nathan et al., 2002); with some volcanic rocks dating back to the Cambrian in age. However, many of these rocks do not outcrop at the surface within the Greymouth area, due to either being at depth or due to now being covered by Quaternary sediments.

The rocks that do outcrop make up much of the topographic features around Greymouth, and these rocks are described, in stratigraphic order, below. However, these descriptions only apply to geology of the area immediately around Greymouth.

The geological time scale, along with a full scale map, stratigraphic legend and detailed geological history are provided in Appendix A.

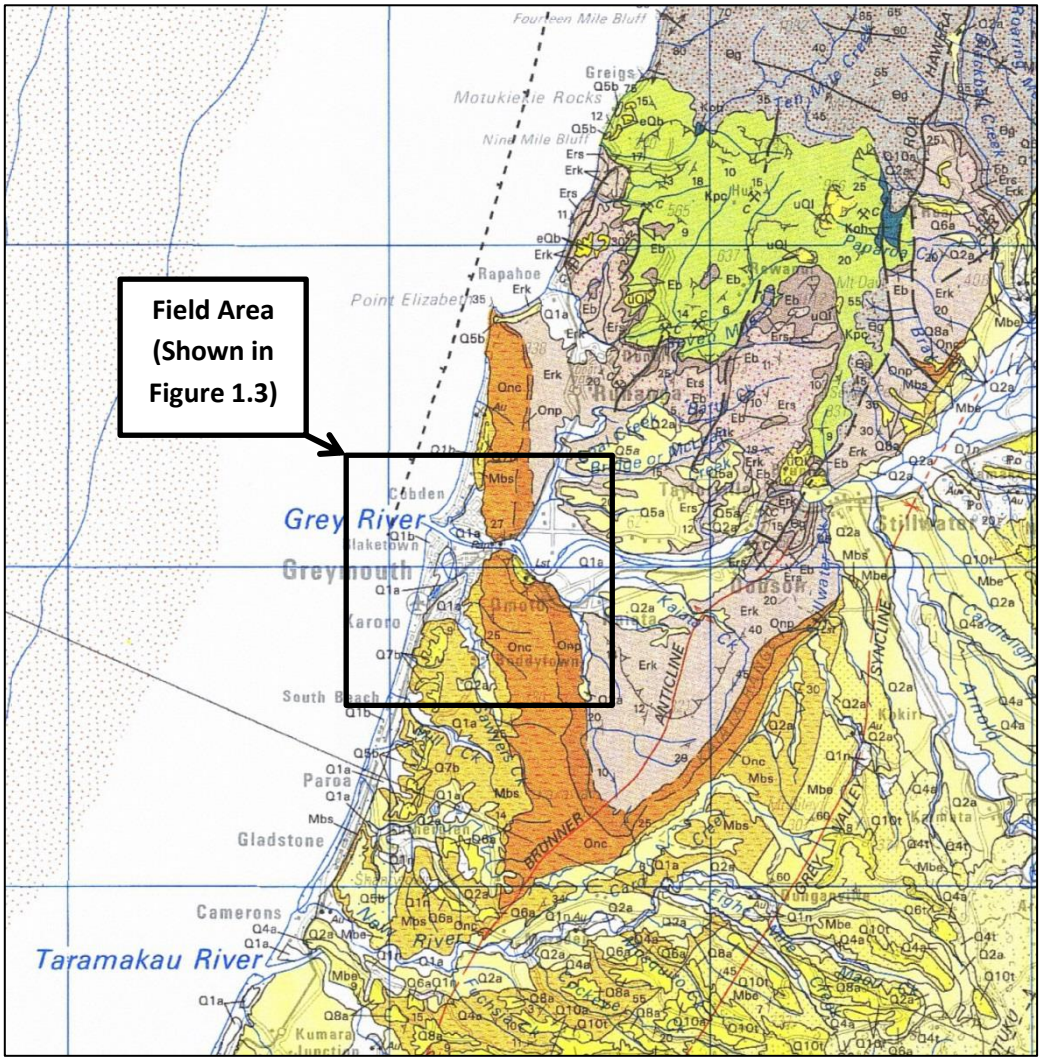

Figure 1.2 - Geological Map of the Greymouth Area (QMAP Series - Nathan et al., 2002)

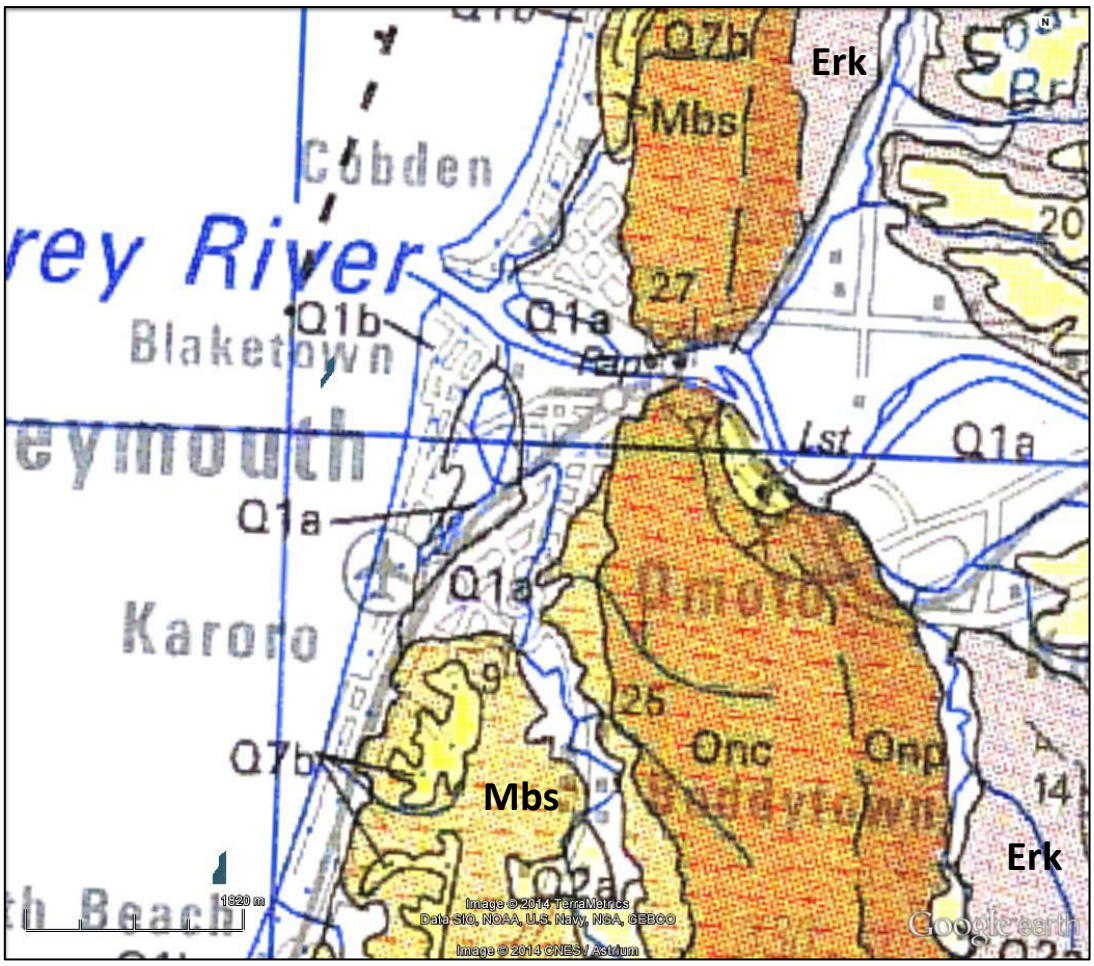

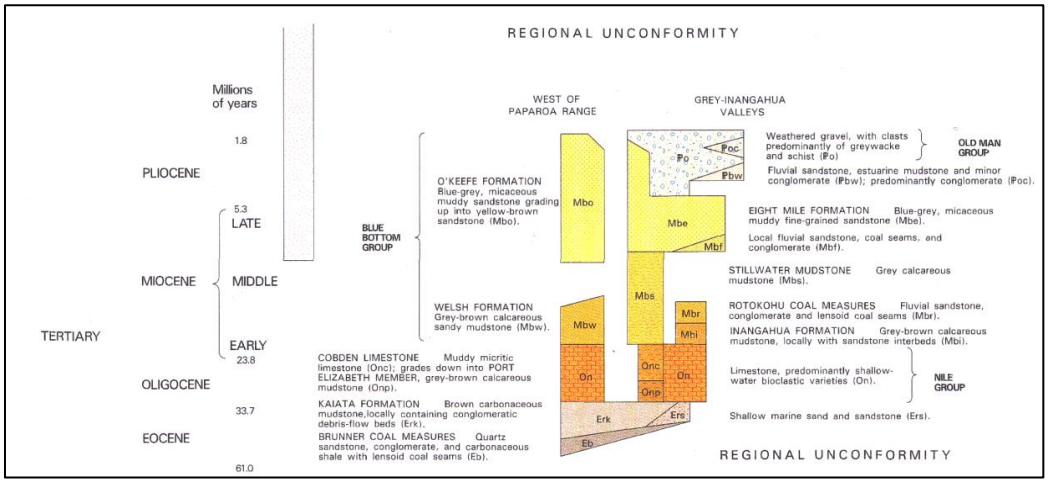

Figure 1.3 - Geology of Field Area (defined by Figure 1.2) with relevant stratigraphic relationship (QMAP Series - Nathan et al., 2002)

The geology of the field area defined by Figure 1.3 comprises a sedimentary sequence ranging in age from Eocene (61 million years ago [Ma]) to the present day. Bedrock material consists of the Nile Group (Cobden Limestone and Port Elizabeth

Member) and marine mudstones that underlie (Kaiata Formation) and overlie (Blue Bottom Group) the limestone. Surficial units unconformably overlie the bedrock and comprise Quaternary material, deposited during a series of glacial and interglacial episodes (Metcalf, 1993).

1.3.1 Bedrock Units

Kaiata Formation (Erk)

The Kaiata Formation is Eocene in age (61 to 33.7 Ma) and is defined as a dark-coloured, fine grained, calcareous mudstone or dark brown muddy micaceous sediments, which are found between the underlying Eocene coal measures (Brunner Coal Measures) and overlying Oligocene limestone unit (Nile Group) in the Greymouth Area (Nathan, 1974; Metcalf, 1993; Nathan et al., 2002). The Kaiata Formation is described as “a massive, brown mudstone, more calcareous towards the top, locally interbedded with coarse sandstone and conglomerate” (Nathan, 1974). These conglomeratic sediments within the unit were later described by Nathan et al. (2002) as interbedded mass-flow (debris-flow) deposits.

Nile Group (Port Elizabeth Member and Cobden Limestone)

The Nile Group (On) is a grouping of all calcareous sediments for much of the West Coast formed during the Oligocene (33.7 to 23.8 Ma) (Nathan, 1974; Metcalf, 1993).

The Port Elizabeth Member (Onp) sits conformably above the Kaiata Formation. This member consists of a grey-brown calcareous mudstone. Nathan (1974) originally included this unit within the Kaiata Formation, though this is revised by Nathan et al. (2002) and is now stated as part of the Nile Group. The Cobden Limestone (Onc) is a muddy micritic limestone, with thin layers of clay/mud infill between some beds, giving the outcrops a wavy appearance due to the less resistant mud layers being eroded quicker than the limestone beds (Nathan et al., 2002).

The Nile Group outcrops in Greymouth as the high relief areas directly east of Greymouth (Twelve Apostles Range and Peter Ridge) as part of the westward-dipping limb of the Brunner Anticline.

Blue Bottom Group (Stillwater Mudstone)

The Blue Bottom Group consists of marine detrital sediments, mainly mudstone and sandy mudstone, which overlie the Nile Group (Nathan, 1974).

The Stillwater Mudstone (Mbs) is a massive blue-grey calcareous mudstone that formed throughout the Early to Middle Miocene (23 to 14 Ma) and sits conformably above the Cobden Limestone of the Nile Group (Nathan et al., 2002).

The Stillwater Mudstone forms the majority of the minor relief found at the foot of the Nile Group ridgelines (Twelve Apostles Range and Peter Ridge) and continues south-east up the valley formed by Sawyers Creek towards Boddytown.

1.3.2 Quaternary Sediments

Much of the Grey Valley and lowlands have a complex cover of late Quaternary moraine, river and alluvial fan gravel, coastal and lagoon deposits, and swamps. These surficial deposits correlate to a succession of ice advances and contemporary periods of low sea levels, and intervening interglacial high sea levels. This sequence is associated with oxygen isotope stages 1 through 10. The ages of these deposits, with associated symbols are described in Table 1.1 below.

These symbols are used in conjunction with the deposit type to classify the Quaternary deposits in the Greymouth area.

Table 1.1 - Quaternary Chronology (kya ≡ thousand years)

Oxygen Isotope	Age of deposits (kya)	Symbol
1	<12	Q1
2	12 – 24	Q2
3	24 – 59	Q3
4	59 – 71	Q4
5	71 – 128	Q5
6	128 - 186	Q6
7	186 – 245	Q7
8	245 – 303	Q8
9	303 – 339	Q9
10	339 – 362	Q10
	>362	eQ

Glacial till deposits (Q4t, Q6t, Q10t) are mapped as discrete units based on their elevation, dissection and the relationship to nearby outwash gravels. These exposures consist of interbedded till (sub-rounded to sub-angular clasts up to boulder size in a tight clayey matrix) and fluvial outwash gravel (Nathan et al., 2002).

Alluvial and fluvioglacial gravels (Q1a, Q2a, Q4a, Q5a, Q6a, Q8a, and Q10a) are widespread, and are well preserved in the floodplains and aggradation surfaces of the major river valleys. They generally consist of rounded boulders in a sandy matrix. Because these deposits can be dated from both glacial and interglacial periods, these deposits occur as terraces and are closely related to terminal moraines. This allows them to be easily identified, though many become fragmentary down-valley especially in narrow valleys where erosion is more widespread. Fluvial gravels from interglacial periods are more recognisable closer to the coast, where they grade to marine surfaces. Further inland these deposits are inferred to be times of down-cutting, with little aggradation. Near Greymouth these deposits are widespread and appear to cover much of the current floodplains (or historic floodplains) and alluvial terraces (Nathan et al., 2002).

Large alluvial fans, screes and colluvial deposits (Q1a, Q2a, and Q6a) occur as localised deposits at the foot of steep streams draining range fronts. They consist generally of moderately to poorly sorted pebble to boulder-size clasts with a sandy matrix. In the map area, these deposits are small due to either the fan deposits being removed due to the fluvial processes (for example, river eroded margins in flood events), or being mapped as part of other alluvial deposits (Nathan et al., 2002).

Coastal marine deposits (Q1b, Q5b, Q7b, eQb) are present near the coast as deposits from successive interglacial periods. They consist mainly of well sorted beach sand and nearshore gravel and sand. Coastal deposits appear around Greymouth on the coastal margins. Some older deposits are seen to be overlying tertiary sediments (Stillwater Mudstone) in the southern part of Greymouth behind the suburbs of Karoro and Paroa. Close to the Paparoa Ranges near Rapahoe, the oldest marine cover beds (eQb) have been identified overlying Kaiata Formation (Nathan et al., 2002).

Swamp deposits (Q1a) are mapped in flat, generally low-lying areas close to the coast, commonly on the landward side of dunes or beach deposits. They consist of

poorly consolidated sand, mud and peat. The only mapped section of these deposits occurs within Greymouth Township where the estuary (Erua Moana) is mapped, or where the historical extents of the estuary were located (Nathan et al., 2002).

Landslides (uQl) are common features in steeper terrain, although many are too small to be mapped separately. Their composition varies from largely coherent but shattered rock to unsorted fragments of rock in a silty clay matrix. Many of the landslides have been triggered by earthquakes, especially during the 1929 Murchison and Arthur's Pass earthquakes and from the 1968 Inangahua earthquake (Nathan et al., 2002).

Areas of ground disturbed by human activities such as sluicing and dredging for gold have been mapped as Q1n. Older dredge tailings have been piled up and show a characteristic hummocky landform. However, since the 1980's it has been mandatory to rehabilitate mined land, and as such mined land is much harder to recognise. These types of ground are distributed randomly around the Greymouth area, with many of them being located south near the Taramakau River and Kumara, where gold mining has been a large productive industry in the past (Nathan et al., 2002).

1.3.3 Greymouth Surficial Geology

Suggate (1965), Suggate (1968), Suggate and Moar (1970), Mew (1980) and Metcalf (1993) describe the nature of the surficial deposits to a greater extent and in greater detail. The surficial units are summarised below.

The Karoro Formation consists of marine sands and gravels (greywacke, granitic and schistose in origin) partially cemented by iron pan development, and is preserved south of Point Elizabeth as a discontinuous coastal terrace (Suggate, 1965; Metcalf, 1993). Suggate (1965) correlated the Karoro Formation with the Terangi Interglacial period (300kya).

The Loopline Formation consists of extensive aggradational surfaces consisting of sands and gravels were formed in conjunction with ice advances down the Arnold Valley during the Otiran glaciation (Suggate and Moar, 1970; Metcalf, 1993). Dating of some deposits indicated that ice advance culminated shortly after 18kya.

The Nine Mile Formation is grouped as all sediments deposited since the glaciers started to retreat, circa 14kya (Metcalf, 1993). Marine sediments include gravels of greywacke and granitic origin, while fluvial sediments include mud, sand and gravel derived from the breakdown of Cobden Limestone, Stillwater Mudstone and erosion of other Quaternary deposits (Metcalf, 1993).

There are also 10 pedological soil types recognised by Mew (1980). The distribution and composition of these soils are functions of areal extent and composition of the underlying parent materials (Metcalf, 1993). These soils will not be discussed here.

The surficial geology of the Greymouth Township itself has been interpreted based on the descriptions in Suggate and Wood and a map was developed by Dowrick, Rhoades and Davenport in 2003 (Figure 1.4) This map divides the town and surrounding areas into microzones based on the types of deposits present.

The lagoonal and estuarine silt represented in Figure 1.4, along with the less consolidated beach sand and gravel is what is believed to be the most liquefiable during cyclic loading, with the clay-rich sediments being unlikely to be susceptible to liquefaction. Carr (2004) noted that due to the rate of accretion, and the less energetic environment in which the sediment is trapped, the sediments in the Blaketown are thought to be loose in comparison to sand dunes subject to wave action, and hence more susceptible to liquefaction.

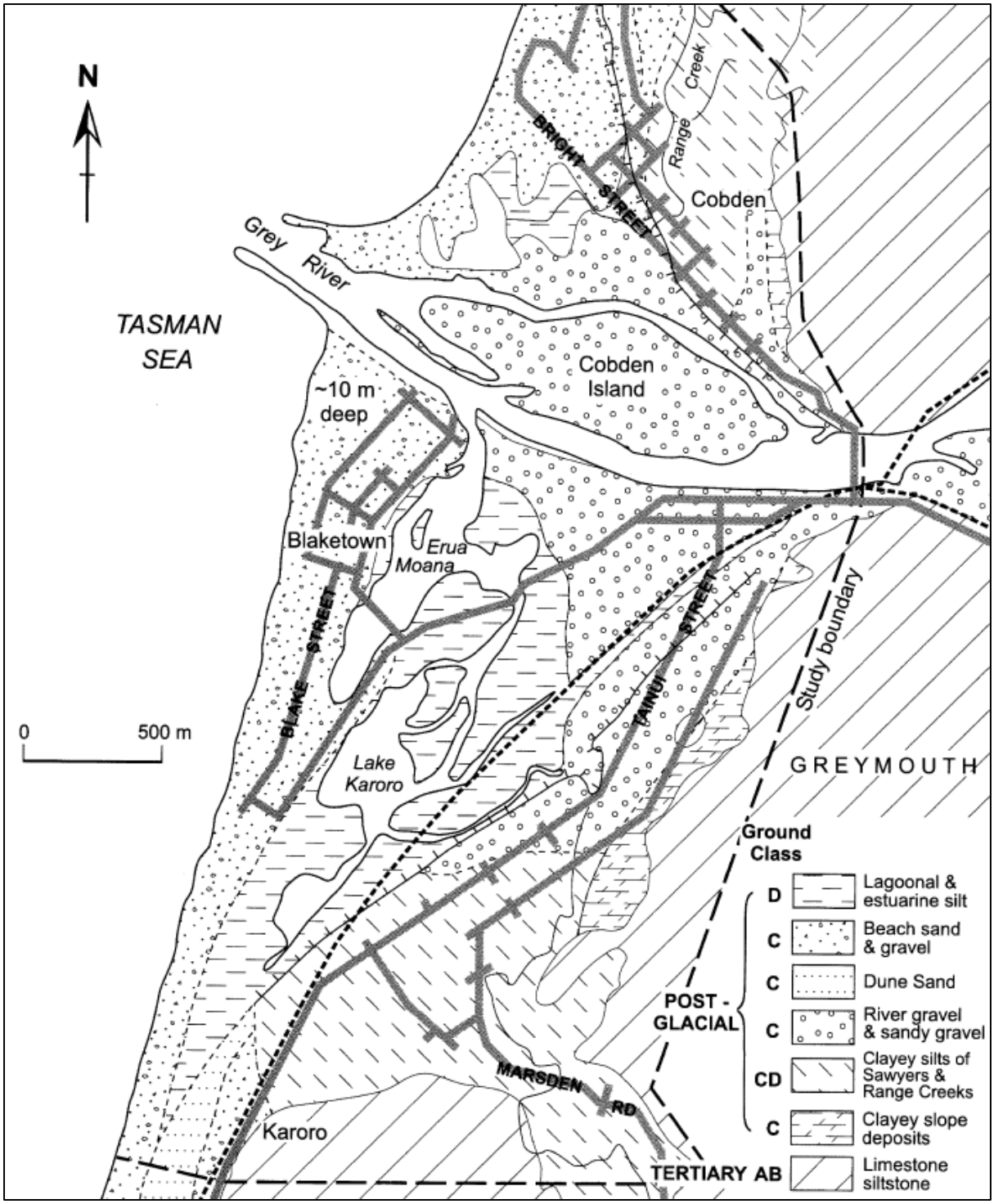

Figure 1.4 - Microzoned map of Greymouth showing different types of surficial deposits (Dowrick et al., 2003)

1.3.4 Tectonic History

The Alpine Fault is the dominant structural element within the region with a predominantly dextral strike-slip movement. It forms the active plate boundary between the Australian Plate to the west and the Pacific Plate to the east. The active compressional tectonic strain along the fault zone is responsible for the high uplift rates (up to 22mm/year) which resulted in the formation of the Southern Alps (Metcalf, 1993), with the eastern side uplifting relative to the western side. Movement is also horizontal based on field evidence of matching rock units offset by upwards of 450km across the fault zone (McCahon et al., 2007).

The most active part of the fault is the central section, which extends from Haast in the south to Inchbonnie in the north, along the western boundary of the Southern Alps. North of this area the fault becomes less active as movement is spread across the Marlborough Fault Zone (McCahon et al., 2007). However, the Alpine Fault is not the only active fault in the region. In Figure 1.5(A) below, the area immediately around Greymouth has known faults represented. There is a trend in the orientation of the faults and folds (Figure 1.5(B)) that run approximately sub-parallel to the orientation of the Alpine Fault. These features are part of a broad shear zone, known as the Paparoa Tectonic Zone (PTZ), extending from the Alpine Fault at the Hokitika River to Kongahu Point. It trends along a NNE orientation. Elements within the PTZ include faulting and folding (e.g. the Brunner anticline and Grey Valley syncline) as seen in Figure 1.2. These are responsible for the deformation of Quaternary sediments (Metcalf, 1993).

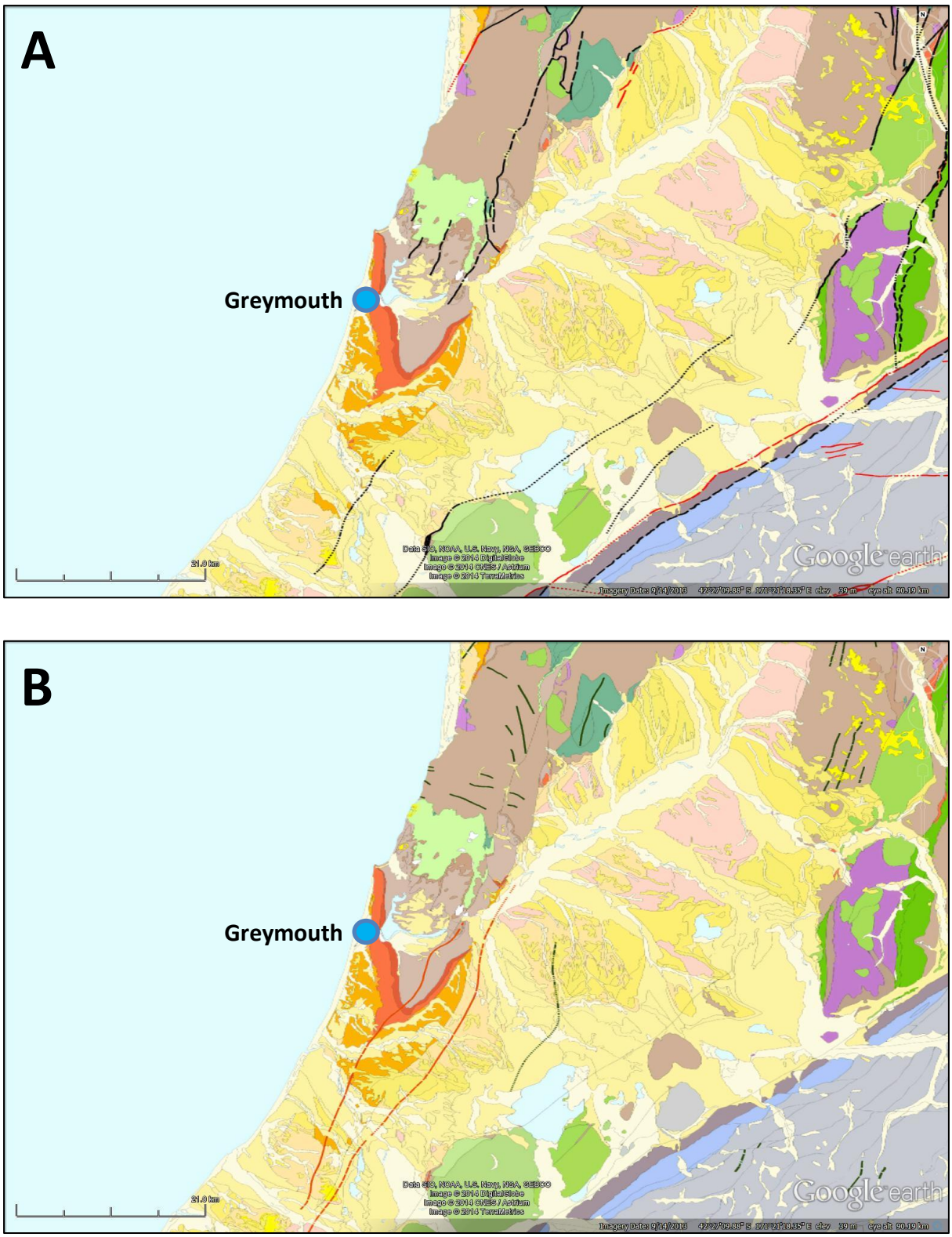

Figure 1.5 - (A) the known locations of active (in red) and inactive (in black) faults in the area surrounding Greymouth; and (B) the location of known folds in the Greymouth Area (Canterbury Geotechnical Database Map CGD5120 - GNS Greymouth Geology [via GeoServer]).

Historically, there have been large earthquakes felt in Greymouth that have caused, or had the potential to cause, damage. Figure 1.5 shows the location of historic large earthquakes with moment magnitudes greater than M_w5.0. The 1929 Murchison and 1968 Inangahua Earthquakes had the greatest effect on Greymouth.

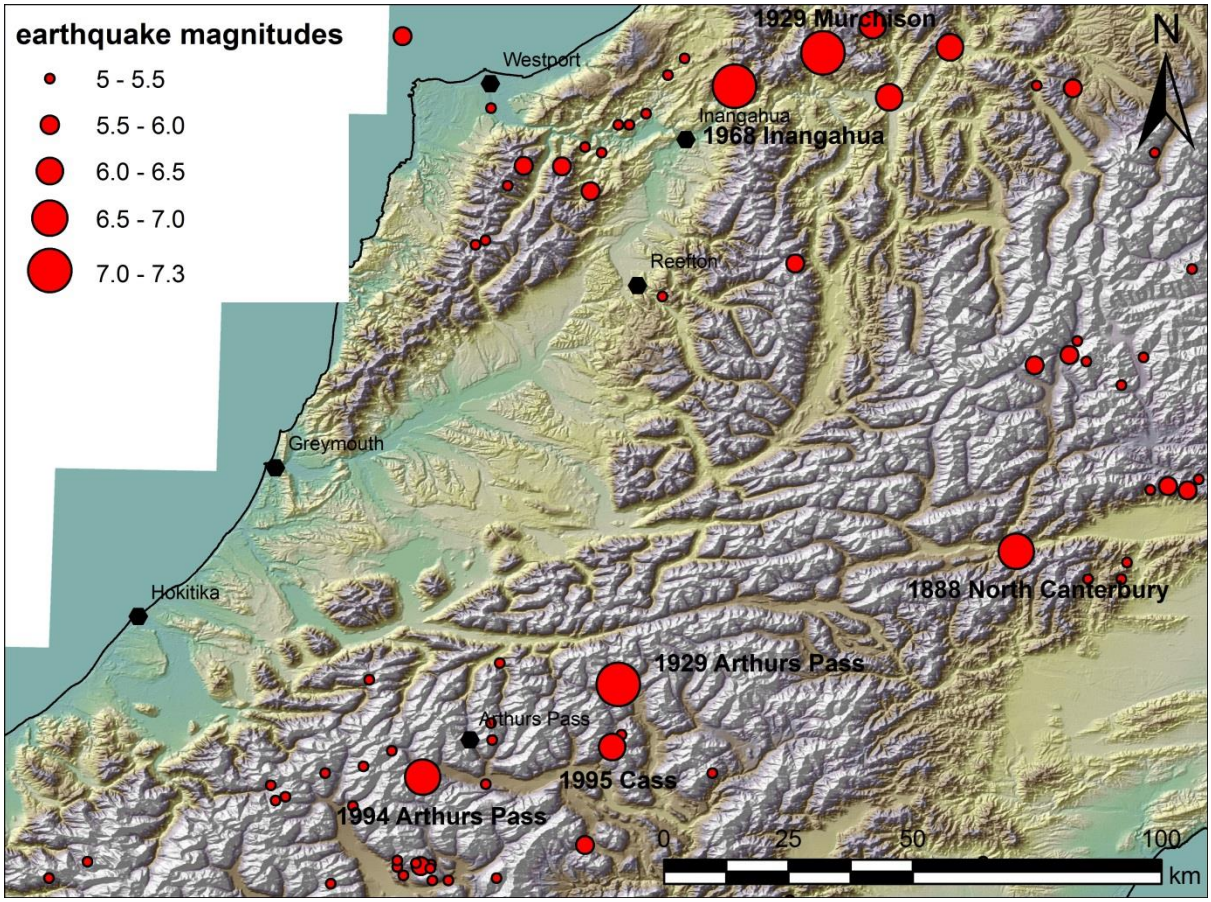

Figure 1.6 - Location of Historical large (>Mw5.0) earthquakes in the Central and Northern South Island

Following the 1929 Murchison earthquake, where shaking intensities were recorded at approximately MM7 on the Modified Mercalli Scale, liquefaction was reported around the Blaketown Lagoon, and damage that occurred was worse on the western side of town in Blaketown than other areas. Most damage occurred in areas of reclaimed land, and where the land has been built up by the combination of longshore deposition and sand trapped by the effective groyne feature, namely the southern breakwater (Figure 1.7). Other anecdotal evidence has been described where sand boils and geysers occurred in paddocks in Coal Creek and fissuring was reported near Victoria Park (possibly as a result of liquefaction-induced lateral spreading). Severe fissuring of the roadway was also reported on Steer Avenue, on

reclaimed land. More details of these accounts are given in Carr (2004) and Metcalf (1993).

Following the 1968 Inangahua Earthquake no sand boils were reported, though Carr (2004) states personal communications with former mayor Kevin Boon, suggested that a number of pipes had to be replaced, suggesting some lateral spreading occurred. The locations and extent of the work is not known.

Figure 1.7 - Sites of Liquefaction following the 1929 Murchison Earthquake (Carr, 2004)

1.4 Principles of Liquefaction

1.4.1 Terminology

The phenomenon of liquefaction and related ground failures are commonly associated with large earthquakes. The common definition of liquefaction is "*loss of strength in saturated, cohesionless soils due to the build-up of pore-water pressures during cyclic loading*" (Rauch, 1997).

Idriss and Boulanger (2008) defines the phenomenon of liquefaction as follows: "*Loose sands tend to contract under cyclic loading imposed by earthquake shaking, which can transfer normal stress from the sand matrix onto the pore water if the soil is saturated and largely unable to drain during shaking. The result is a reduction in the effective confining stress within the soil and an associated loss of strength and stiffness that contributes to deformations of the soil deposit*".

Marcuson (1978) also defines liquefaction: *"…the transformation of a granular material from a solid to a liquefied state as a consequence of increased pore-water pressure and reduced effective stress."*

A more precise definition, as stated by Rauch (1997), is the definition provided by Sladen et al. (1985): *"Liquefaction is a phenomenon wherein a mass of soil loses a large percentage of its shear resistance, when subjected to monotonic, cyclic, or shock loading, and flows in a manner resembling a liquid until the shear stresses acting on the mass are as low as the reduced shear resistance."*

The granular nature of New Zealand soils and the location of many New Zealand cities and towns, such as Christchurch and Greymouth, on such soils mean that the potential risk of liquefaction would be likely, especially in areas more prone to seismic events or in areas where liquefaction has occurred before. Understanding the phenomenon of liquefaction and identifying where liquefaction is likely to occur is highly important as the stability of the supporting ground beneath developed areas play a key role in the ability of towns and cities to survive following a significant seismic event.

1.4.2 Liquefaction Mechanism

The mechanism of liquefaction is well understood. In order for a soil deposit to liquefy it must be saturated (i.e. below the water table), loose and fine grained, and generally consist of either sand or a coarse silt, though loose gravels can liquefy. Under shaking conditions, the soil grains try to compact to a denser configuration (Carr, 2004). Youd et al. (2001) state that increased pore-water pressure is induced by the tendency of granular materials to compact when subjected to cyclic shear deformations. Greene et al. (1994) add that seismic waves passing through the granular layers distort the structure and cause loosely packed groups of particles to collapse. These collapses increase the pore-water pressure between the grains if drainage cannot occur. If the pore-water pressure rises to a level approaching the weight of the overlying soil, the granular layer temporarily behaves as a viscous liquid rather than a solid.

As liquefaction occurs, the soil stratum softens, allowing large cyclic deformation to occur. In loose materials, the softening is also accompanied by a loss of shear strength that may lead to large shear deformations or even flow failure under moderate to high shear stresses, such as beneath a foundation or sloping ground (Youd et al., 2001). The liquefaction phenomenon is generally limited to the top 10 to 15 metres, as beneath this depth pressure cannot be relieved by venting the material to the surface due to the weight of the overlying soil (Carr, 2004). Rauch (1997) describes the mechanism of liquefaction in greater detail.

1.4.3 Liquefaction Effects

The liquefaction phenomenon by itself may not be particularly damaging or hazardous. However, when liquefaction is accompanied by some form of ground failure or displacement is it destructive to the built environment. Adverse effects of liquefaction can take many forms, including: flow failures; lateral spreading; ground oscillation; loss of bearing capacity; sand boils; differential and/or uniform settlement; and rise of buried structures (Greene et al., 1994; Carr, 2004). Diagrams of some of these failures are shown in Figure 1.6.

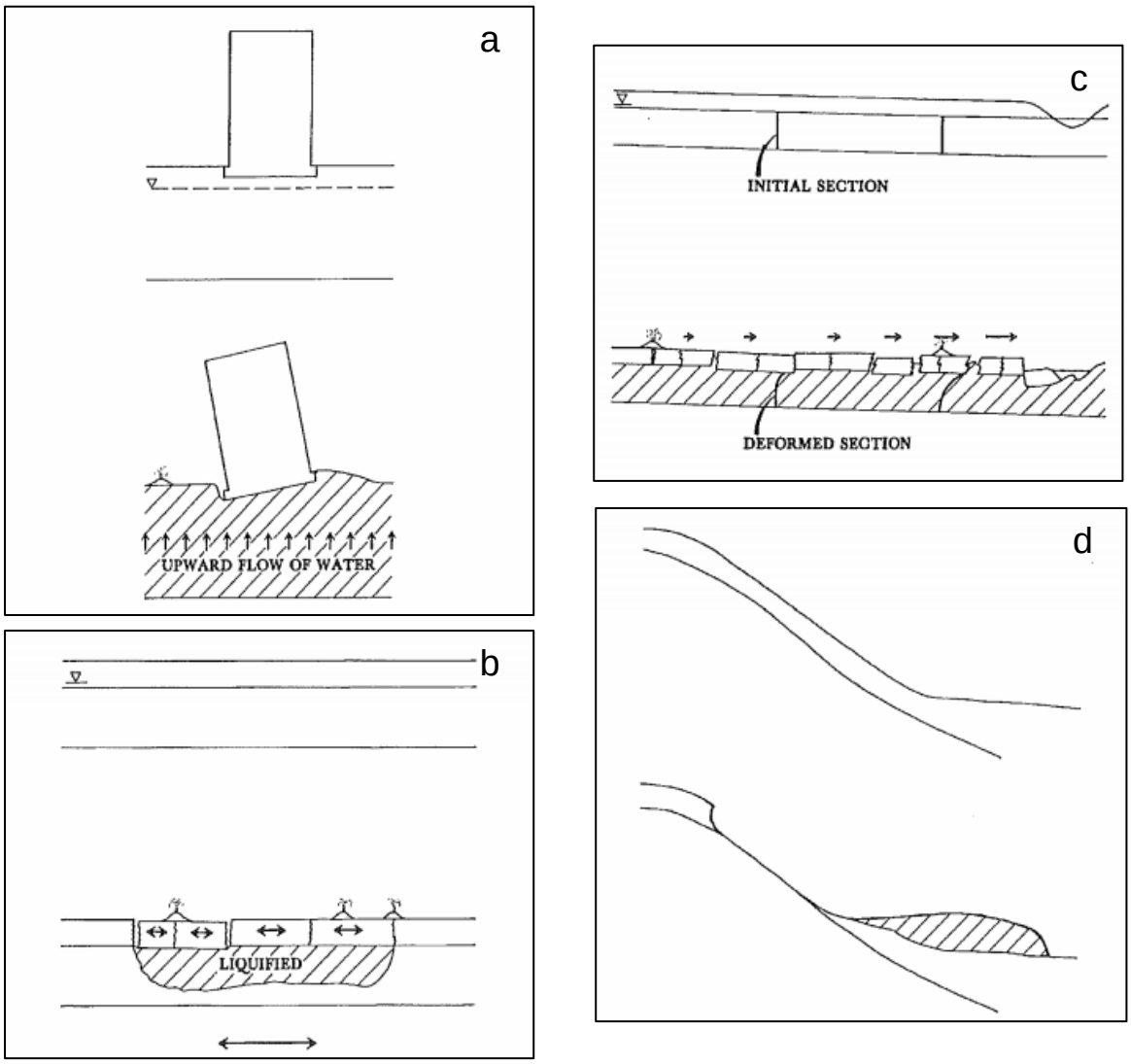

Figure 1.8 - Diagrams showing some of the types of failure associated with liquefaction processes: (a) Loss of bearing strength – Liquefaction weakens the soil reducing the foundation support, allowing heavy structures to settle and tip; (b) Ground Oscillation – Shows decoupling of the surface layers through liquefaction (cross-hatched zone). The decoupled layer oscillates in a different mode than the surrounding ground causing fissures to form; (c) Lateral Spreading; and (d) Flow Failure – Failure is caused by liquefaction and loss of soil strength lying on a steep slope, creating instability (Youd 1992; Greene et al, 1994)

Flow Failures

Flow failures are the most catastrophic ground failures caused by liquefaction. They usually develop on slopes greater than 3 degrees and occur in loose saturated sand and silts. The liquefiable layer loses strength and flows down a slope either en masse (i.e. as blocks of intact material sliding on a layer of liquefied material) or as completely liquefied material. Failures commonly extend tens of metres, though run-outs of kilometres have been known to have occurred (Greene et al., 1994; Carr, 2004).

Lateral Spreading

Lateral spreading involves lateral displacement of large surficial blocks of soil as a result of liquefaction of a subsurface layer, and generally occurs on shallow slopes (0.3 to 3 degrees [Greene et al., 1994]). Displacement occurs in response to the combination of gravitational forces and inertial forces generated by a seismic event, causing the upper layer to break up into blocks through fissuring, which move down slope or towards a free face, such as an incised river channel. Horizontal displacements commonly range up to tens of metres.

Damage associated with lateral spreading include damage to foundations of building located on or across the failure surface, rupturing of pipelines and other utilities, and failure of abutments and toes of engineering structures, such as bridges (Greene et al., 1994; Rauch, 1997; Carr, 2004).

Ground Oscillation

Where the ground is generally flat or the slope is too gentle to allow lateral displacement (less than 0.3 degrees), liquefaction can decouple the overlying sediment layers, allowing the upper soil to oscillate back and forth in the form of ground waves. These oscillations are usually accompanied by opening and closing of fissures, and fracturing of rigid structures such as paths and pavements as well as subsurface utilities (Greene et al., 1994).

Loss of Bearing Capacity

When liquefaction of a soil occurs, the substantial reduction of soil strength can result in large deformations. If this soil is supporting a structure, it can result in a reduction of foundation support, leaving the structure to experience differential settling. This can occur gradually where liquefaction propagates upwards through the overlying soil, and thus weakening the soil and allowing the building to slowly settle differentially. (Greene et al., 1994; Carr, 2004).

Sand Boils

Carr (2004) states that sand boils (though actual grainsize of liquefied material can range from coarse silt [0.03mm in diameter] to fine gravel [6mm in diameter]) are an

unambiguous indicator that liquefaction has occurred. They are easily recognisable, making them useful as the basis for discerning whether or not a site has liquefied. Sand boils are formed during earthquake shaking when the compaction of granular materials creates zones of high “slurry” pressure, and to relieve this pressure the slurry is expelled through the cracks in the overlying strata or through vents formed vertically through the overlying sediment to reach the ground surface. The water can flow violently, carrying sediment with it, which then settles and forms a conical shape around the vent hole (Carr, 2004).

Settlements

The densification of a soil deposit due to earthquake shaking can result in the subsidence of an area (Carr, 2004). Furthermore, the weight of a structure may not be great enough to cause the large settlements associated with bearing capacity failures. However smaller settlements may occur as soil pore-water pressure dissipates and the soil consolidates. These settlements can be damaging, but not on the magnitude of the effects identified above (Greene et al., 1994). Also, if ejecta was observed at the surface (e.g. sand boils) then the removal of the material from underground can cause voids underground, leading to differential settlement over time as the overlying sediment subsides to fill the void areas where material has been removed.

Rise of Buried Structures

When surrounding soil liquefies, buried structures that are less dense than the surrounding soil (such as pipes, piles and tanks), can rise buoyantly. This has an impact on lifeline services (Carr, 2004).

1.5 Thesis Organisation

Chapter 2 comprises a literature review of the MASW method, summarising the various stages from data acquisition to final production of shear-wave velocity profiles. It also discusses the limitations of the method.

Chapter 3 considers the geomorphology of the Greymouth Township, with particular regard to the evolution of the land over the last 150 years.

Chapter 4 describes the individual site investigations undertaken as part of this study. This chapter presents the specific site conditions, details of the data and the initial results obtained.

Chapter 5 details the analysis undertaken on the initial results obtained following the MASW test processing. It concentrates specifically around the simplified procedure outlined by Andrus and Stokoe (2000) and how liquefaction susceptibility can be estimated using shear-wave velocity. Further analysis to determine the factor of safety of the areas tested is also provided.

Chapter 6 provides discusses the results obtained, with particular regard to the surficial geology and geomorphology. It also discusses the implications of the results for the seismic hazard and critical infrastructure. Together with the analysis, the potential for future work in this area and an effective way of making estimates for liquefaction potential is outlined. It will also discuss how the results obtained in this study can be further enhanced to provide more accurate results.

2 The Multichannel Analysis of Surface Waves technique

2.1 Introduction

The multichannel analysis of surface waves (MASW) method was first introduced into the geotechnical and geophysical community in early 1999, although earlier development versions came out several years prior (Park et al., 1999; Park and Brohammer, 2003; Yuan, 2011). MASW is a seismic method that generates a shear-wave velocity (Vs) profile versus depth. This method analyses Rayleigh-type surface waves on a multi-channel record, as Rayleigh waves make up more than two-thirds of the energy imparted in a seismic survey (Park et al., 1999; Park and Brohammer, 2003; Ivanov et al., 2005; Duffy, 2008;). MASW utilises energy commonly considered noise on conventional reflection seismic surveys (Park et al., 1999), and uses multichannel recording and processing concepts widely used for decades in reflection surveying for oil exploration (Park and Brohammer, 2003). Construction of a shear-wave velocity profile through the analysis of planar, fundamental-mode Rayleigh waves is one of the most common ways to use the dispersive properties of surface waves. This type of analysis provides key parameters commonly used to evaluate near-surface stiffness, which is a critical property in geotechnical studies (Park et al., 1999).

Rayleigh waves are the result of interfering P- (compressional body waves) and S-waves (oscillating body waves) (Figure 2.1). Rayleigh waves, in general, are surface waves that travel along a free surface, such as the earth-air interface, with the depth of penetration dependent on the wavelength.

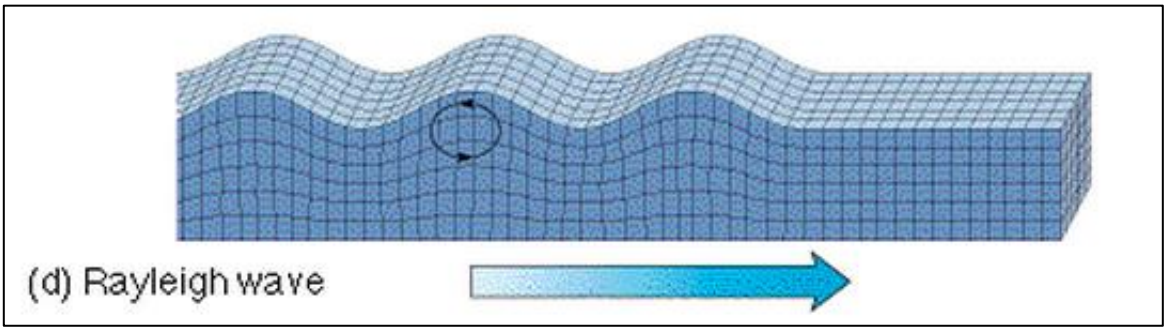

Figure 2.1 - Particle motions associated with a Rayleigh wave. Rayleigh waves are a result of interfering P- and S- waves and this is illustrated here with particles undergoing dilation and compression associated with P-waves, and oscillations associated with S-waves

Ground roll is a particular type of Rayleigh wave that travels along or near the ground surface and is usually characterised by being relatively low velocity, low frequency, and high amplitude (Park et al., 1999; Xia et al., 1999). Long wavelengths penetrate deeper and are more sensitive to the elastic properties of the deeper layers. Longer wavelengths generally also exhibit greater phase velocities. The shorter wavelengths are sensitive to the physical properties of the surface layers. Based on this reasoning a particular mode of surface wave will possess a unique phase velocity for each unique wavelength, leading to the dispersion of the seismic signal (Xia et al., 1999).

Rayleigh waves propagate as different modes, with a mode being a 'packet' of acoustic energy that propagates in one direction whilst confined in the other two directions. Being surface waves, this means that Rayleigh waves are confined to the earth-air interface (Duffy, 2008). Therefore, as mentioned above, a particular mode of Rayleigh wave will have a particular propagation velocity for a given frequency. Of these modes, fundamental mode Rayleigh-waves, which travel in an anticlockwise motion, are the slowest and so appear closer to the origin in a frequency versus phase velocity plot. This is known as a dispersion plot.

There are 3 common types of MASW survey: active source MASW, where data collection is impact triggered; passive source MASW, measured over longer times without an active source (Park and Miller, 2006); and walkaway active source MASW surveys, where 2-4 shot records are 'stitched' into composite records, keeping either the source or receiver static (Figure 2.2) (Vincent et al., 2006).

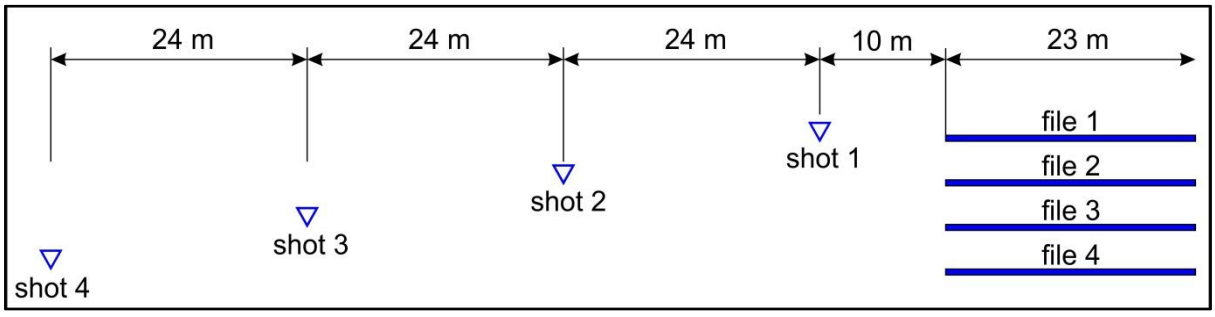

Figure 2.2 - Typical shot sequence for a fixed-receiver walkaway record

The methodology described below in Section 2.2 is generally for the active source MASW survey. Descriptions of the walkaway methods are given in Section 2.3 of this chapter.

2.2 MASW Data Acquisition

The MASW process requires a multichannel record with at least 12 traces to produce reliable results. The method described in this chapter is related to the use of a 24-channel recording device, with the geophones oriented in a linear array (Figure 2.3).

There are three stages to the MASW process: data acquisition; dispersion curve extraction; and finally, inversion of the dispersion curve.

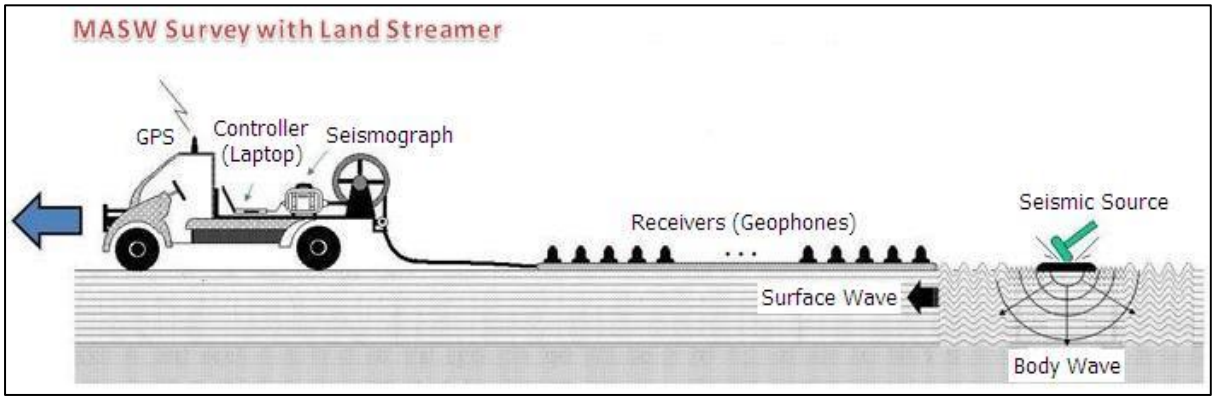

Figure 2.3 - Schematic of a linear array of geophones on a land-streamer (Park Seismic)

The first step in the MASW process is the data acquisition in the field. The purpose of this is to acquire broadband high frequency planar fundamental-mode Rayleigh wave records, in either an ‘active’ or ‘passive’ manner.

The correct selection of an appropriate source is essential to ensuring that enough energy is delivered (Park et al., 2005). Impulsive sources are cheaper and more convenient so are used for all surveys conducted as part of this study. An 8kg sledgehammer and plate was chosen as the seismic source and the signal recorded with a 24-channel array of 4.5Hz sled-mounted vertical geophones, which are suitable for materials in the top 30 m (Park et al., 2005).

The basic field configuration and acquisition procedure is generally similar to that used in conventional common midpoint (CMP) body-wave reflection surveys. The results obtained from MASW testing can be affected by the field setup with key factors including source type, source location, geophone spacing and type, the number of geophones and the site conditions (Yuan, 2011).

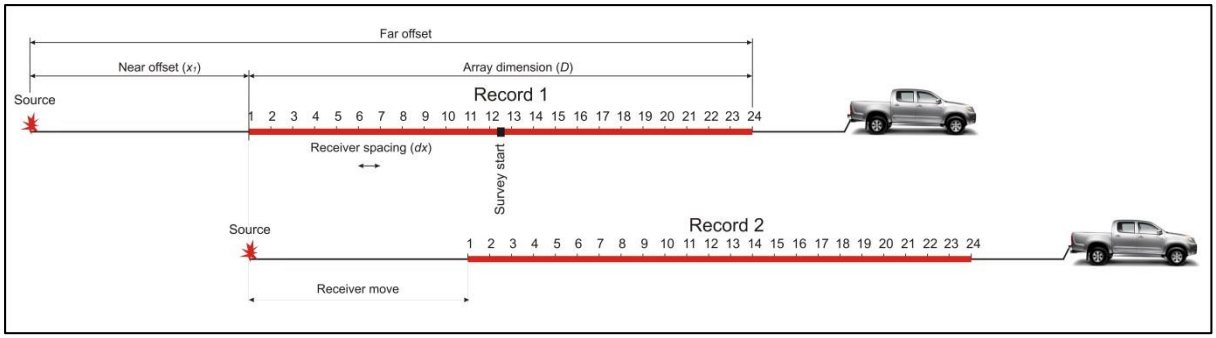

Figure 2.4 - MASW survey geometry using a linear array, known as a land streamer (sled-mounted geophones). The key acquisition parameters (near offset, array dimension, far offset and receiver spacing are illustrated here and selection of these is discussed in the text (Image courtesy of Brendan Duffy)

Selection of an appropriate near offset (x_1 in Figure 2.4) (the distance between the source and nearest geophone), is critical to avoid the near-field and far-field effects. Near-field effects are caused by cylindrical rather than planar propagation of the Rayleigh-waves close to the source (Figure 2.5), manifesting themselves as a lack of linear coherency at lower frequencies (Park et al., 1999).

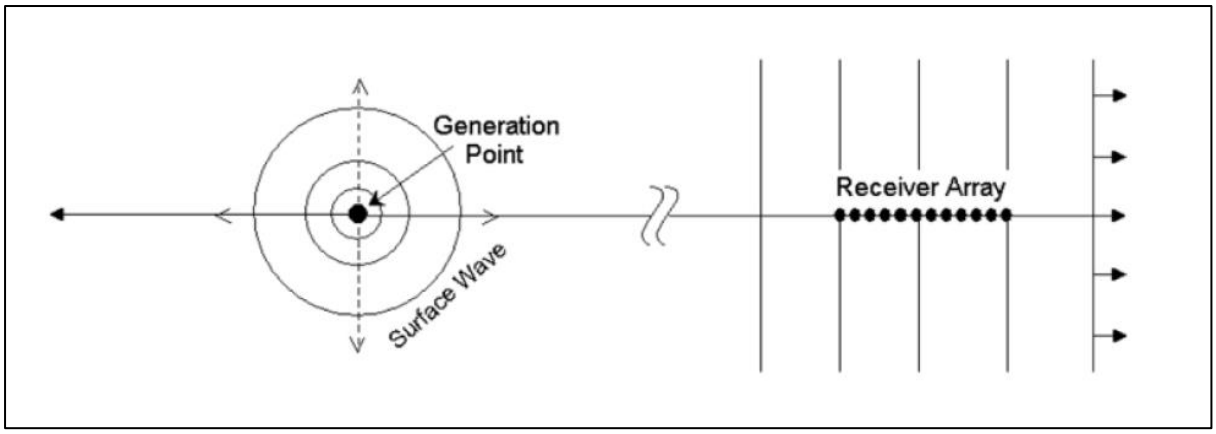

Figure 2.5 - Rayleigh wave propagation away from a generation point. Near the sources the wavefront is cylindrical, whilst further away it becomes planar (Park and Miller, 2006)

It is assumed that the Rayleigh wave is planar only after near-offset (x_1) is larger than approximately half of the maximum desired wavelength (λ_{max}):

$$x_1 \geq 0.5\lambda_{max}$$

This means that the longer a wavelength, the further it must travel before becoming planar, thus requiring a larger near offset for deeper investigations (Richart et al., 1970; Park et al., 1999; Duffy, 2008; Yuan, 2011).

A conservative estimate of the reliable investigation depth for surface wave surveys (z_{max}) (e.g. Stokoe, 1994) is given by:

$$x_1 \geq z_{max}$$

where;

$$z_{max} = 0.5\lambda_{max}$$

This half wavelength criterion is based on the premise that the maximum depth (z_{max}) for which the shear wave velocity (v_s) can be calculated is about half the longest wavelength (λ_{max}) measured (Park et al., 1999). However Park et al. (2001; 2005) state that a near-offset of 10 meters as used in this study can be used to sample wavelengths as large as 50 metres without interference of near-field effects, though this assumption is dependent on the site conditions.

Far field effects are defined as contamination of the body-wave record due to attenuation of high-frequency ground roll at longer offsets (Park et al., 1999) or high-frequency component dissipation at larger distances from the source (Stokoe, 1994). At excessive offsets higher mode surface waves (Ivanov, 2001; 2005) dominate over fundamental mode surface waves and this limits the array dimension *D* (Figure 2.1). This effect limits the highest frequency at which phase velocity (f_{max}) can be measured, and thus the minimum reliable surface layer thickness (Stokoe et al., 1994; Duffy, 2008; Yuan, 2011) such that:

$$Minimum\ layer\ thickness\ (H1) \geq 0.5\lambda_{min} = 0.5C_{min}/f_{max}$$

where C_{min} and λ_{min} are phase velocity and wavelength, respectively, corresponding to a particular f_{max} (Park et al., 1999). Although the final inverted shear-wave profile may possess shallow layers thinner than H1, calculated v_s values for these upper layers should be considered unreliable (Park et al., 1999; Duffy, 2008). Furthermore, the geophone spacing (*dx* in Figure 2.1) cannot be smaller than half the shortest wavelength measured, to ensure that spatial aliasing is avoided (Park et al., 1999; Yuan, 2011):

$$dx \geq 0.5\lambda_{min}$$

By convolving a full wavefield impulsive record with a sweeping stretch function and examining the swept frequency record obtained, a near offset can be selected that minimises near and far field effects for a useful range of wavelengths. As stated above the reliable investigation depth is approximately half the maximum wavelength, so by optimizing the near offset this results in the maximisation of the investigation depth (Park et al., 1999; Duffy, 2008). However in most soil site surveys a full wavefield survey is unnecessary and general parameters can be adopted from Park et al. (2005). Table 2.1 summarises these general parameters.

Table 2.1 - Optimum field parameters for MASW surveys for most common soil sites (Reproduced from Park et al. (2005))

Receiver (Hz)	Max. Depth [z_{max}] (m)	Minimum Offset [x_1] (m)	Maximum Offset (m)	Receiver Spacing [dx] (m)
4.5	50	10	100	1
10	30	10	100	1
40	15	10	100	1

2.3 Dispersion Curve Extraction

Dispersion is the property of frequency-dependent velocity. Generation of a dispersion curve is one of the most critical steps for generating an accurate shear-wave velocity profile. Dispersion curves are generally displayed as phase velocity versus frequency (Figure 2.6).

The shot records must be processed in SurfSeis to image the dispersion to extract fundamental mode dispersion curves (Duffy, 2008). Surfseis applies a wavefield transformation to generate a dispersion image. A multichannel coherency measure is applied to a swept-frequency record in the offset-frequency domain and used to calculate phase velocity with frequency. These variables are mapped continuously to produce a dispersion map from which a curve can be picked (Duffy, 2008).

The accuracy of a dispersion curve can be enhanced by the analysis and removal of noise on ground roll data (Park et al., 1999), however this was not necessary in this study.

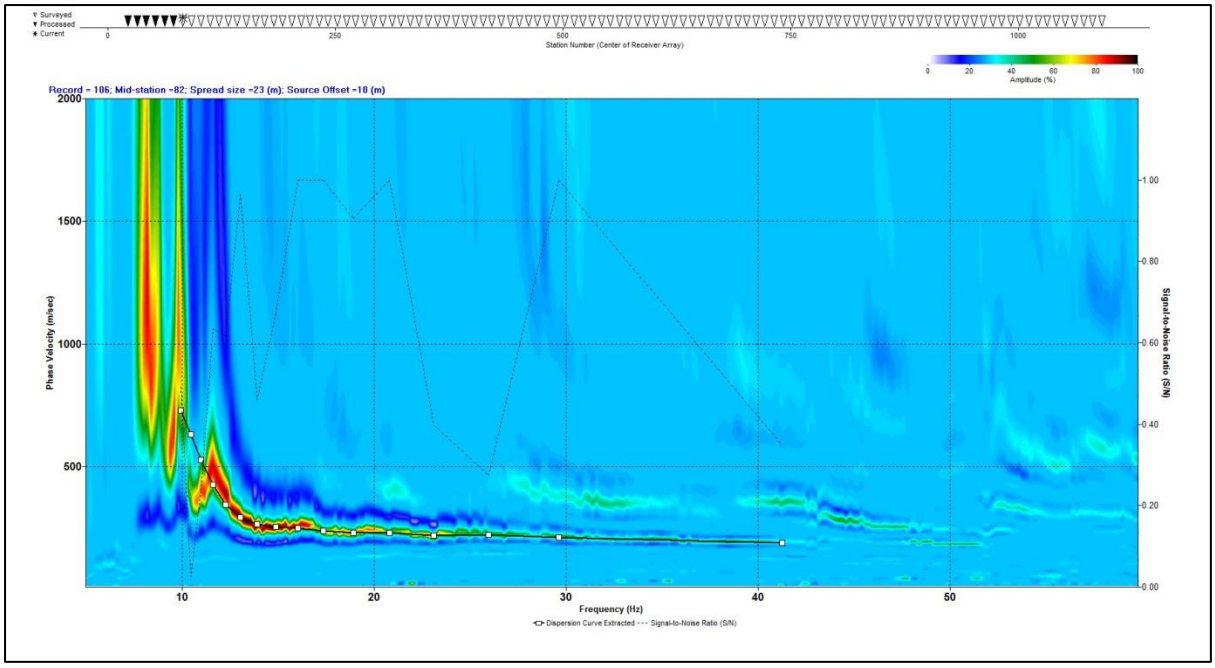

Figure 2.6 - Typical Dispersion Curve Plot with phase velocity (y-axis) versus frequency (x-axis)

It is normally assumed that the fundamental mode of surface waves dominates the recorded wavefield and higher modes can be ignored. In reality, however, higher modes are commonly generated and can sometimes possess significant amounts of energy (Park et al., 1998). Contribution of higher modes tends to become more significant at higher frequencies than normally analysed in conventional application of surface waves. Near-surface application of surface waves deals with these higher frequencies. Reliable separation of different modes is possible only through a multi-channel recording method combined with an appropriate multi-channel data-processing technique (Park et al., 1998; Ivanov et al., 2001; 2005).

2.4 Inversion

Xia et al. (1999) modelled the contribution of elastic properties to fundamental mode Rayleigh-wave phase velocity. They found, for both their models and in-field testing, that S-wave velocity is the dominant property at frequencies greater than 5Hz. The low sensitivity of Rayleigh-wave phase velocity to P-wave velocity and density allows these properties to be estimated to within 25% without a significant adverse effect on the convergence of model and inversion. Definition of a layer model by division of the subsurface into layers of constant velocity removes layer thickness as a variable, leaving S-wave velocity as the only remaining variable. S-wave velocities can thus be derived by inverting Rayleigh-wave dispersion data to fit a layer model with fixed

estimates of layer thickness, Poisson's ratio or P-wave velocity and density. Once individual dispersion curves are inverted, the resulting 1-D profiles are interpolated to construct a 2-D S-wave velocity profile (Figure 2.7) (Duffy, 2008).

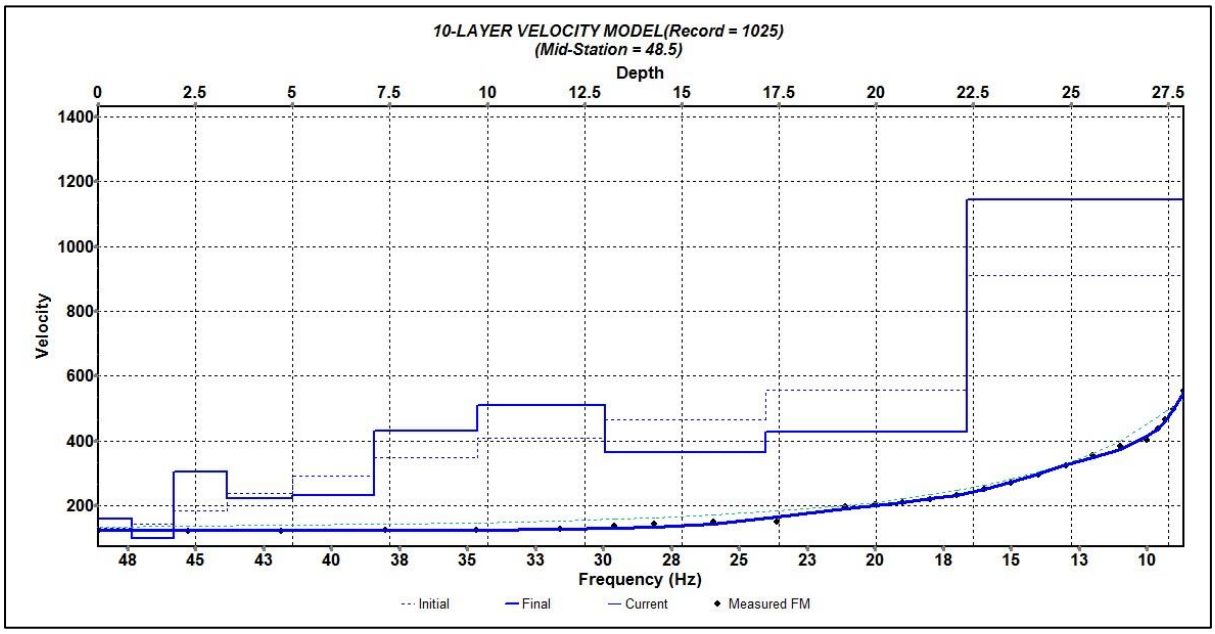

Figure 2.7 - Typical 1-D inverted profile showing depth (frequency) vs velocity

The validity of an inversion of a fundamental mode Rayleigh-wave dispersion curve is heavily dependent on the accuracy of the curve (Xia et al., 2003; Zhang and Chan, 2003; O'Neill and Matsuoka, 2005) A well picked fundamental mode dispersion curve will invert to a model that closely resembles the earth model, but if the dispersion curve is inaccurate at any point along its length a partly or completely imitation S-wave velocity profile can result.

Zhang et al. (2003) observed that cross-mode mixing of up to 40% at middle to high frequencies made little difference to the inverted result, but anything more than 5% mixing at low frequencies adversely affected the inverted model. Mixing <10% dramatically reduced penetration depth whilst higher mixing ratios produced similarly reduced penetration depth and significantly higher velocities within those penetration depths. (Duffy, 2008)

Xia et al. (2003) proposed an alternative approach based on inverting both fundamental and higher mode Rayleigh-waves. This is implemented in the SurfSeis 3 software. Higher mode Rayleigh-waves are even more strongly dependent on S-wave velocity than are fundamental mode Rayleigh waves. This means that a small

change in S-wave velocity at a given wavelength produces a many times larger standard deviation in the phase velocity of the higher mode than that of the fundamental mode The higher modes stabilise the inversion procedure.

2.5 Walkaway surveys

This study used fixed receiver (source move-out – Vincent et al., 2006) walkaway survey geometry at several sites. The process for conducting walkaway surveys is the same to that of a rolling MASW survey, described above, with only the data acquisition being different, thought the processing is generally the same. The term walkaway is defined as a survey performed by moving source points to progressively larger offsets while keeping geophones fixed, or the source point can remain fixed while the geophones are moved to progressively larger offsets. In fixed-receiver walkaway surveys (FRW), the geophone spread remains stationary, whereas the source location moves out one geophone spread length at a time (Vincent et al., 2006). This study used fixed-receiver walkaways for deep soundings only. Using the fixed-receiver walkaway method, rather than the fixed-source walkaway method, we reduce the effect of heterogeneity in the subsurface (Vincent et al., 2006).

The source is placed at 10 metre spacing between the source and first geophone, then moved at multiples of the array length. Individual shot records are added to produce a pseudo-96-channel record. A schematic of the FRW process is shown in Figure 2.3 above.

2.6 Parameters used for this study

The active source MASW method was used for the field investigations as part of this study. The field data was collected as roll along methodology, with some deep walkaway soundings. The survey parameters used as part of this study are shown below in Table 2.2.

Table 2.2 - Summary of parameters used for the roll-along MASW data acquisition as part of this study

Receiver (Hz)	Minimum Offset (m)	# of Geophones	Maximum Offset (m)	Geophone Spacing (m)	Stack number
4.5	10	24	33	1	6 (12)

As part of the surveys completed for this study, a geophone array consisting of 24 4.5Hz geophones at 1m spacing was used. The stack number indicates the number of records that were taken at each distance along a profile. Generally 6 stacks were taken at each location, while up to 12 stacks were taken when ambient noise from the surroundings would register on the equipment.

The processing of the data was all completed using the SurfSeis 3 software.

The data obtained was encoded with geometry. The geometry-encoded fixed-receiver walkaway records were added to build 96-channel records. Dispersion maps (overtone images) were generated using the active overtone technique. Frequency ranges were typically from 5 to 50Hz.

Fundamental mode dispersion curves were extracted within user-defined boundaries. Representative dispersion curves for the different sites are shown below in Figure 2.4. The dispersion curve was typically coherent, clear of higher modes and strongly dispersive.

The dispersion curves were inverted using the default 10-layer model and interpolated in SurfSeis to produce 2-D profiles. Further analysis is reported in Chapter 5 and the results discussed in Chapter 6. All dispersion curves plots are provided in Appendix E.

Greymouth Aerodrome

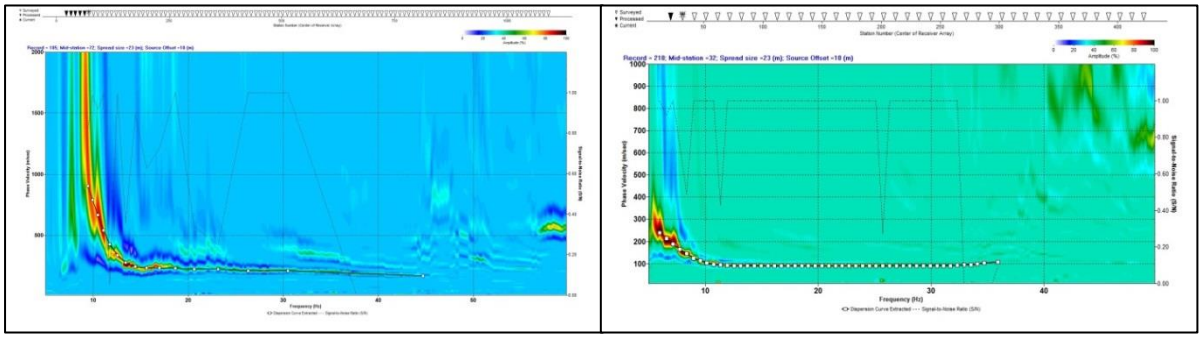

Victoria Park Racecourse

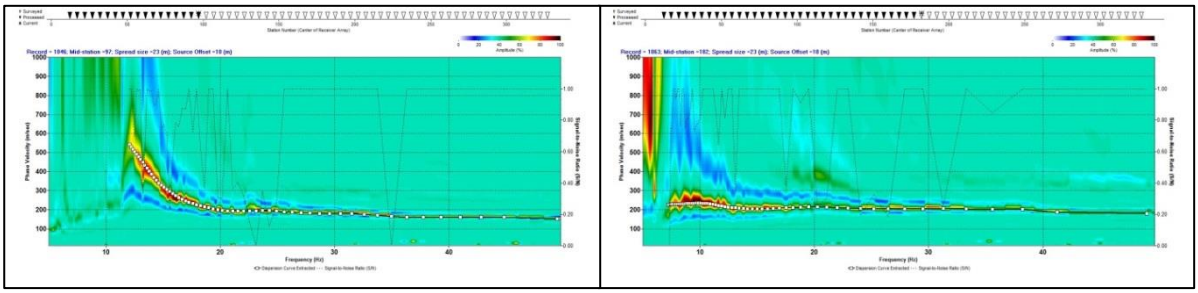

Truck Stop on Charles O'Connor Street

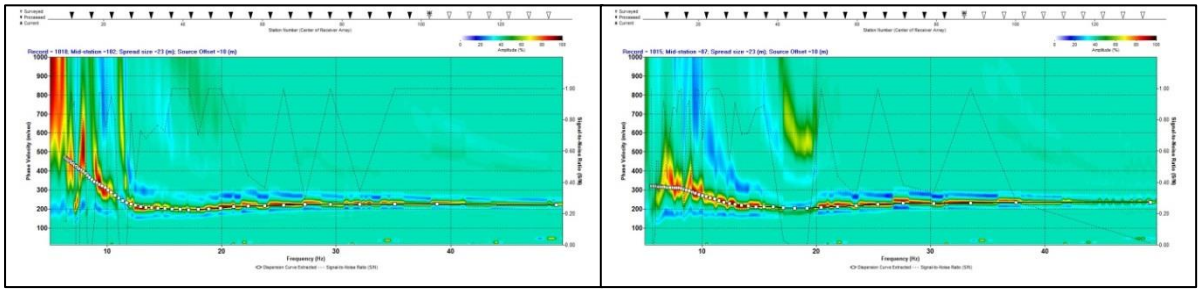

Figure 2.8 - Sample of the dispersion curves produced through the SurfSeis Software. The top 2 images are from the Greymouth Aerodrome, the middle 2 images are from Victoria Park Racecourse, and the bottom 2 images are from the Awatuna Freighters Truck Stop on Charles O'Connor Street

3 Geomorphology

3.1 Introduction

The Greymouth area has been affected by a combination of late Cenozoic uplift and erosion, the effects of Quaternary glaciation, and coastal erosion (Nathan et al., 2002). The Greymouth township is situated on a narrow coastal plain extending immediately south of Point Elizabeth to beyond the southern extent of the field area (Metcalf, 1993). This chapter describes the current structural (Figure 3.2) and surficial geomorphology and processes, and also describes the geomorphic evolution over the last 150 years from natural and anthropogenic factors.

3.2 Structural Geomorphology

The dominant structural geomorphological feature in the area surrounding Greymouth is the steep hill country, including the Twelve Apostles Range and Peter Ridge described in Chapter 1.3. This steep hill country feature has formed on erosion-resistant Tertiary limestone (Cobden Limestone) that forms the landward boundary of the coastal plain to the east, with less dominant hills formed at the base of the limestone beds from the less erosion-resistant mudstone (Stillwater Mudstone). The dip in these limestone beds formed with the active development of the Brunner-Mt Davy Anticline, resulting in the western limb dipping at approximately 30°. This structure possesses the highest relief in the area, with elevations of 330m above sea level (asl) for the Twelve Apostles Range and 270m asl. for Peter Ridge (Figure 3.1) (Metcalf, 1993). The digital elevation map shown in Figure 3.2 shows the location of the dominant structural features.

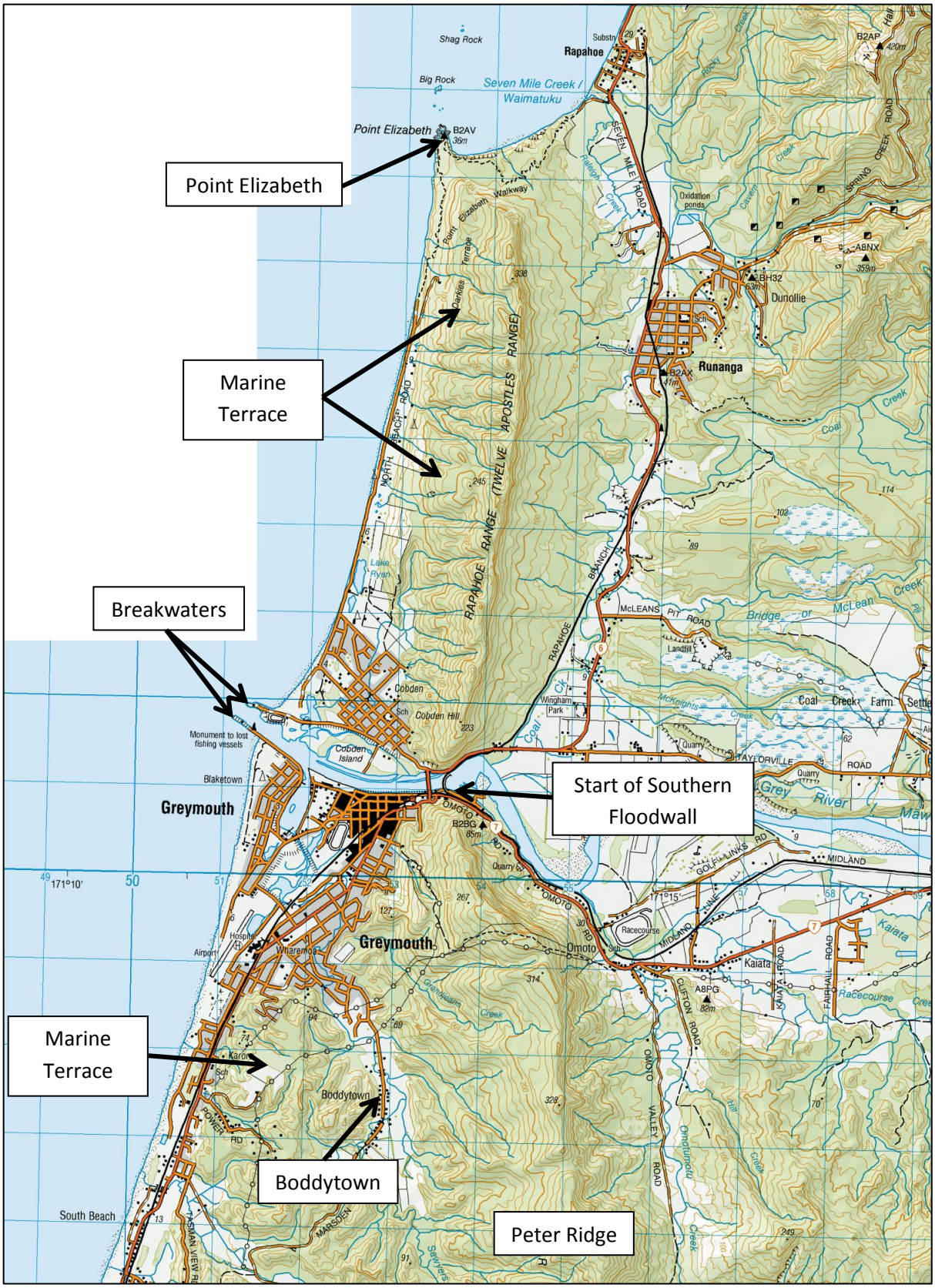

Figure 3.1 - Topographic map showing the Twelve Apostles Range and Peter Ridge constraining Greymouth to the east, and locations of marine terraces (Sourced from NZ Topo Maps)

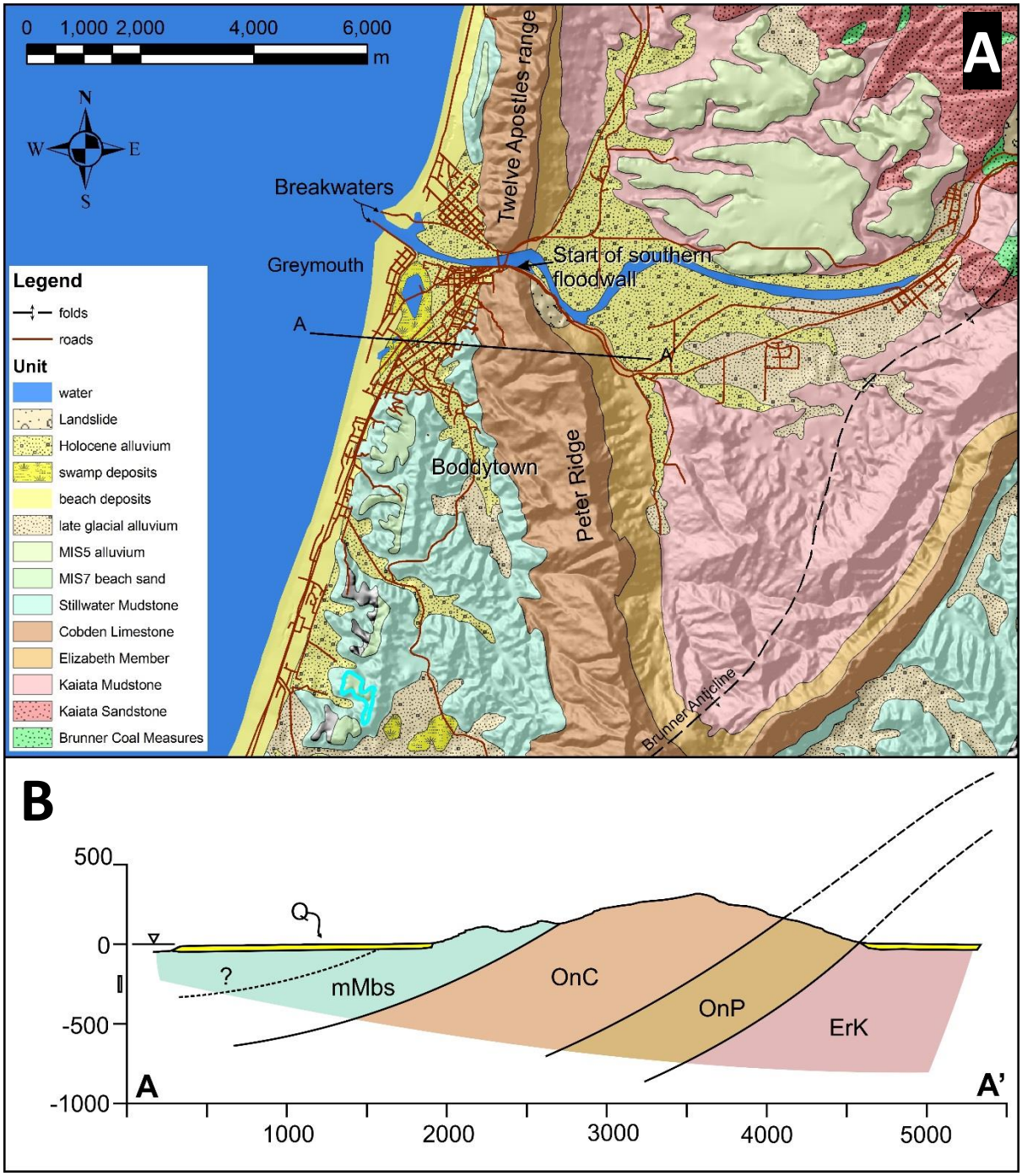

Figure 3.2 - (A) Digital elevation map of the Greymouth Area with bedrock and Quaternary geological units represented. Major structural features are also represented. (B) Schematic cross-section of Greymouth

Tectonically uplifted marine terraces at approximately 6–9m asl form a higher section of the coastal plain. Another terrace at 70–80m asl is also present north and south of the Grey River (Metcalf, 1993). These terraces generally overlie eroded marine mudstone (Stillwater Mudstone). The uplift of these terraces has preserved the marine mudstone and overlying Quaternary deposits from coastal and alluvial processes during interglacial periods. The susceptibility to erosion of this mudstone

unit results in the removal of the mudstone from above the limestone units forming the ridges. As a result of this, the relief developed above the mudstone is much more subdued. This is observed in the southeast of the township that extends towards Boddytown (as seen in Figure 3.1 and Figure 3.2), where a broad valley has eroded into the mudstone during incision of Sawyer's Creek (Figure 3.2) (Metcalf, 1993).

3.3 Present Day Geomorphology of Greymouth

The dominant geomorphic agents are the Grey River, and also the Tasman Sea coastline. The river has been completely constrained on the southern bank from the Cobden Rail Bridge east of the town, westwards to the coastline through construction of the wharves for boat moorings and more recently a floodwall (Figure 3.1, 3.2). This has not allowed the river to form meanders on the southern bank. It is also partially constrained on the north bank through the entrainment walls, though these are smaller than, and not as continuous as, the floodwall constructed on the southern bank. Flood protection was built between 1988 and 1990, following two major floods in 1988. Flooding has historically been an issue with floods recorded since European occupation (Figures 3.4, 3.5 and Appendix D).

Figure 3.3 - Flooding on Mawhera Quay following the 1887 flood (McMillan Brown Library, UC)

Figure 3.4 - Greymouth town following the September 1988 Flood event. Photo is looking west towards the Tasman Sea (Grey District Library Charlton Collection)

The other dominant geomorphological feature is the coastline, which constrains the western side of Greymouth, extending north and south. The coastline is broken by two breakwaters, which were built in the early 20th century (see Greymouth Argus excerpt dated 11 August 1904 [Appendix B]).

The Erua Moana lagoon and Lake Karoro (Figure 3.2) make up the modern extent of the estuary. The entrance to the estuary is located in the floodwall along the south bank of the Grey River. The entrance is constrained by the presence of the floodwall and the Port of Greymouth. The estuary extends through Greymouth, with the southern extent being Lake Karoro located at the Greymouth Aerodrome. Apart from Lake Karoro, the estuary is bounded on all sides by floodwalls, though the bounds of Lake Karoro have still been influenced by anthropogenic methods.

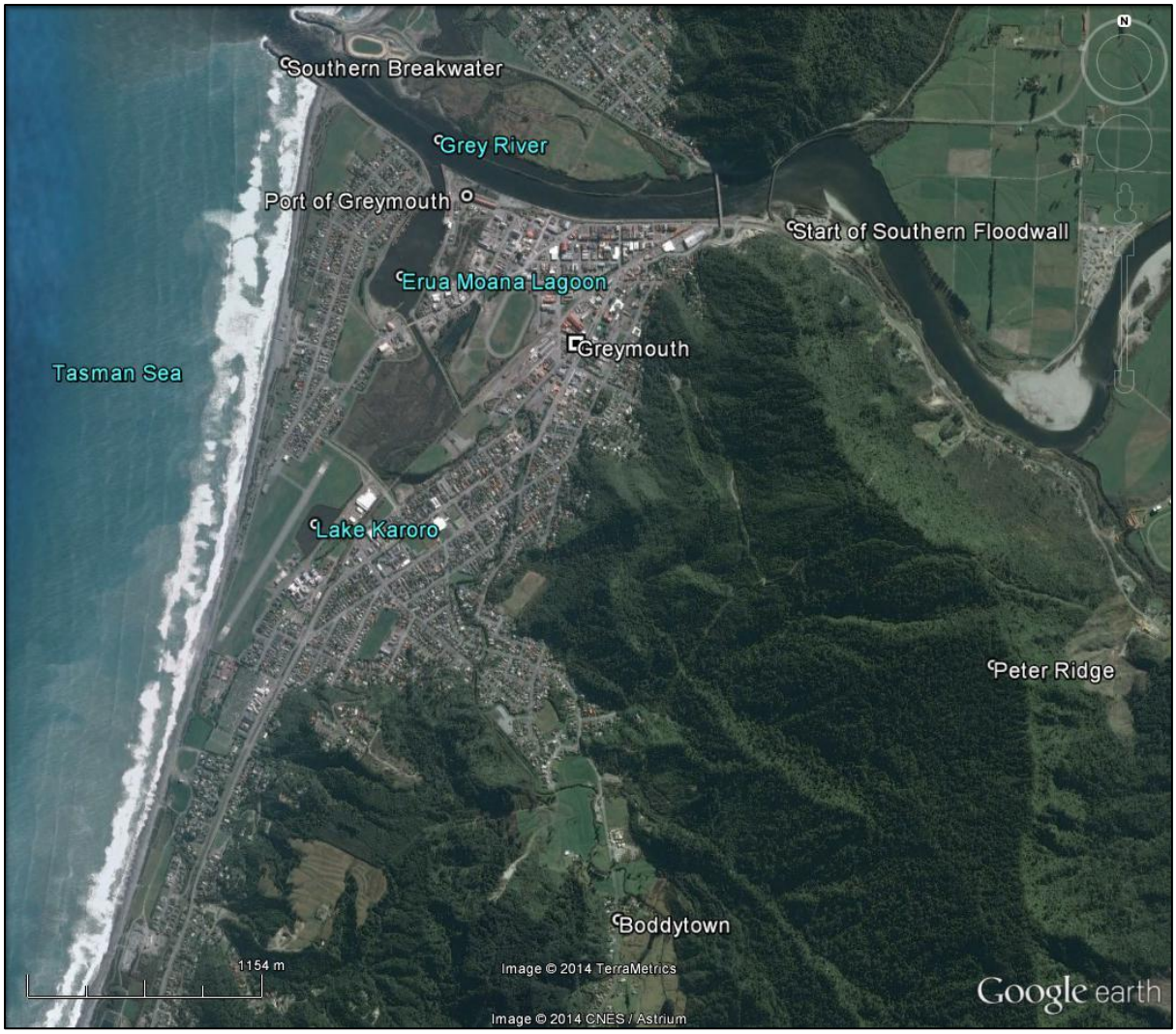

Figure 3.5 - Current Geomorphological features in the Greymouth Area

3.4 Geomorphic Evolution over the past 150 years

The current geomorphology of Greymouth is heavily constrained by human influences. The geomorphological evolution outlined below has been based on historical maps, which can be found in Appendix C, along with larger versions of the maps used below. This section focuses on the southern bank of the Grey River, the estuary and the Tasman Sea coastline south of the Grey River mouth.

It should be noted that not all maps have the same extents, so only the interpretation that can be observed has been documented below. A site-specific geomorphological evolution has also been provided in each section of Chapter 4 relevant to each site.

1871 to 1873

The extent of the Grey River, Tasman Sea coastline and location of the estuary as mapped in 1871, and the change over time to 1873 is shown in Figure 3.6. Based on the 1871 extent (purple line) the Grey River mouth flowed into the Tasman Sea in a northwest direction. The entrance to the estuary was very narrow, and the presence of sand bar at the mouth of the river indicates the influence of the river meeting the north-flowing longshore drift in the Tasman Sea. The map for 1871 only defines the area around the river mouth.

From the 1871 extent to the 1873 extent (green line), the mouth of the Grey River had migrated south and the meander in the river had begun to straighten. However, the entrance to the estuary was still narrow. There is no information on presence of the sandbar across the mouth of the river in 1873. In addition the extent of the estuary (Erua Moana and Lake Karoro) is defined. Several tributaries to the estuary are shown, predominantly as drainage from the elevated area making up Peter Ridge, also associated sources from Sawyers Creek flowing from the southeast of the map. The coastline of the Tasman Sea is shown also.

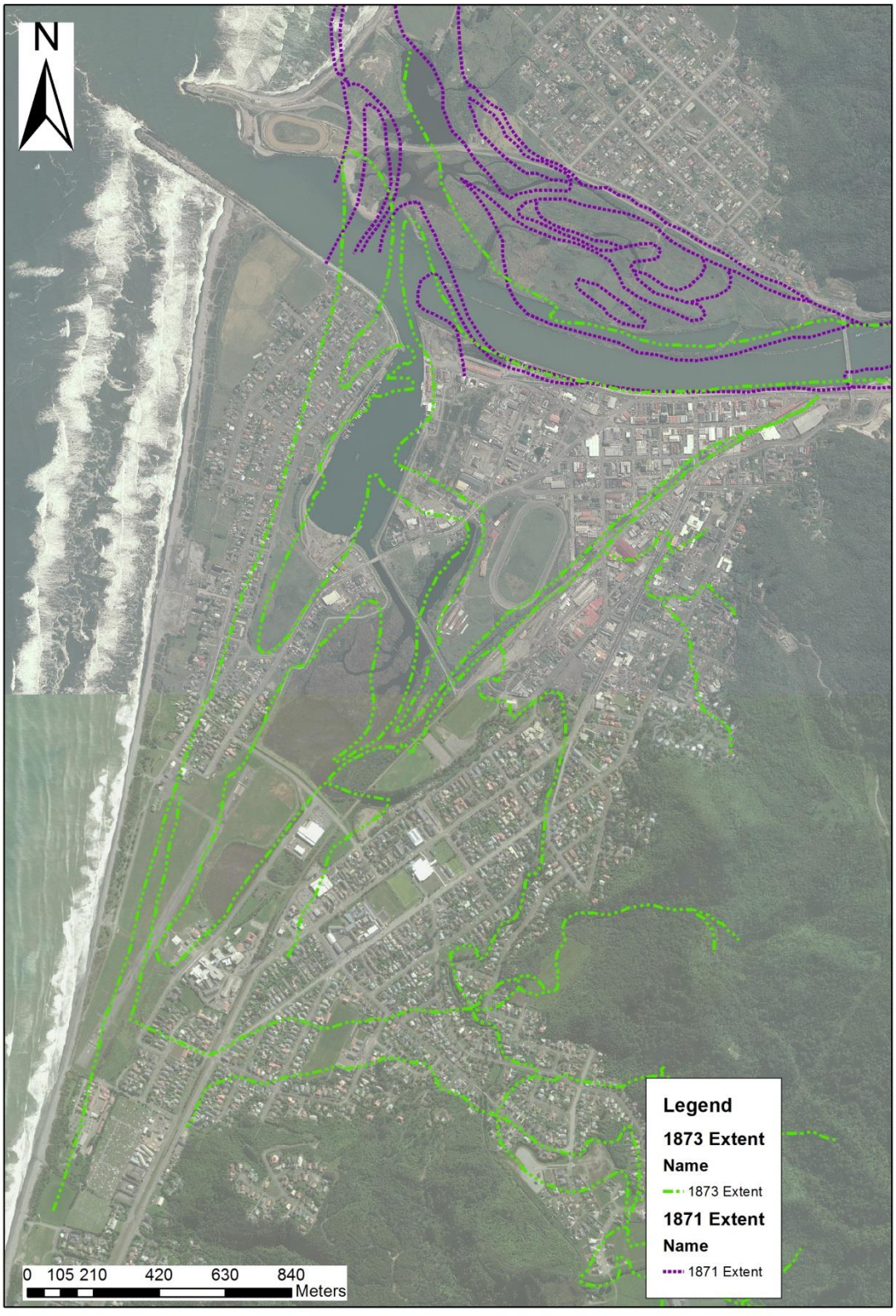

Figure 3.6 - Changes in the extents of geomorphic features from 1871 (purple) to 1873 (green)

1873 to 1879

The evolution from 1873 to 1879 (orange line) is shown in Figure 3.7. The construction of the Port of Greymouth, which picked up in the 1880's to meet the demand associated with the gold and coal at the time (Grey District Council, 2014) can be seen on the southern bank of the Grey River. The river had continued to migrate south during this time. The entrance to the estuary was still narrow and appears to have been constrained on its eastern edge by the Port of Greymouth construction. The river had straightened further, possibly caused by a large flood event or by dredging of the channel, which had removed much of the material that made up river mouth on the southern bank.

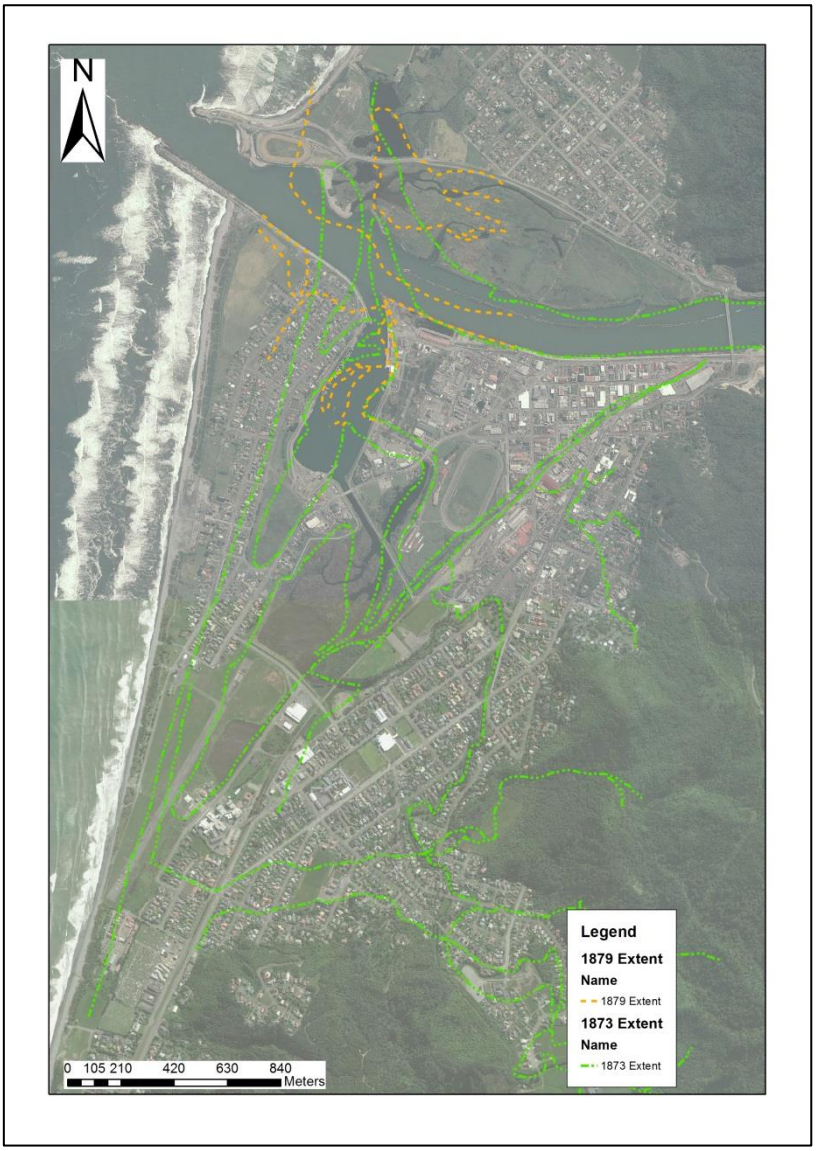

Figure 3.7 - Changes in the extents of geomorphic features from 1873 (green) to 1879 (orange)

1879 to 1888

Figure 3.8 demonstrates the changes from 1879 to 1888 (yellow). Continuing construction of the port had further constrained the eastern portion of the southern bank of the river. The entrance to the estuary had widened and initial construction of the floodwall and breakwater west of the estuary entrance is apparent. Dredging of the channel along the southern bank allowed for the reclamation for the port to be developed on the river (Westfleet). The river channel appears to be narrower.

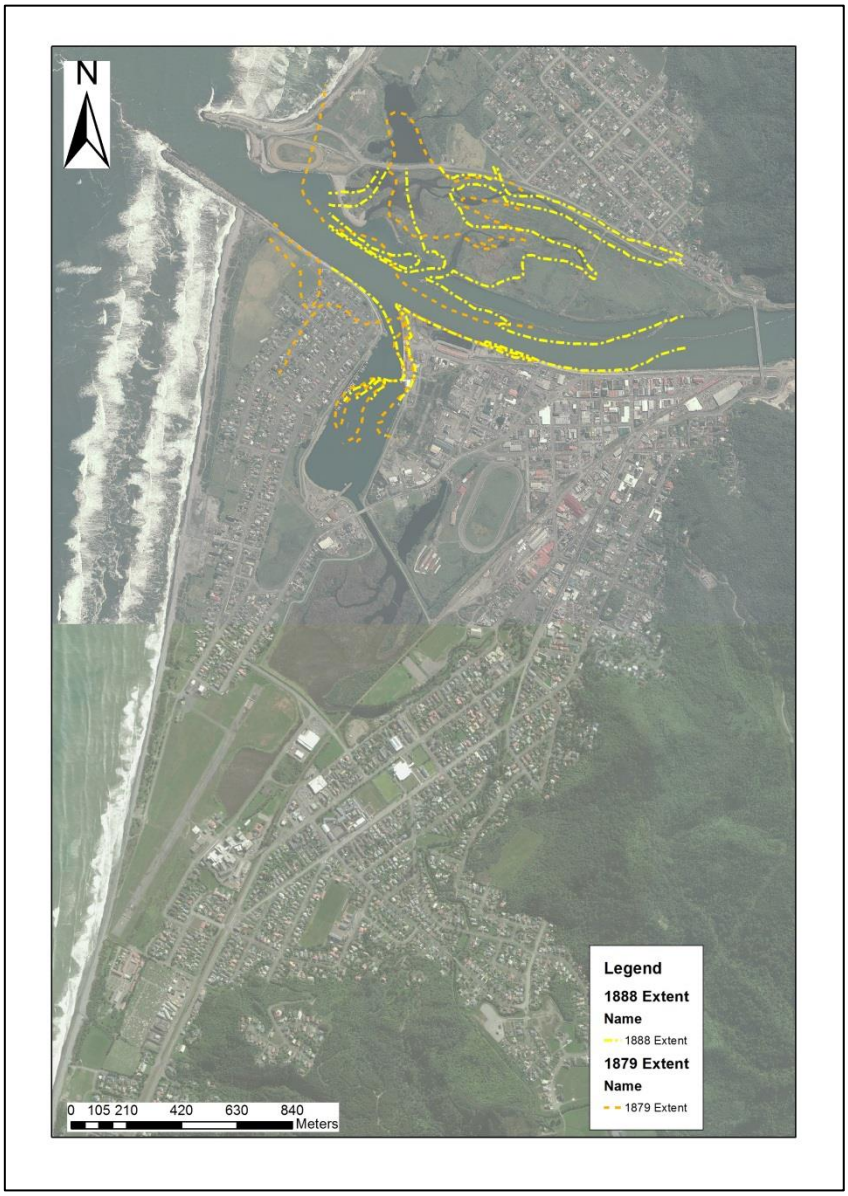

Figure 3.8 - Changes in the extents of geomorphic features from 1879 (orange) to 1888 (yellow)

1888 to 1895

The changes from 1888 to 1895 (pink) are shown in Figure 3.9. By 1895 the initial construction of the southern wall, both east and west of the estuary entrance appears to have been completed. The estuary entrance had widened further also. The entrainment walls appear to have influenced the northern bank of the river, through a reduction of energy allowing more material to be deposited. Historically, build-up of a sandbar at the mouth of the Grey River caused significant issues for vessels attempting to leave or arrive at the Port of Greymouth. It's likely these were constructed as a way to entrain the flow to naturally remove the sandbar build-up at the river mouth.

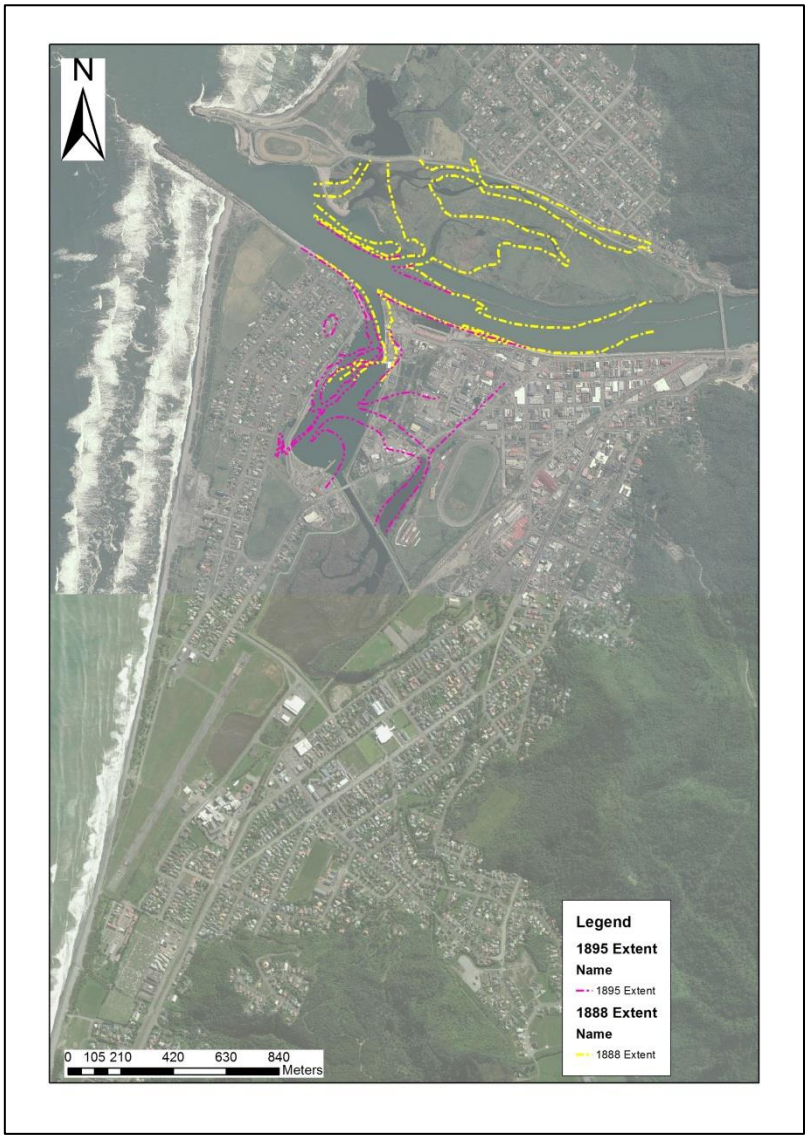

Figure 3.9- Changes in the extents of geomorphic features from 1888 (yellow) to 1895 (pink)

1895 to 1945

Figure 3.10 shows the geomorphological evolution from 1895 to 1945 (red). This is a considerable time gap (50 years) and as such, the changes in the Greymouth area were extensive. The constraint through the port construction on the southern bank was completed as far east as the current Cobden Bridge location. The southern and northern breakwaters were completed during this period (Greymouth Argus, 1904) along with the wall between the southern breakwater and the estuary entrance. Erua Moana has been constrained on the eastern, southern and western bounds, with some land being reclaimed on the western boundary when compared to the 1873 extent. Though the 1873 extent isn't shown it is referred to from Figure 3.7 due to it being the last map that had the extents shown for the area south of the river.

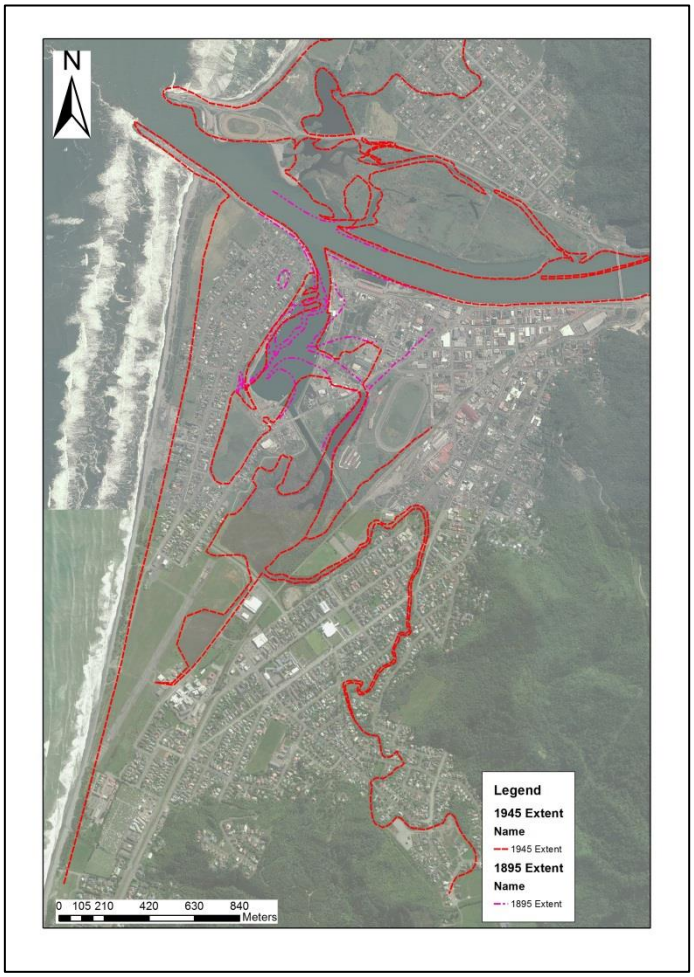

Figure 3.10 - Changes in the extents of geomorphic features from 1895 (pink) to 1945 (red)

The channel connecting Erua Moana and Lake Karoro remained intact. Lake Karoro had also been constrained through the reclamation on land within when compared to

the 1873 extent. This is largely in part to the development of an airfield on the site west of Lake Karoro. The coastline appears to have prograded westward, probably due to accretion of material behind the newly constructed southern breakwater.

1945 to 1979

Figure 3.11 shows the change between 1945 and 1979 (blue), and generally the extent of the major water bodies has not changed during this time. The main change is the further progradation of the coastline to the west. It is unclear whether the small changes in the size/shape of Erua Moana were due to seasonal fluctuations or minor reclamation work.

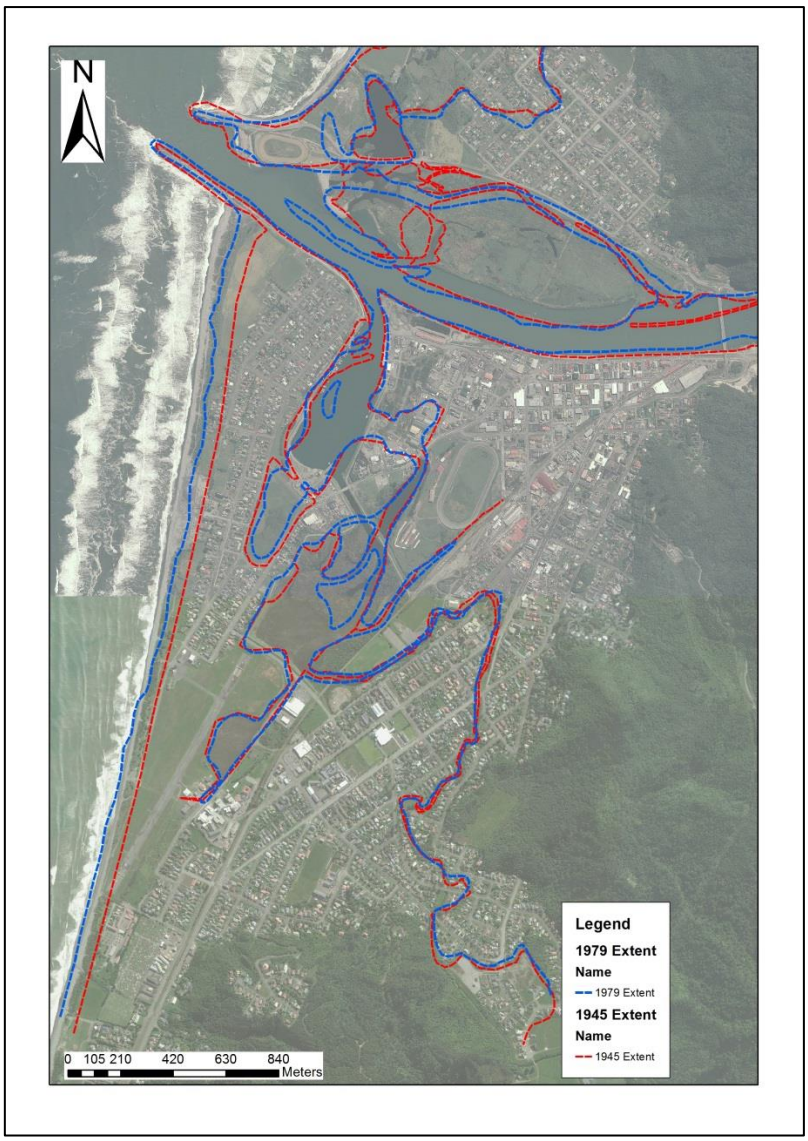

Figure 3.11 - Changes in the extents of geomorphic features from 1945 (red) to 1979 (blue)

1979 to present

From 1979 to the present day there have been several significant changes (Figure 3.12), and areas of reclamation are visible in Figure 3.9, particularly around Erua Moana lagoon. The southern portion of Erua Moana has been reclaimed, along with the historic channel connecting Erua Moana to Lake Karoro. A new channel has been constructed at the southeast part of the newly confined Erua Moana Lagoon to Lake Karoro. A floodwall has also been constructed around all of the reclamation land, confining the estuary, and not allowing it to increase in size or migrate. Further seaward progradation has occurred on the coastline as material continues to likely accrete behind the southern breakwater.

Figure 3.12 - Changes in the extents of geomorphic features from 1979 (blue) to present

Summary of geomorphological evolution

In the time from 1871 to the present day, some 143 years, the landscape of the Greymouth delta has changed significantly. While initially the changes were likely due to natural causes (e.g. flood events), around the turn of the century anthropogenic influences became the major factor in the changing geomorphology. Numerous areas of reclamation especially around the estuary (Erua Moana and Lake Karoro), and the constraint of southern bank of the Grey River have been the major human influences during this time. These areas are shown in Figure 3.13 below.

Areas of natural accretion have resulted from:

- The construction and extension of the breakwaters in the early 1900's extensive accretion of the southern coastline of the Tasman Sea has occurred. This is a result of longshore drift being disrupted causing the suspended sediment load to be deposited;
- The accretion of material on the northern coastline is likely to be also a result of the construction of the southern and northern breakwaters. Material being transported by the river is delivered into the Tasman Sea, where wave action then moves it north into the area north of the northern breakwater, causing subsequent deposition. This accretion has not been on the scale interpreted on the southern coastline, though it is still extensive.

Areas of reclamation have resulted from:

- Primarily it is anthropogenic processes that have resulted in reclamation. The major areas of reclamation are around the Aerodrome site at Lake Karoro and the construction of both breakwaters between 1873 and 1945. Also the southern extent of Erua Moana at the current Messenger Park location and the historical channel connecting Erua Moana to Lake Karoro, with this land being reclaimed post-1979;
- Minor areas of reclamation occurred between 1873 and 1945 where a thin historical extent of the estuary moved north-east towards the present day Cobden Bridge. This could be either due to natural infilling of the channel or anthropogenic emplacement of fill.

The areas of land removal have resulted from:

- Natural removal of material between 1873 and 1945. This is likely to be a result of high-energy events such as floods removing the natural obstruction of the material at the mouth of the river. Anthropogenic influences were possibly involved with the removal of this ground (e.g. dredging of the river mouth) though it is unlikely;
- Anthropogenic removal of the land post-1979 occurred at the south-eastern extent of the current Erua Moana lagoon to allow for the construction of the new channel connecting it to Lake Karoro. This was required as a result of the reclamation of the land where the historical channel used to reside.

It should be noted that Cobden Island, which is clearly visible in Figure 3.12, has been evolving continuously throughout this time. The constant changing shape of Cobden Island gives an idea of how active this environment has been, and continues to be. Numerous channels have formed within it (as seen in Figures 3.6, 3.8 and 3.10), while Figures 3.11 and 3.12 show large reductions in the size and number of channels. This gives a prime example of how dynamic this environment continues to be.

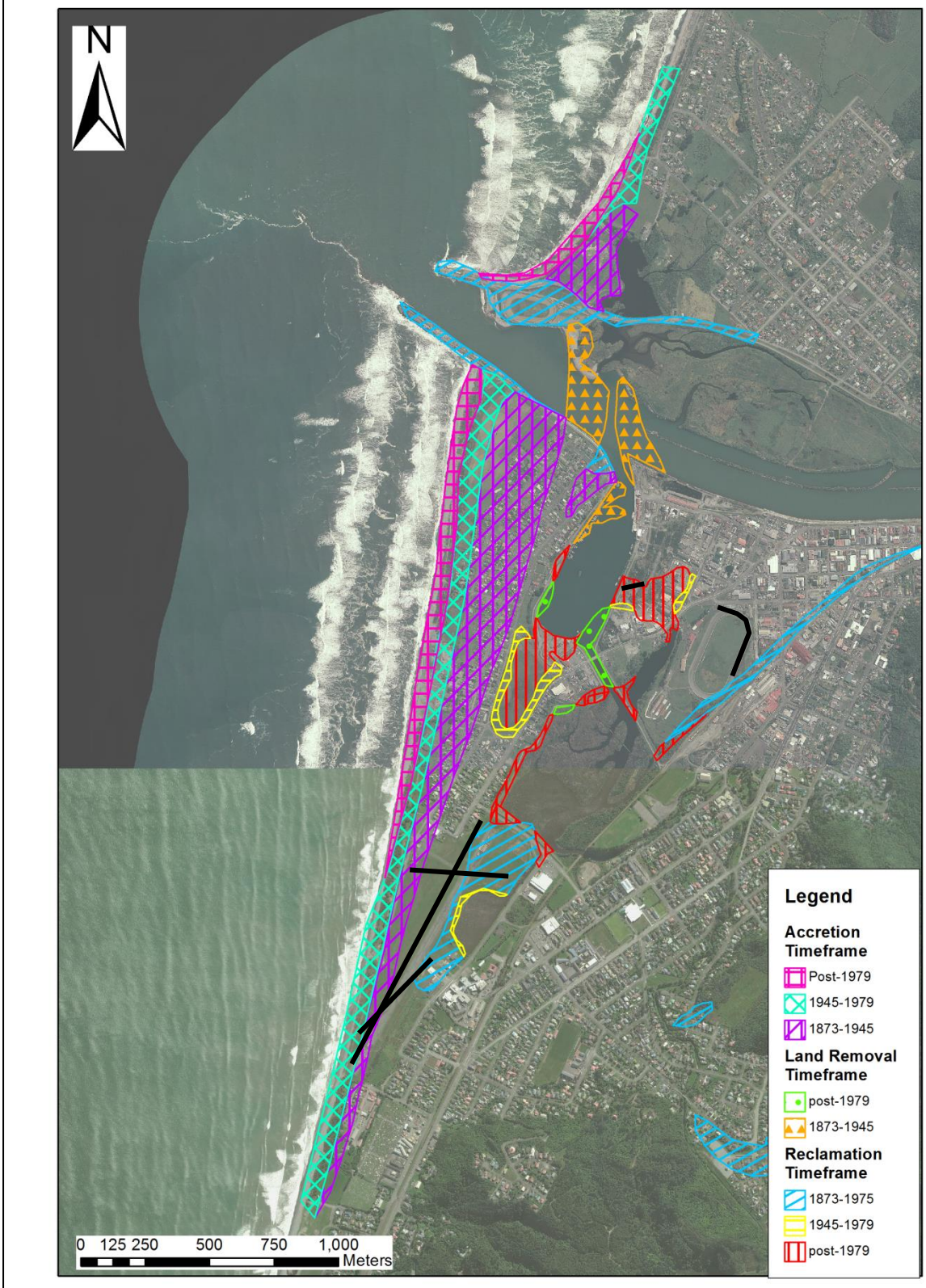

Figure 3.13 - Areas of different types of landscape modification (with MASW testing lines overlain [black lines])

4 Site Investigations

4.1 Introduction

The sites that were chosen for the field investigative testing were based on the historical geomorphology of the site and also on observations made during previous seismic events that induced liquefaction. The three sites chosen were based on the common criteria that they were influenced at some stage during the Holocene by the estuary (Erua Moana and Lake Karoro), while there was anecdotal evidence of liquefaction occurring at 2 of the 3 sites. The 3 sites and their locations are shown below in Figure 4.1.

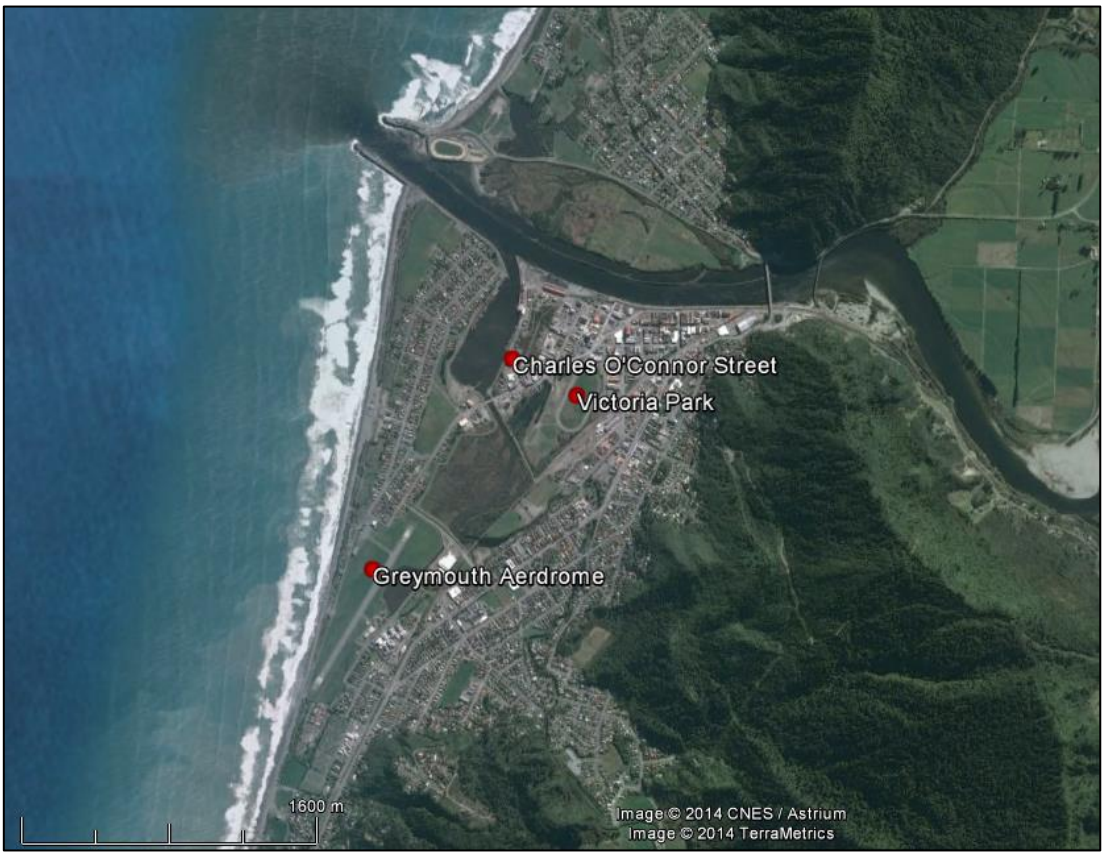

Figure 4.1 - Locations of site investigations

The sites are all located on the low lying land on the western side of the Greymouth Township, in areas that are in close proximity to the estuary. Photos of the sites are included in Appendix D, and all original historic drawings are included in Appendix C.

4.2 Greymouth Aerodrome

4.2.1 Site Description

The Greymouth Aerodrome is located close to the coastline on the west side of the town, and is situated within the suburbs of Blaketown and Karoro. It is a large cleared, relatively flat area with a single concreted runway running northeast-southwest. There are several buildings on site, all located on the western edge of the area, consisting of control buildings and storage hangars.

4.2.2 Site Geomorphology

The current geomorphology of the Greymouth Aerodrome consists of a large flat area with no distinctive features other than the lake that bounds the northern part of the eastern boundary on the site. Historically the site has experienced significant change over the last 140 years, as can be seen in Figure 4.2.

The two major geomorphological changes that have occurred during this timeframe is the reduction in the size of Lake Karoro, which makes up part of the estuary, and the westward movement of the beach and coastline.

Large areas of the estuary have been reclaimed from 1873 to 1945 (1945 Historic Drawing; Aerial Photographs dated 1945). There were no available maps between these dates to better constrain when the reclaim occurred. There was further reclamation work completed from 1945 to 1979 (Aerial Photographs dated 1945; Dowrick et al., 2003), though that was on a smaller scale around Lake Karoro, likely to allow for the construction of the concrete runway, as it was still a grass landing strip in the 1945 aerial photos. Post-1979 a further reclamation took place at the northern boundary to allow for the construction of a roadway, with material being removed and replaced as fill in other areas for what appears to be the realignment of the road. The channel between Lake Karoro and Erua Moana, the main estuary, also appears to have been narrowed (Current Aerial Photographs, dated 2004).

The coastline south of the Grey River has prograded approximately 120m since 1873, as seen in Figure 4.2, and appears to coincide with the construction of the breakwaters at the river mouth in the late 1880's (Greymouth Argus excerpt [Appendix B]).

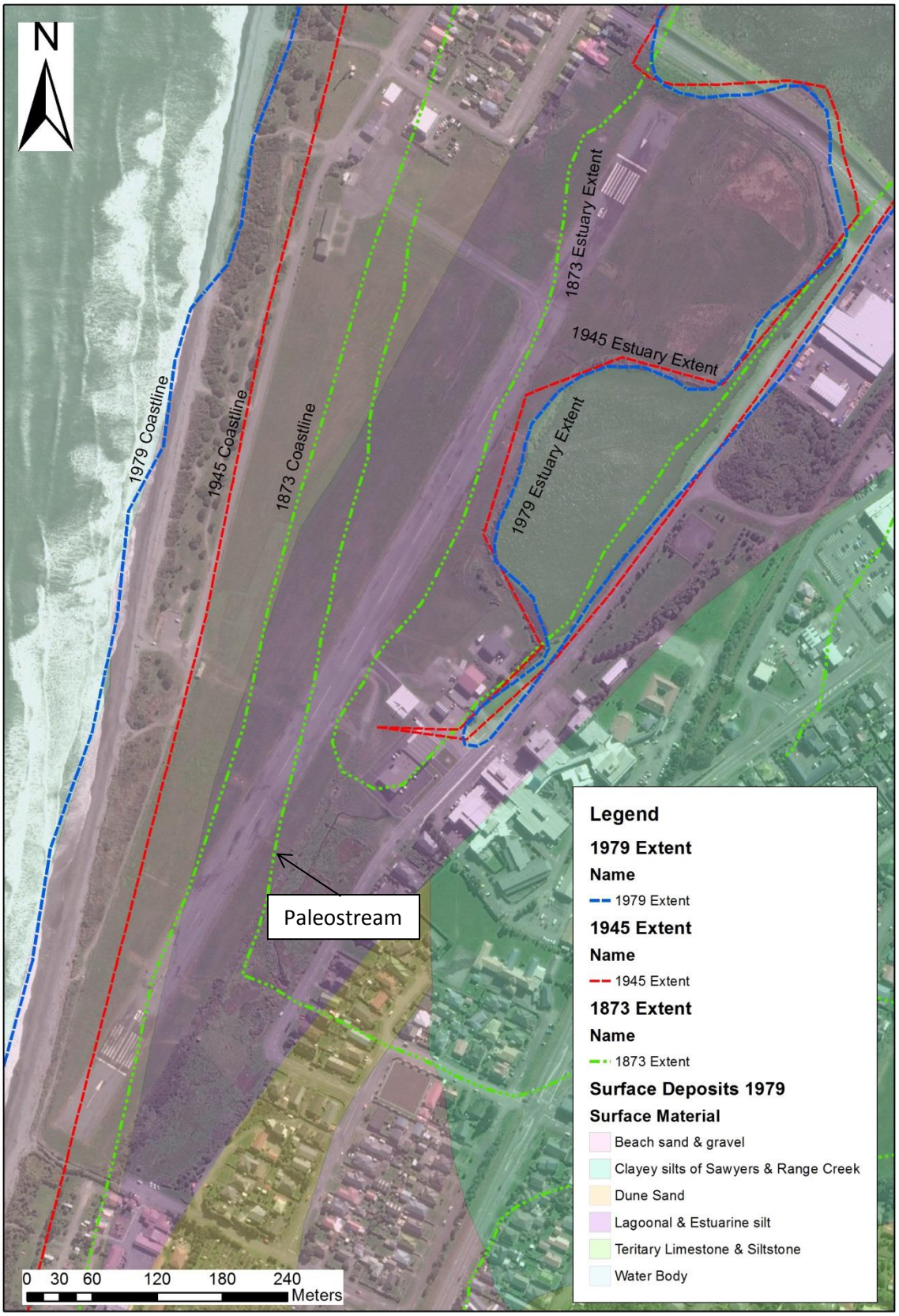

Figure 4.2 - Geomorphology of the Greymouth Aerodrome with known historical estuary and coastline extents shown (Image redrawn based on West Coast Business Unit Historic Drawing, dated 1873; Aerial Photographs dated 1945; and Microzoning map of Greymouth, Dowrick et al., 2003).

Northward-flowing longshore drift has caused material being transported to encounter the breakwaters, and subsequently deposit its sediment load.

The other geomorphological change is the clearance of land at the southern boundary. Since 1945 approximately 470 metres of land has been cleared to allow for the extension and construction of the current runway. Much of the land appears to have been scrubland though a quarry stockpile yard makes up some of the area which is now incorporated into the aerodrome.

Based on Dowrick et al. (2003) the site appears to be dominated by lagoonal and estuarine silt for the eastern half, while beach sand and gravels make up the western half, which correlates to the approximate locations of the historical estuary and coastline extents respectively.

4.2.3 Test Locations

The locations for the seismic testing at the Greymouth Aerodrome are shown in Figure 4.3 below. The testing consisted of 3 MASW seismic lines completed in September 2013, totalling approximately 1900 metres. Line 1 was a profile running north-eastwards, parallel to the runway. Line 2 was an east-west oriented line

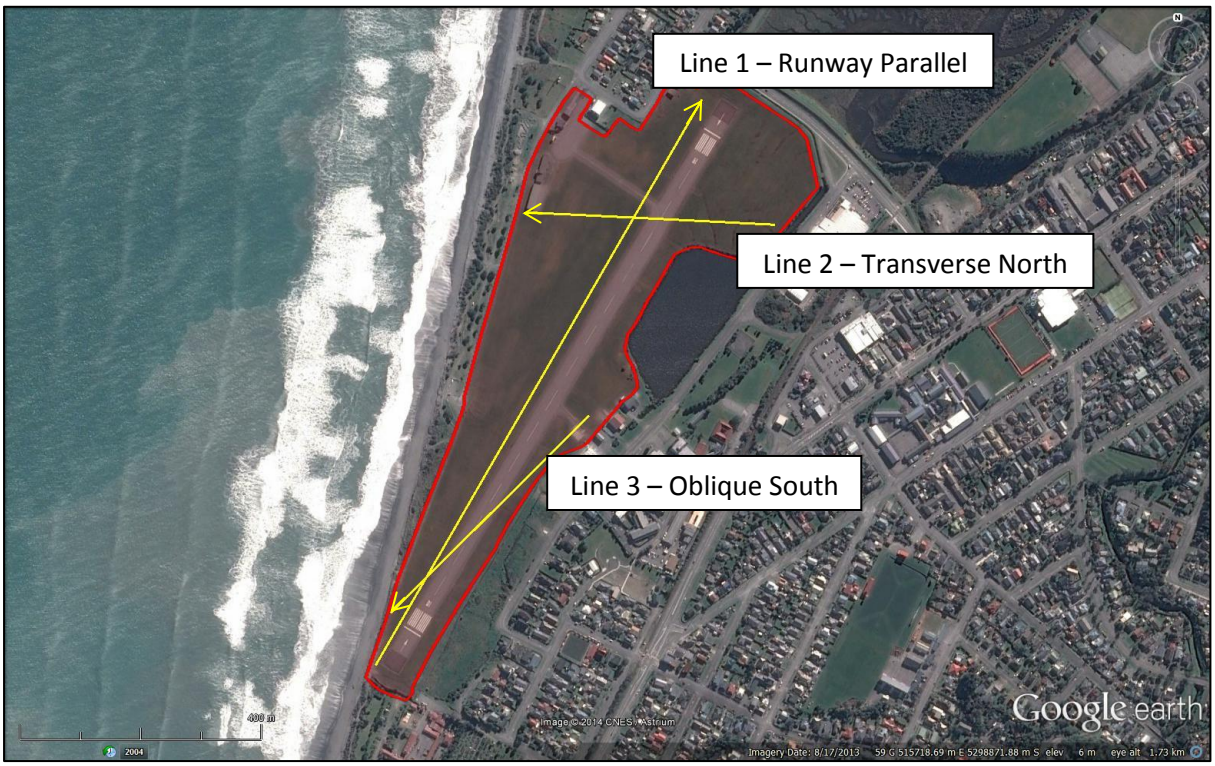

Figure 4.3 - Greymouth Aerodrome MASW Profile Locations

running from the eastern boundary near Lake Karoro, to the western boundary. Line 3 was run south-westwards, starting near the newly constructed St. John's Ambulance building on the eastern boundary to the southwest corner of the site.

4.2.4 Test Results

The initial seismic velocity profiles for Line 1, Line 2 and Line 3 are shown below in Figure 4.4, 4.5 and 4.6, respectively.

Line 1 was the longest line, running parallel to the runway, with the length of the seismic profile being approximately 1090 metres and it reached a depth of 29 metres.

Lines 2 and 3 were smaller lines, extending across the site, intersecting with Line 1. Line 2 had a total length of about 420 metre and reached a depth of 23 metres, while Line 3 was 390 metres long and reached a depth of 20 metres.

The details of the seismic lines are summarised below in Table 4.1.

Table 4.1 - Summary Table of Seismic Line at Greymouth Aerodrome

Line Number	Name	Length	Heading	Depth
Line 1	Runway Parallel	1090m	030° NNE	29m
Line 2	Transverse North	420m	273° W	23m
Line 3	Oblique South	390m	225° SW	20m

Based on the initial results obtained through the testing, the following observations were made:

- The velocities for much of the top 10m on the runway line are less than 250m/s, which is consistent with potentially liquefiable soils (Andrus and Stokoe, 2000). These low velocities extend deeper to approximately 15m depth as we approach the northern end of the profile.
- Velocities of 600m/s were encountered relatively consistently at 25 metres depth in Line 1; with high velocities (>1000m/s) being reached at places along the profile at approximately 26m to 27m depth, though these velocities are not consistent throughout.

- In Line 2, low velocity (≤250m/s) material is observed up to ~23m depth for the eastern extent of the profile; with very low velocities of less than 100m/s being encountered in the top 5m.
- High velocity material (>600m/s) is encountered up to 20m depth on the western end of the survey.
- Line 3 has low velocity material (<250m/s) reaching a depth of 10m, with a small layer of very low velocity (<100m/s) material is initially encountered.
- Velocities of >600m/s are encountered from approximately 15m depth throughout the profile.

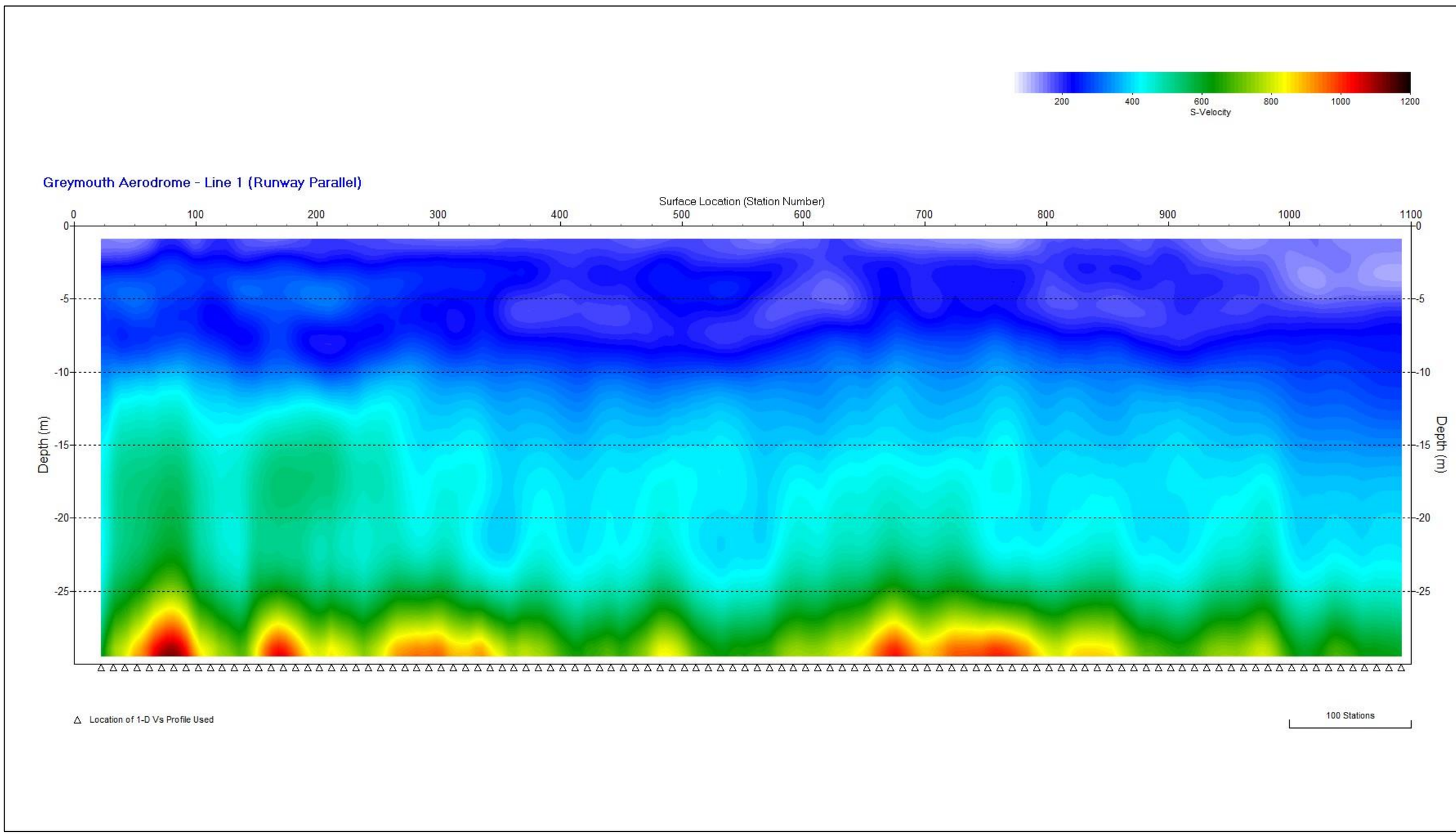

Figure 4.4 - Seismic Velocity Profile for Greymouth Aerodrome Line 1 (Runway Parallel)

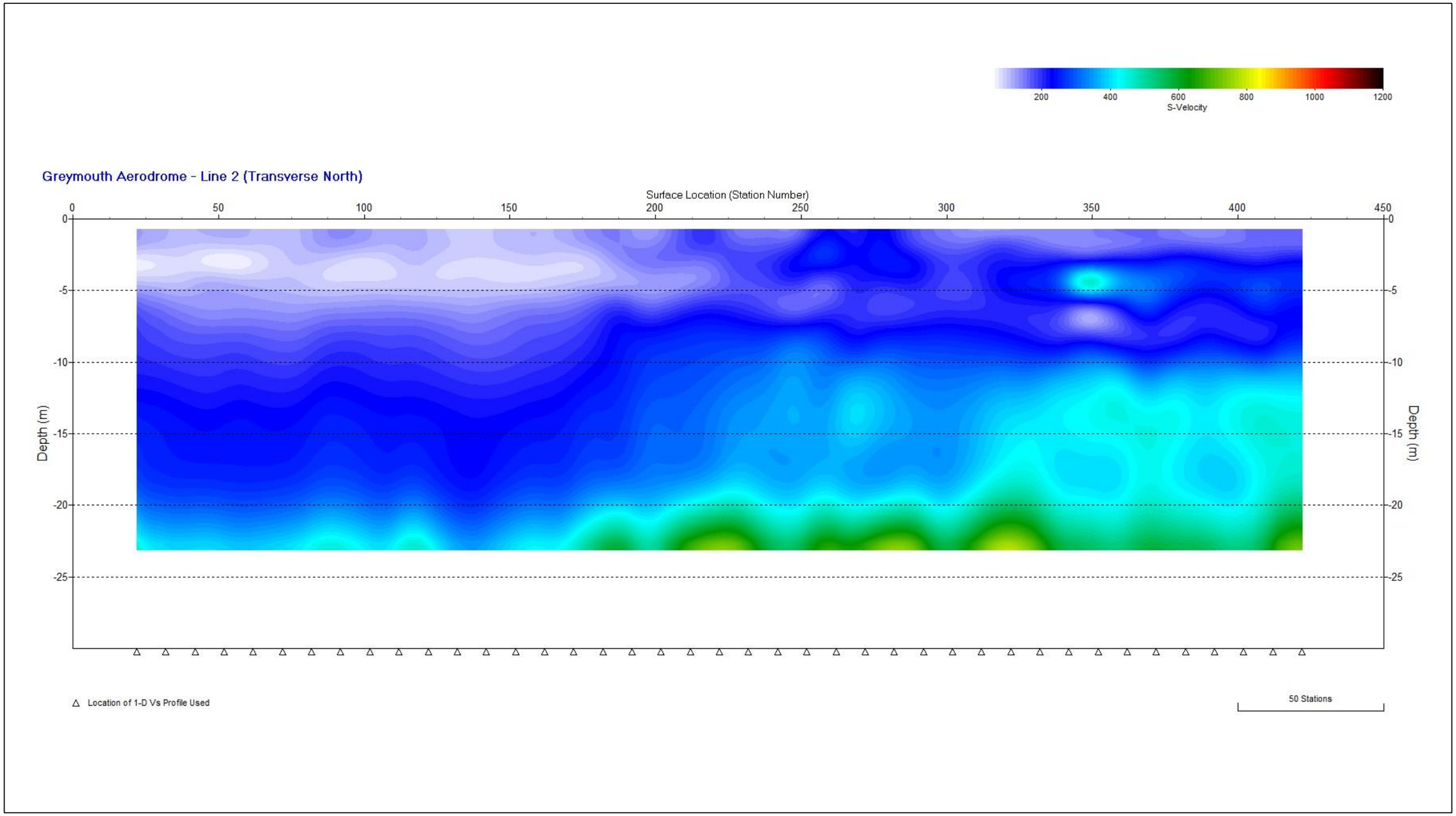

Figure 4.5 - Seismic Velocity Profile for Greymouth Aerodrome Line 2 (Transverse North)

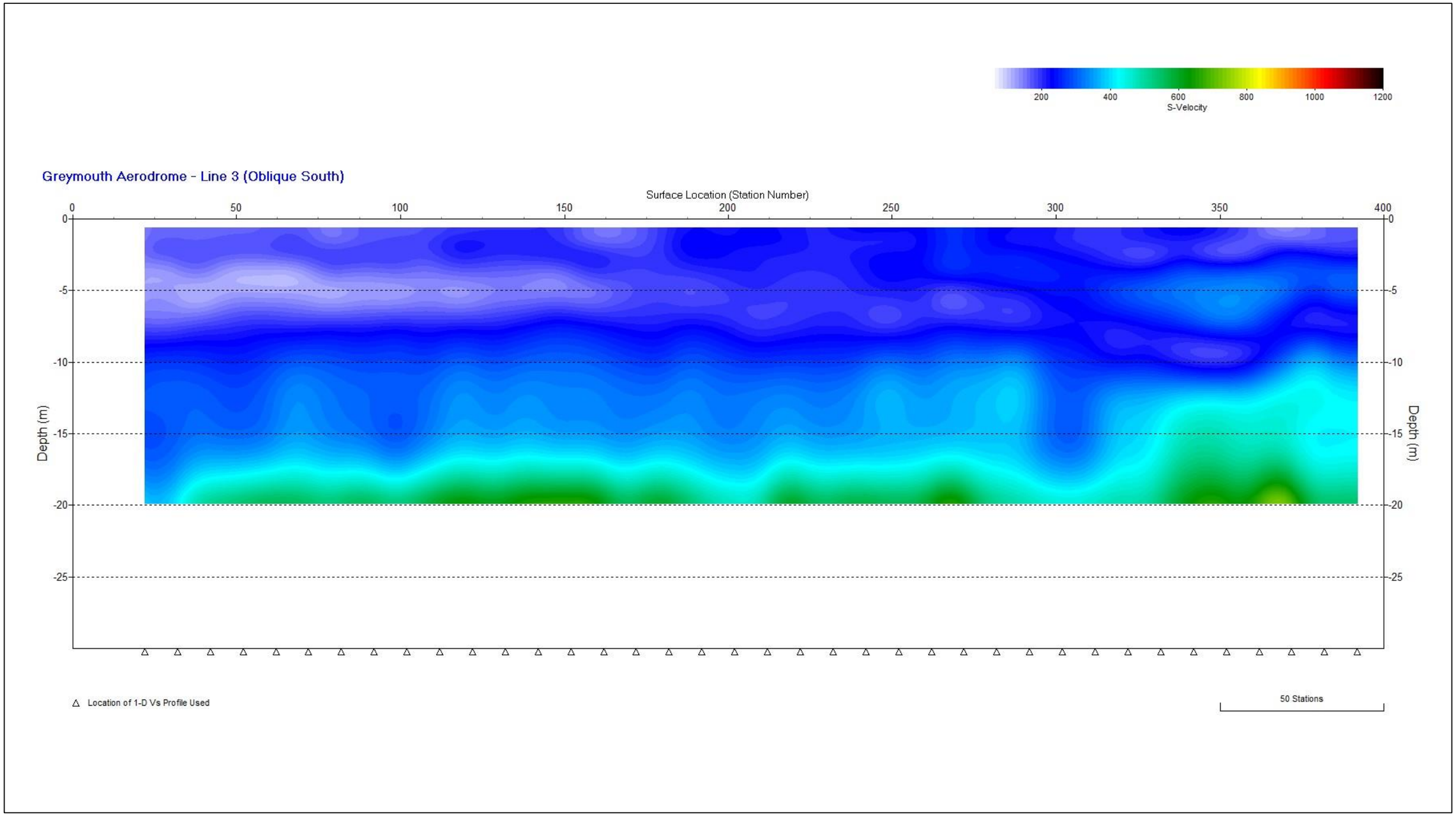

Figure 4.6 - Seismic Velocity Profile for Greymouth Aerodrome Line 3 (Oblique South)

4.3 Victoria Park Racecourse

4.3.1 Site Description

Victoria Park Racecourse is located approximately 550 metres southwest of the town centre, with the southern boundary of the site bounding the estuary. It is a relatively flat site, with a gravel racecourse making up the northeast side of the site. Within the racecourse, there is a grassed area, which is lower than the surrounding ground. Historically there has been a grandstand on the western edge of the track and stables in the southwest section of the site which, at the time of testing, have both been removed.

4.3.2 Site Geomorphology

As seen in Figure 4.7 below, the geomorphology of the Victoria Park Racecourse appears to be relatively flat, a low point within the racetrack itself. There are no distinctive geomorphological features within the site; however there is a remnant channel of the estuary on the western boundary.

It appears that only the estuary has affected the geomorphological evolution of the site. The major change in the geomorphology is the apparent reduction in the size of the estuary channel along the western boundary and another paleochannel along the eastern boundary.

The main channel of the estuary in 1873 formed part of what is now the Victoria Park Racecourse. Based on the available maps for 1873 to 1895 (1873 Historical Drawing; 1895 Historical Drawing), much of the estuary channel between Lake Karoro and Erua Moana becomes confined, with the eastern side of the channel reduced in size to the apparent extent that exists today. On the eastern boundary the estuary appears to have covered an area that appears as a “finger” moving north. There was no information on when this area was reclaimed between 1873 and 1895; however the next map for 1945 shows that size of this part of the estuary is considerably reduced with it now appearing as small stream or inlet.

The next stage of reclamation between 1895 and 1945 (1945 Aerial Photographs) shows that there was minimal land reclaimed on the site in this time, other than the small inlet on the eastern boundary mentioned prior.

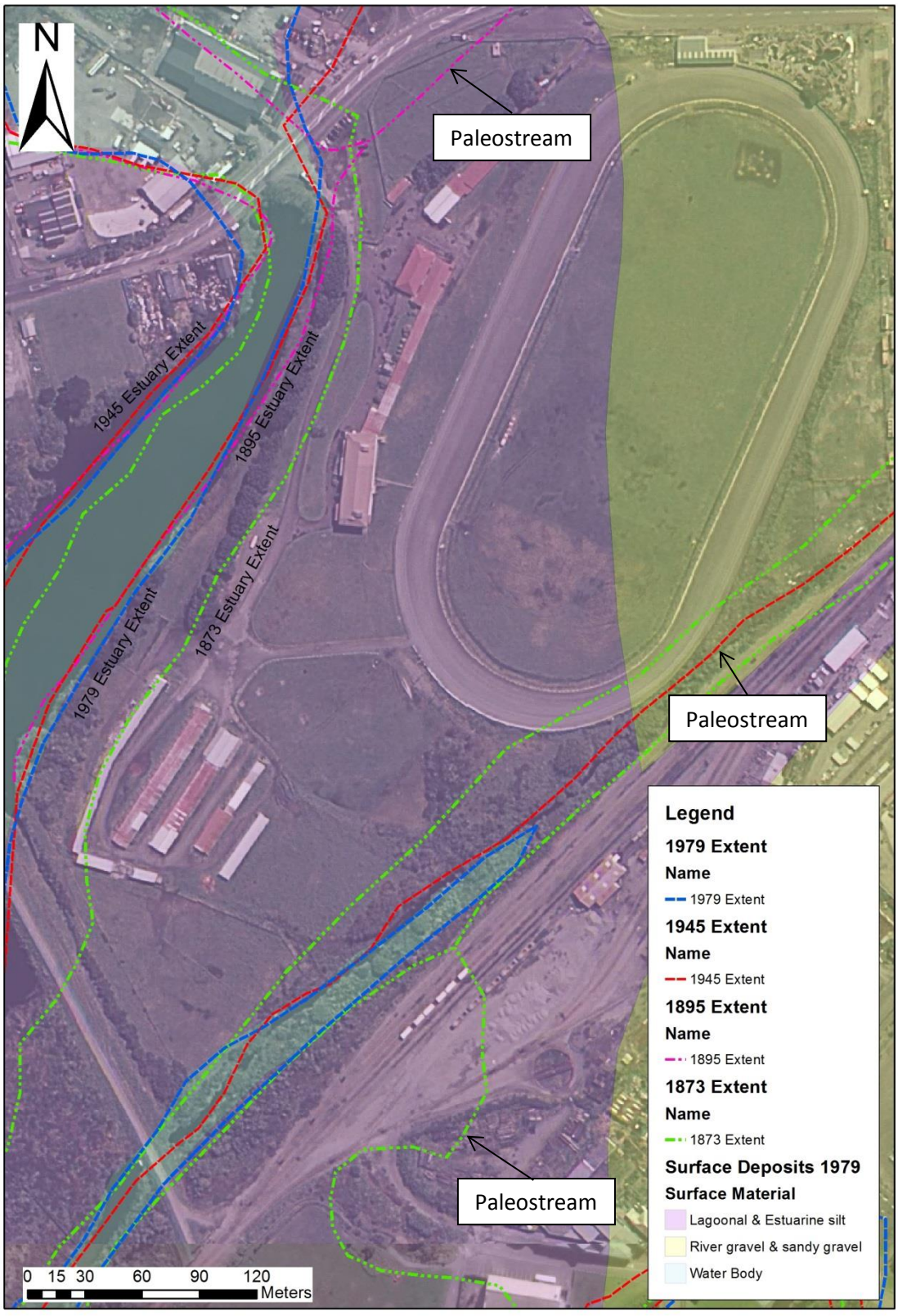

Figure 4.7 - Geomorphology of Victoria Park Racecourse with known historical extents of the estuary shown (Image redrawn based on West Coast Business Unit Historic Drawing, dated 1873; West Coast Business Unit Historic Drawing, dated 1879; Aerial Photographs dated 1945; and Microzoning map of Greymouth, Dowrick et al., 2003)

Between 1945 and 1979 (Dowrick et al. 2003), again there was no discernable change in the area around and within the Victoria Park site, with the estuary channel still observable on the west side of the site and the small inlet on the east side of the site, though the size of the inlet appears to be reduced, through possible reclamation work.

Post-1979 the inlet on the eastern side of the site has been completely reclaimed and is no longer present on the site. The major change has occurred with the historical channel of the estuary connecting Erua Moana and Lake Karoro. It has been reclaimed from the road to Erua Moana, with a new artificial channel being constructed further south. The banks of the new channel also act as flood walls and as a result have cut off the southern end of the channel from the estuary, confining the old channel as a lake-like feature.

The map produced by Dowrick et al. in 2003, based on the geology of Suggate and Wood in 1979, there appear to be two different surficial deposits making up the site. These deposits are described as ‘lagoonal and estuarine silt’ and ‘river gravel and sandy gravel. The lagoonal and estuarine silt material is assumed to be the same material mapped at the Greymouth Aerodrome site described in Section 5.2 and makes up the western side of the site while the river gravel and sandy gravel makes up the eastern part of the site. There also appears to be a thin strip of the silt material extending northeast from the eastern boundary of the silt. This is potentially associated with the historical extent of the apparent inlet.

4.3.3 Test Locations

The locations for the seismic testing completed at the Victoria Park Racecourse as shown in Figure 4.8 below. The testing consisted of a single MASW seismic line, as well as two deep soundings using MASW completed in April 2014.

Line 1 was a MASW seismic profile line that followed the racetrack, starting on the eastern straight, which extended north-northeast before turning left and continuing in a westerly direction toward the estuary. The intention was to align the survey with three boreholes, completed by Opus International Consultants, at the site. The locations of these boreholes are shown in Figure 4.8 and the borehole logs are attached in Appendix E.

Figure 4.8 - Victoria Park Racecourse Test Locations

The deep soundings (also shown in Figure 4.8) were completed with the intention of obtaining the seismic velocity of the material at a depth greater than was achieved with the normal MASW survey. The first sounding (Deep Sounding 1) was completed at the same location that Line 1 started, while the second sounding (Deep Sounding 2) was completed on an old access road to the stables on the southwestern side of the site.

4.3.4 Test Results

The initial seismic velocity (Vs) profile for Line 1 is shown below in Figure 4.9. The individual sounding profiles for Deep Sounding 1 and Deep Sounding 2 are also shown below in Figure 4.10 and 4.11, respectively.

Line 1 extended for approximately 330 metres, from the back straight to near the entrance gate, and reached a deep of about 26 metres.

The deep soundings were unable to reach greater depths, with penetration only obtaining a few metres deeper than the normal seismic test.

Deep Sounding 1 reached a depth of approximately 28 metres, while Deep Sounding 2 reached a depth of approximately 29 metres.

The details are summarised below in Table 4.2 for the seismic profiles and Table 4.3 for the soundings.

Table 4.2 - Summary Table of Seismic Line at Victoria Park Racecourse

Name	Length	Initial Heading	Final Heading	Depth
Line 1	330m	025° NNE	289° WNW	26m

Table 4.3 - Summary Table of Soundings at Victoria Park Racecourse

Name	Array Length	Array Orientation	Depth
Deep Sounding 1	96m	025° NNE	28m
Deep Sounding 2	48m	266° W	29m

Based on the initial results obtained through the testing, the following observations were made:

- A high velocity (500 – 600m/s) material is initially encountered at a depth of approximately 10m in Line 1, though this stops at about 140 metres along the profile.
- Material with a velocity as low as 200m/s is observed to a depth of 25m from 140m along the survey, signifying that this material is potentially liquefiable (Andrus and Stokoe, 2000).
- Thin layers (~1 – 2m thick) are observed within the top 5m, though this is not consistent across the survey.
- Deep Sounding 1 appears to confirm what was found at the start of Line 1, with velocities of ~500m/s observed between 10 and 12.5m, before dropping down below 400m/s to a depth of 22m. A sharp increase to >1100m/s is then observed. Material with a velocity less than 100m/s is confined to the top 2m.
- For Deep Sounding 2 we see a relatively uniform increase in velocity, from ~150m/s at 2m depth, to 500m/s to a depth of about 18m. A maximum velocity of 900m/s was attained at approximately 23m depth.

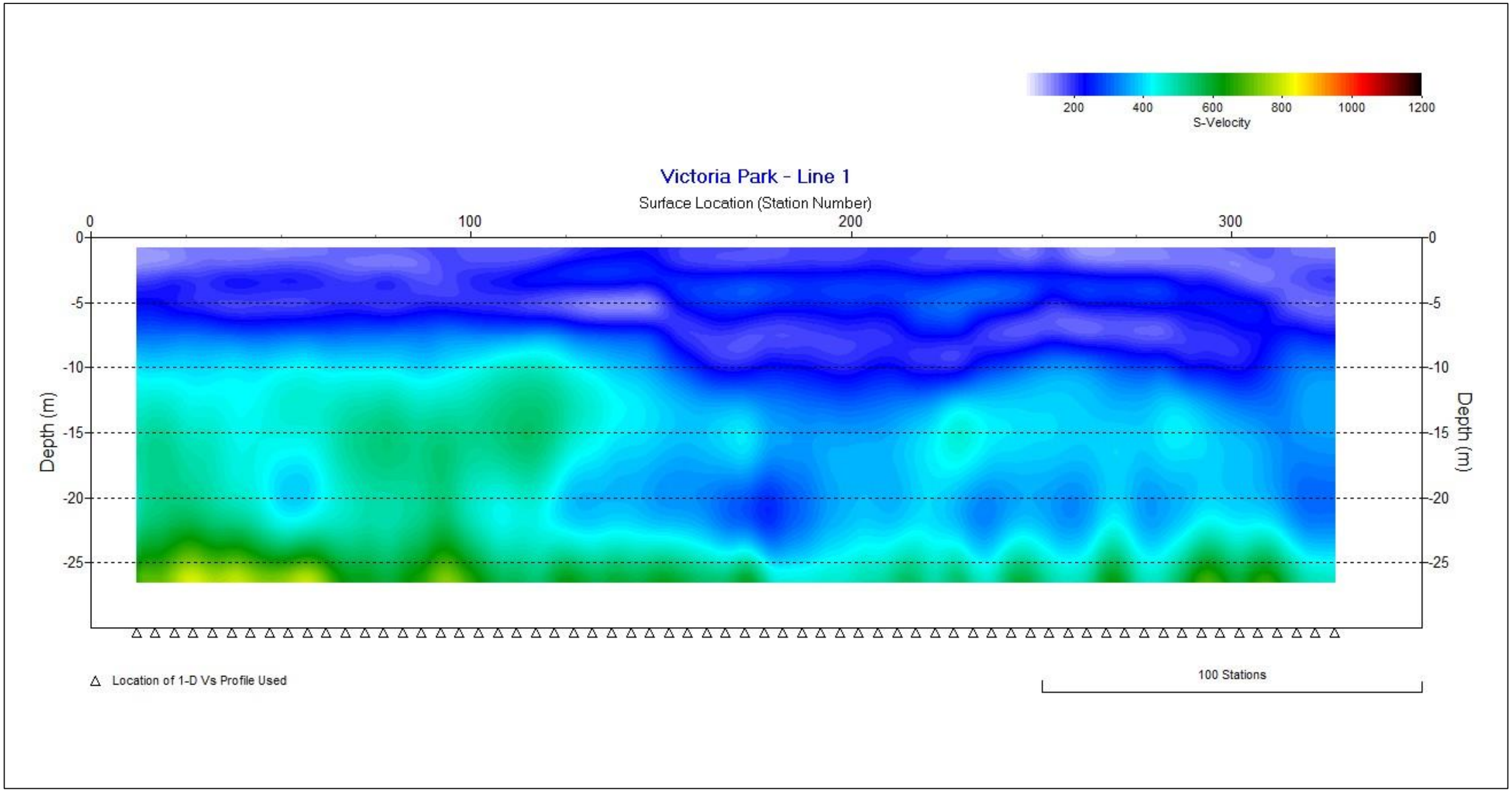

Figure 4.9 - Seismic Velocity Profile for Victoria Park Racecourse Line 1

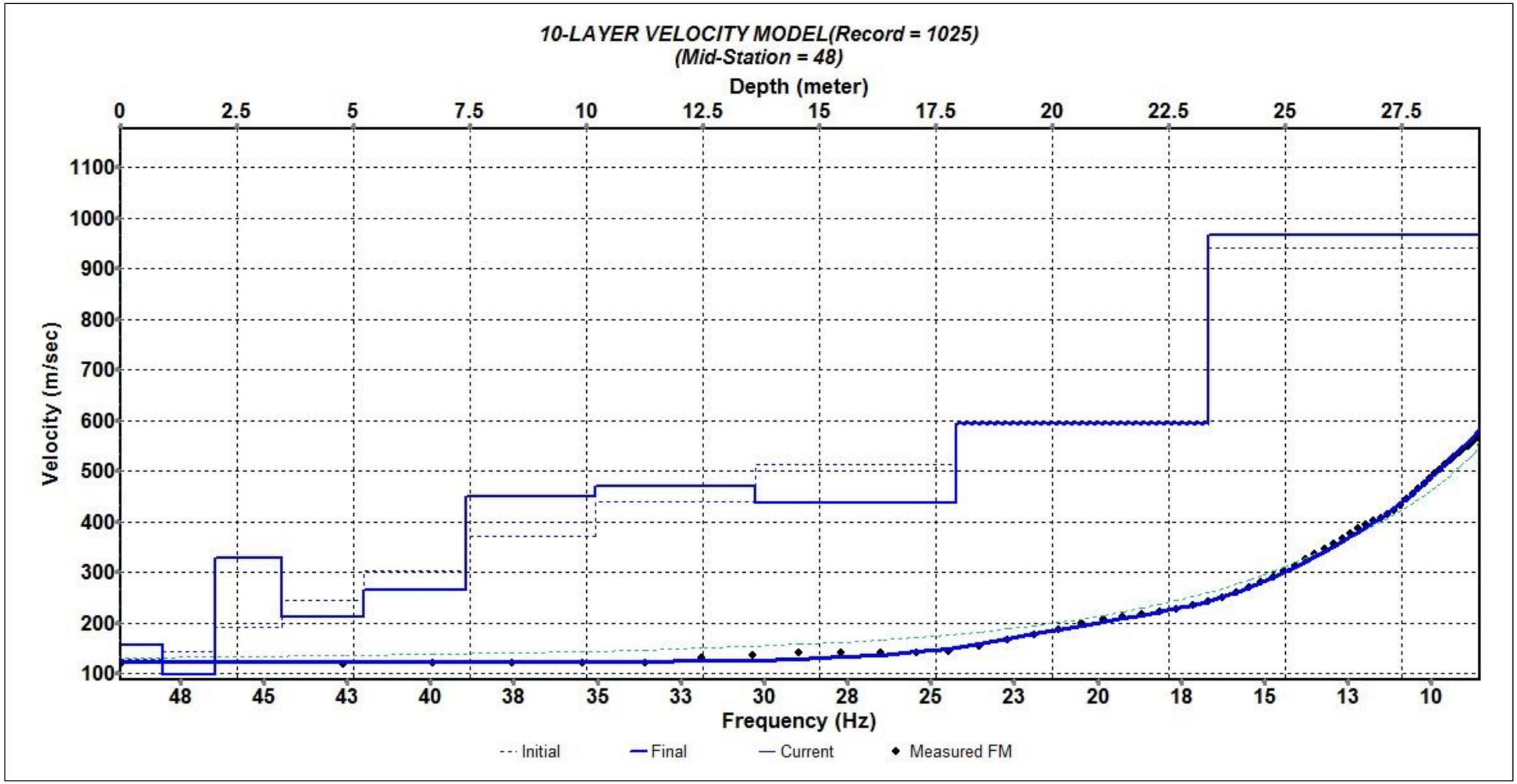

Figure 4.10 - Fixed-Receiver Walkaway Deep Sounding 1 (Eastern Straight of Racecourse Track)

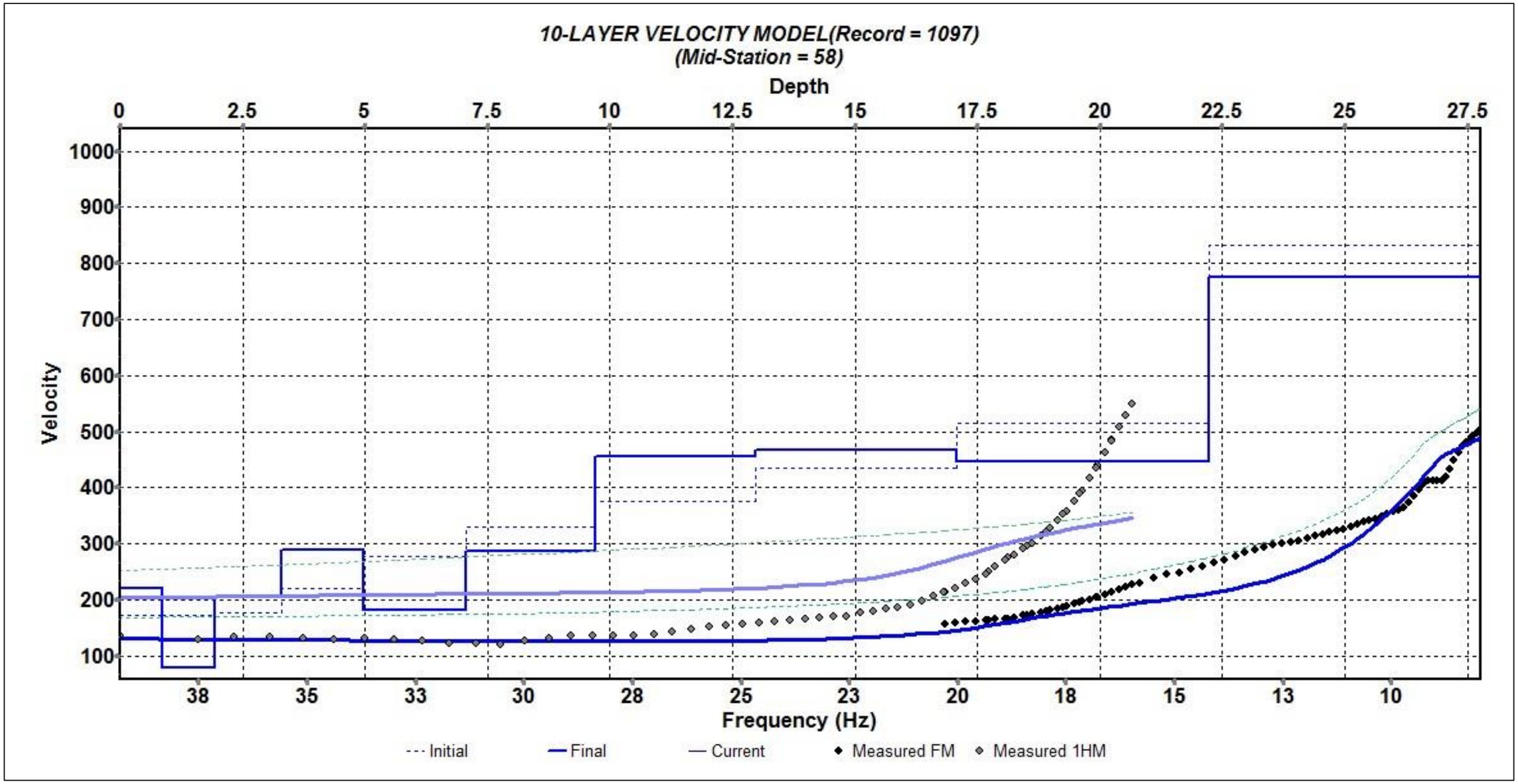

Figure 4.11 - Fixed-Receiver Walkaway Deep Sounding 2 (Southwest corner of Victoria Park site)

4.4 Charles O'Connor Street Truck Park

4.4.1 Site Description

The Truck Stop located on Charles O'Connor Street is located next to the estuary on northern end of the street and it is owned by Aratuna Freighters. It is situated within Greymouth and currently consists of a cleared site with perimeter fencing. No buildings were present at the time of testing though construction has been planned for the near future.

4.4.2 Site Geomorphology

The current geomorphology of the Truck Stop is largely anthropogenic in nature. It consists of a relatively flat lot with gravel shingle making up the surficial material. Historically the area has experienced significant change, largely within the 35 years. The changes can be seen in Figure 4.12.

The major geomorphological change that has occurred over the last 140 years is the reclamation of the historical estuary channel. As seen in Figure 4.12 the channel connecting Erua Moana and Lake Karoro has been situated in the vicinity of the Truck Stop. There has been very little geomorphological change from 1873 to 1979, with only apparent minor migration of the channel, though the general location has not changed during this time.

Post-1979 however, the construction of the floodwall and confinement of the estuary has led to the reclamation of this area with the channel, historically, making up a large portion of the current site.

Based on Dowrick et al. (2003), the surficial material in 1979 was categorised as "lagoonal and estuarine silt", though much of the site was categorised as water due to the old channel.

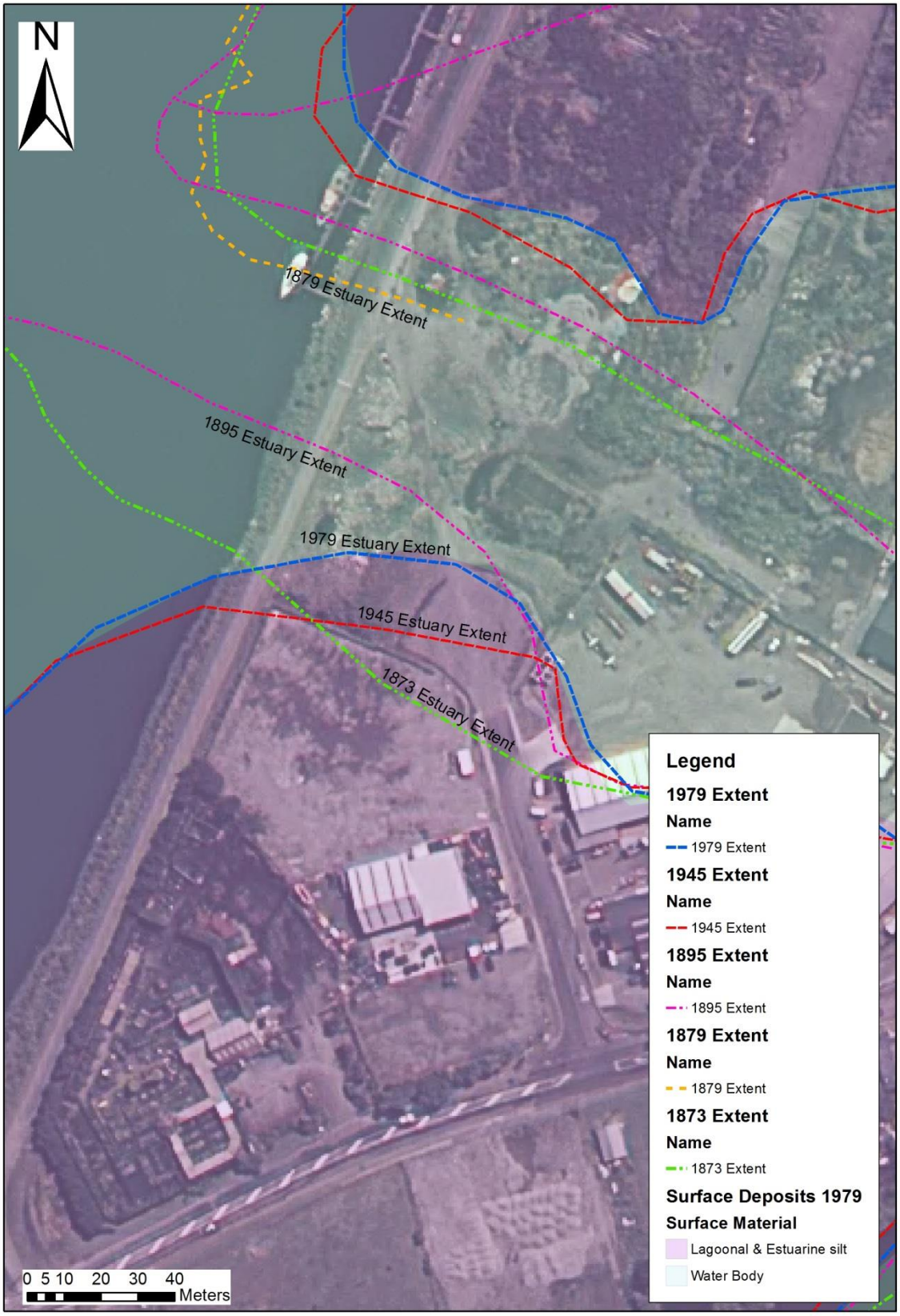

Figure 4.12 - Geomorphology of the Charles O'Connor Street Truck Stop with known historical extents of the estuary shown (Image redrawn based on West Coast Business Unit Historic Drawing, dated 1873; West Coast Business Unit Historic Drawing, dated 1879; West Coast Business Unit Historic Drawing, dated 1895; Aerial Photographs dated 1945; and Microzoning map of Greymouth, Dowrick et al., 2003)

4.4.3 Test Locations

The testing location at the Aratuna Freighters Truck Stop on Charles O'Connor Street is shown below in Figure 4.13. Testing at this site consisted of a single MASW seismic line, with the intention to lineate the historical channel under the reclamation material.

Though the image below shows vegetation on the site, at the time of testing this had been cleared to allow for construction to occur. The single line ran in a northeast direction diagonally across the site.

Figure 4.13 - Charles O'Connor Street Truck Stop Test Locations

4.4.4 Test Results

The initial seismic profile for Line 1 is shown in Figure 4.14. Line 1 was approximately 150 metres in length and reached a depth of nearly 30 metres.

The details of the testing is summarised below in Table 4.4. Again the initial results displayed areas of interest, which will be discussed further in Chapter 6.

Table 4.4 - Summary Table of Seismic Line at Aratuna Freighters Truck Stop on Charles O'Connor Street

Name	Length	Initial Heading	Depth
Line 1	150m	066° ENE	30m

Based on the initial results obtained through the testing, the following observations were made:

- Velocities of <250m/s are encountered up to 25m depth, and based on Andrus and Stokoe (2000) means it is potentially liquefiable.
- The presence of higher velocity (400 – 500m/s) material is observed from approximately 27m depth, and is relatively consistent across the profile.
- A very low velocity layer, of less than 100m/s, extends across the profile at a depth of 5m, though the layer is only ~1m thick.

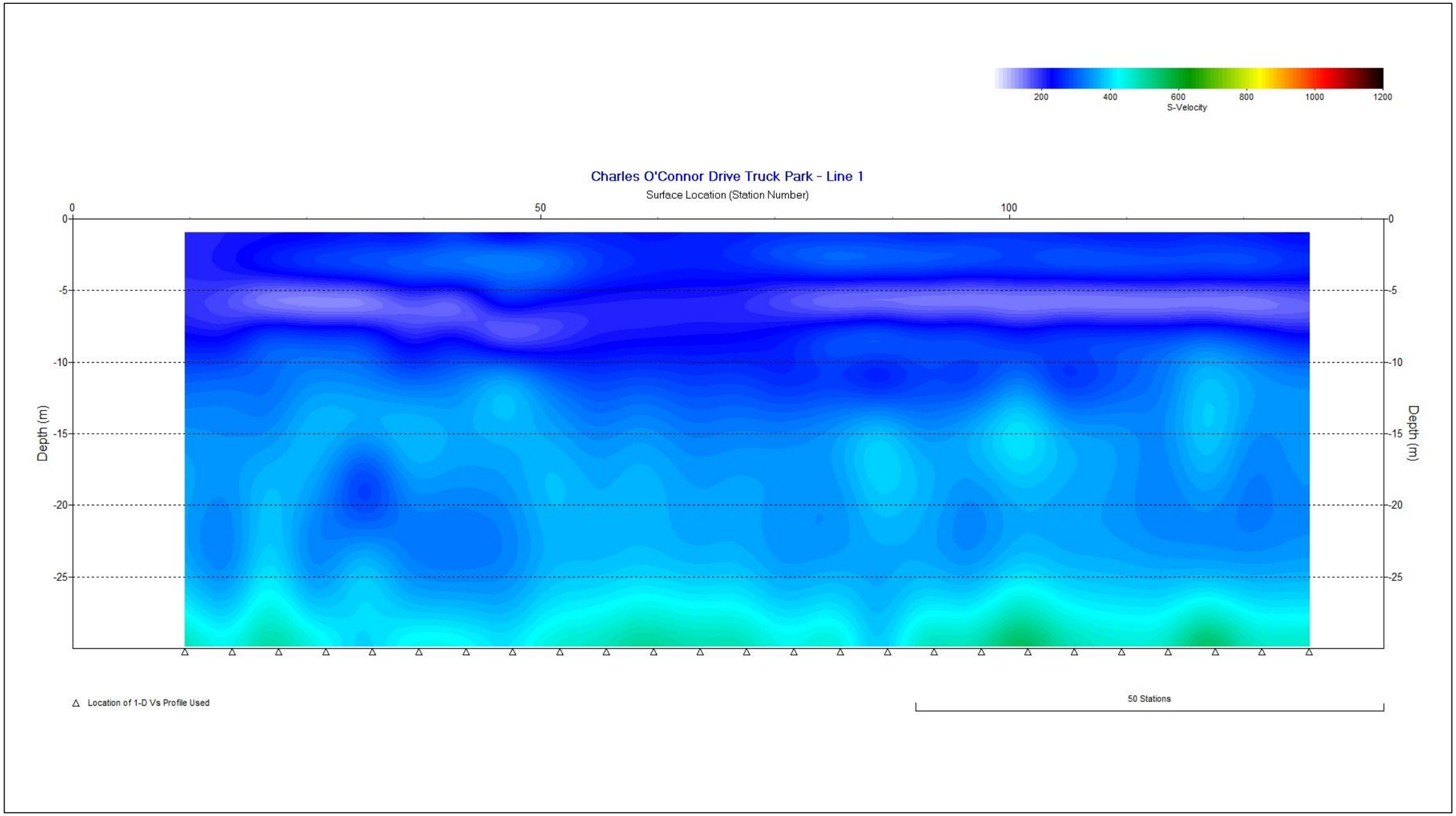

Figure 4.14 - Seismic Velocity Profile for Aratuna Freighters Truck Stop on Charles O'Connor Street

5 Analysis for Susceptibility of Liquefaction

5.1 Introduction

Over the past 35 years, numerous studies have been conducted to investigate the relationship between shear-wave velocity (V_S) and liquefaction resistance. These studies involved field observations (e.g. Andrus and Stokoe, 1997), penetration-V_S correlations (e.g. Seed at al., 1983), analytical investigations (e.g. Stokoe et al., 1988), and laboratory tests (e.g. Tokimatsu and Uchida, 1990). Several of the liquefaction evaluation procedures developed from these studies follow the general format of the Seed-Idriss simplified procedure, where V_s is corrected to a reference overburden stress and correlated with the cyclic stress ratio (Andrus and Stokoe, 2000).

5.2 Procedure for assessment of liquefaction susceptibility

The analysis conducted as part of this study for liquefaction susceptibility follows the guidelines outlined in Andrus and Stokoe (2000), and summarised by Youd and Idriss (2001). This procedure requires the calculation of three parameters: (1) the level of cyclic loading on the soil caused by the earthquake, expressed as a cyclic stress ratio (CSR); (2) stiffness of the soil, expressed as an overburden stress-corrected shear-wave velocity; and (3) resistance of the soil to liquefaction, expressed as a cyclic resistance ratio (CRR).

Following calculation of these parameters, a factor of safety can be determined to predict whether liquefaction will or will not occur during a specific design earthquake.

5.2.1 Cyclic Stress Ratio (CSR)

The cyclic stress ratio at a particular depth in a level soil deposit can be expressed by:

$$CSR = \frac{\tau_{av}}{\sigma'_v} = 0.65 \left(\frac{a_{max}}{g}\right)\left(\frac{\sigma_v}{\sigma'_v}\right) r_d$$

where τ_{av} = average equivalent uniform cyclic shear stress caused by the earthquake and is assumed to 0.65 of the maximum induced stress (Andrus and Stokoe, 2000); a_{max} = peak ground acceleration; g = acceleration of gravity; σ'_V = initial effective vertical overburden stress at the depth in question; σ_V = total vertical overburden stress at the same depth; and r_d = shear stress reduction coefficient to adjust for the flexibility of the soil profile.

The initial effective overburden stress is given by:

$$\sigma'_v = \rho_S g d$$

where ρ_S = the soil density; and d = depth (in metres below ground level [m bgl]).

The total overburden stress is given by Terzaghi's Principle:

$$\sigma_V = \sigma'_V + u$$

where u = the pore-water pressure at a given depth. The pore-water pressure is given:

$$u = \rho_w g h$$

Where ρ_w = density of water; and h = depth below the water table.

The values for r_d are estimated from the chart by Seed and Idriss (1971) shown in Figure 5.1. The values used for the analysis are shown in the spreadsheets in Appendix E. This coefficient, as stated above, accounts for flexibility in the soil profile (Youd and Idriss, 2001), while Idriss and Boulanger (2014) describe the parameter as the ratio of cyclic stresses for a flexible soil column to the cyclic stresses for a rigid soil column. Seed and Idriss (1971) determined the average curve analytically using a variety of earthquake motions and soil conditions. Idriss (1999) proposed revised average r_d values based on the analytical work by Golesorkhi (1989). Unlike the original values, these revised r_d values are magnitude-dependent and reflect the differing CSR caused by different magnitude earthquakes.

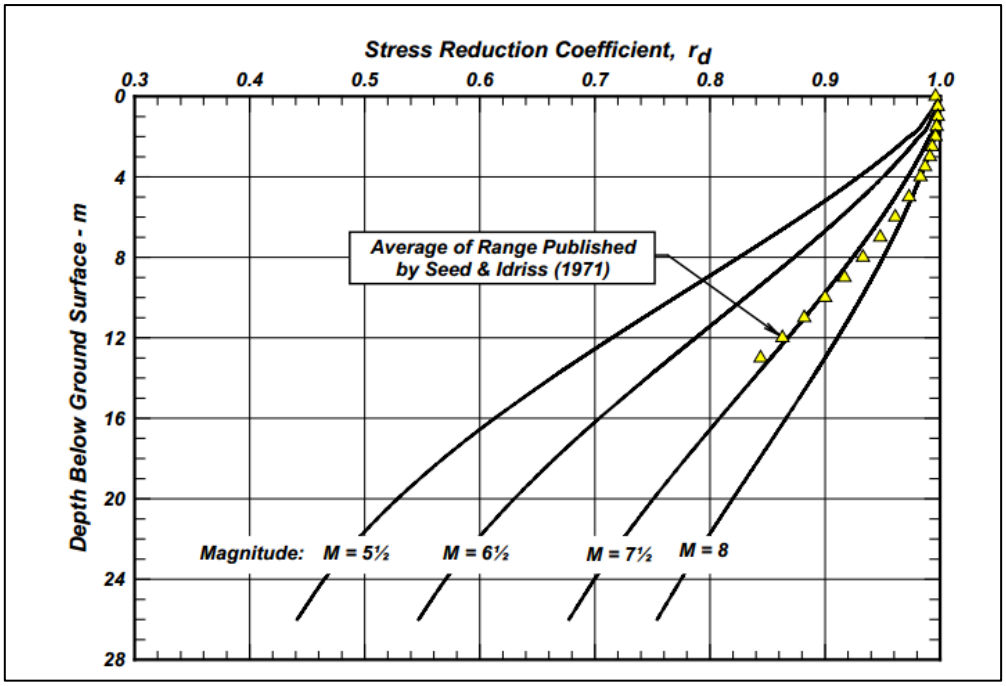

Figure 5.1 - Variations of stress reduction coefficient (r_d) with depth and earthquake magnitude (Idriss and Boulanger, 2014)

5.2.2 Overburden Stress-Corrected Shear-Wave Velocity

Shear-wave velocities can be measured in situ by several seismic tests, including cross hole, downhole, seismic cone penetrometer, suspension logger, and surface wave inversion (i.e. SASW and MASW). Following the traditional procedures for correcting Standard Penetration Test (SPT) blow count and Cone Penetration Test (CPT) tip resistance to account for overburden stress, V_S can also be corrected to a reference overburden stress by the expression (Andrus and Stokoe, 2000):

$$V_{s1} = V_S C_V = V_S \left(\frac{P_a}{\sigma'_V}\right)^{0.25}$$

where V_{S1} = overburden stress-corrected shear-wave velocity at a given depth; C_V = factor to correct measured shear-wave velocity for overburden pressure; P_a = reference stress of 100 kPa or about atmospheric pressure; and σ'_V = initial effective vertical overburden stress at the depth in question. A maximum C_V value of 1.4 is generally applied to V_s data at shallow depths. By applying this formula it is assumed that the initial effective horizontal stress is a constant factor of the effective overburden stress. It is assumed that V_S is measured with both particle motion and

wave propagation polarized along principal stress directions, and that one of those directions is vertical (Stokoe et al., 1985; Andrus and Stokoe, 2000; Youd and Idriss, 2001).

5.2.3 Cyclic Resistance Ratio (CRR)

The value of CSR separating liquefaction and non-liquefaction occurrences for a given V_{S1} is called the cyclic resistance ratio (CRR). Figure 5.2 compares seven CRR-V_{S1} curves. These curves were determined through various laboratory (Tokimatsu and Uchida, 1990) and field performance data from various sites in California (Kayen et al., 1992; Robertson et al., 1992; Lodge, 1994). Andrus and Stokoe (1997) developed their curve based on uncemented, Holocene-aged (<10,000 year old) soils with 5% or less fines using field performance data from 20 earthquakes and over 50 measurements sites. Andrus and Stokoe (2000) revised this curve based on new information and an expanded database that includes 26 earthquakes and more than 70 measurement sites (Youd and Idriss, 2001).

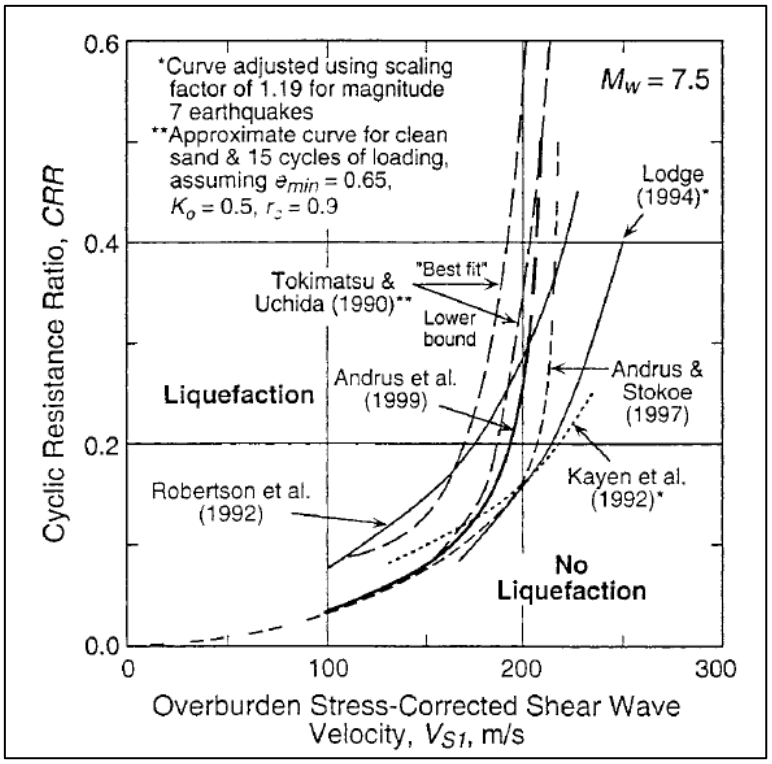

Figure 5.2 - Comparison of seven relationships between liquefaction resistance (CRR) and overburden stress-corrected shear wave velocity for granular soils (Andrus and Stokoe, 2000; Youd and Idriss, 2001)

Andrus and Stokoe (1997) proposed the following relationship between CRR and V_{S1}:

$$CRR = a\left(\frac{V_{S1}}{100}\right)^2 + b\left(\frac{1}{V_{S1}^* - V_{S1}} - \frac{1}{V_{S1}^*}\right)$$

where V_{S1}* = limiting upper value of V_{S1} for liquefaction occurrence; and *a* and *b* are curve fitting parameters. The assumption of a limiting upper value of V_{S1} is equivalent to the assumption commonly made in CPT- and SPT-based procedures dealing with clean sands, where liquefaction is considered not possible above a corrected tip resistance of about 160 and a corrected blow count of about 30 blows per 300mm for CPT and SPT respectively (Andrus and Stokoe, 2000; Youd and Idriss, 2001). Dobry (1989) explains that in dense soils settlement is insignificant and no sand boils or failure take place because of small amounts of water being expelled. This is important because the definition of liquefaction used to classify the field behaviour, as well as the penetration-based procedures, is based on surface manifestations (Andrus and Stokoe, 2000).

CRR-V_{S1} curves recommended for engineering practice by Andrus and Stokoe (2000) for magnitude 7.5 earthquakes and uncemented Holocene-age soils with various fines contents (≤5% fines, 20% fines, and ≥35% fines), are shown in Figure 5.3. Also plotted on this figure are points calculated from liquefaction case history information from magnitude 5.9 – 8.3 earthquakes. The three curves shown were determined through an iterative process of varying values of *a* and *b* until nearly all points indicative of liquefaction were bounded by the curves with the least number of non-liquefaction points plotted in the liquefaction region.

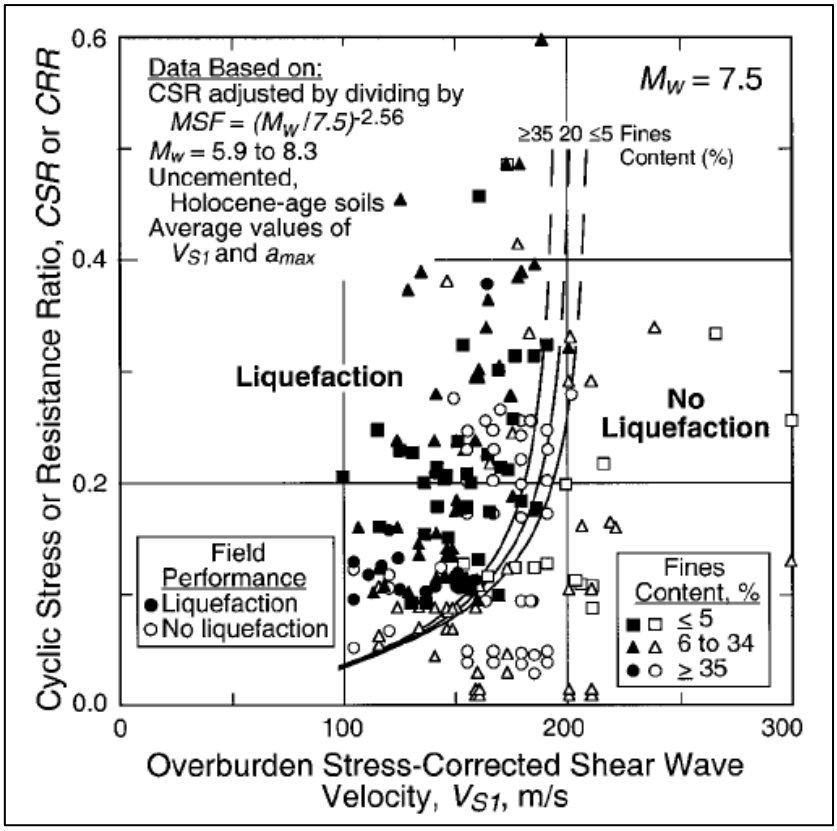

Figure 5.3 - Liquefaction Relationship (CRR-V_{S1}) curves recommended for clean, uncemented soils from liquefaction case histories (Andrus and Stokoe, 2000; Youd and Idriss, 2001)

The final values of *a* and *b* used to create these curves were 0.022 and 2.8, respectively. Values for V_{S1}* were assumed to vary linearly from 200m/s for soils with fines contents greater than or equal to 35%, to 215m/s for soils with fines contents of 5% or less.

The equation for CRR provided above can be scaled for other magnitude values, it was based on a magnitude 7.5 event. The magnitude scaling factor (MSF) is traditionally applied to CRR rather than CSR, and equals 1.0 for earthquakes with a magnitude of 7.5, while other magnitudes can be represented by (Youd et al., 1997; Youd and Idriss, 2001):

$$MSF = \left(\frac{M_W}{7.5}\right)^n$$

where M_W = moment magnitude; and n = exponent. Moment magnitude is the scale most commonly used for engineering applications and is preferred for liquefaction

resistance calculations. The lower bound for MSF recommended by Youd et al. (1997) is defined as n = -2.56; while the upper bound of the recommended range is defined as n = -3.3 (Andrus and Stokoe, 1997) for earthquakes with magnitudes ≤7.5 (Andrus and Stokoe, 2000).

By applying these values listed above, the equation for CRR can be rewritten as follows:

$$CRR = \left\{0.022\left(\frac{K_C V_{S1}}{100}\right)^2 + 0.28\left(\frac{1}{V_{S1}^* - K_C V_{S1}} - \frac{1}{V_{S1}^*}\right)\right\} MSF$$

where K_C = correction factor for high values of V_{S1} caused by cementation and aging of the soil profile. Average estimates of K_C for Pleistocene-age (10 to 2600 kya) soils range from 0.6 to 0.8 based on penetration-V_{S1} correlations (Andrus and Stokoe, 2000).

5.2.4 Factor of Safety (FoS)

A common way to quantify the potential for liquefaction is in terms of factor of safety. The factor of safety against liquefaction can be determined by (Andrus and Stokoe, 2000):

$$FoS = \frac{CRR}{CSR}$$

Liquefaction is predicted to occur when FoS ≤ 1, and liquefaction is predicted not to occur when FoS > 1. The acceptable value of FS will depend on several factors, including the acceptable level of risk for the project, potential for ground deformation including lateral spreading, extent and accuracy of seismic measurements, availability of other site information, and conservatism in determining the design earthquake magnitude and expected value of a_{max} (Andrus and Stokoe, 2000; Youd and Idriss, 2001).

5.3 Stress-Corrected Shear-Wave Velocity Profiles for Greymouth

The following section outlines the parameters used as part of the analysis for the study completed in Greymouth with the outputs for both overburden stress-corrected

shear-wave velocity, and the factor of safety profiles for the tested areas provided in Section 5.3.2 and 5.3.3, respectively. The analysis follows that which is outlined by Andrus and Stokoe (2000), as described above.

5.3.1 Parameters used in this study

The parameters used for the analysis are summarised below in Tables 5.1 and 5.2. All calculations were completed on spreadsheets, and are provided in Appendix E.

Three different design earthquake events were completed as part of the analysis for this study: a magnitude 8 Alpine Fault earthquake (based on McCahon et al., 2007); a localised M_w5.5 earthquake, with accelerations similar to that experienced during the 1991 Hawks Crag earthquake (Dowrick and Sritharan, 1993); and a localised M_w6.5 earthquake with accelerations similar to that experienced following the February 2011 Christchurch earthquake (Bradley and Hughes, 2012a; 2012b).

Table 5.1 - Summary Table of Design Earthquake Parameters used in this study

Event Name	Moment Magnitude (M_w)	PGA* expected in Greymouth (m/s^2)	Magnitude Scaling Factor (MSF)
Alpine Fault Event	8.0	0.3	0.848
Localised M_w5.5 Event	5.5	0.2	2.212
Localised M_w6.5 Event	6.5	0.45	1.442

** Peak Ground Accelerations*

Table 5.2 - Summary Table of all constant values used in the analysis as part of this study

Parameter	Soil Density (ρ_s) (t/m^3)	Upper Limit of V^*_{S1} (m/s)	Correction factor for cementation and aging (K_c)	Water Table (m below ground level	Shear Stress Reduction Factor (R_d)
Value	1.8	215***	0.6	1.0	Dependent on depth**

** *Based on Figure 5.1*

*** *Conservative value (i.e. maximum)*

Due to a lack of subsurface data through CPT and SPT-based approaches, the factors stated in Table 5.2 are hypothetical. The values for K_c and V^*_{S1} are based on values outlined by Andrus and Stokoe (2000). The value for the limiting upper value for overburden stress-corrected shear wave velocity is defined by the fines content of the soil. Due to no particle size distribution tests being conducted (as a result of no soil samples) this was set to the most conservative value (i.e. 215m/s). The correction for the age and cementation of the soil (K_c) is generally based on penetration data and known information on the age of deposition of the material. Andrus and Stokoe (2000) state that K_c equals one if the soil to be evaluated is uncemented and <10000 years old. The surficial material can be assumed to be younger than this in Greymouth, though as Andrus and Stokoe (2000) outline; if penetration data is not available, a value of 0.6 can be assumed for K_c. The soil density used was conservative and based on geologically young gravel with an approximate density of 1.8t/m^3 (David Bell, per comm., 2014). A water table depth of 1m bgl was assumed due to the general low-lying elevation in respect to nearby water features (i.e. Lake Karoro and Erua Moana Lagoon).

5.3.2 Overburden stress-corrected Shear Wave Velocity

The overburden stress-corrected shear-wave velocity profiles for the Greymouth Aerodrome, Victoria Park Racecourse and Charles O'Connor Street are shown below in Figures 5.4, 5.5 and 5.6, respectively. The overburden stress-corrected

profiles strongly outlined areas of soft or loose (soft refers to cohesive material and loose refers to granular material (NZGS, 2005)) sediment. The clear definition of soft or loose sediments provides an initial estimate for locations for potential future penetration-based testing (CPT or SPT). The upper boundary defined in Andrus and Stokoe (2000) for liquefaction to occur in gravelly soil is proposed as 215m/s for the stress-corrected shear-wave velocity. This boundary is shown as the sharp change from blue to green on the profiles. Several of the profiles show areas of overburden stress-corrected shear-wave velocities less than 215m/s.

AT the Greymouth Aerodrome site, the most notable area is observed within Line 2 (Figure 5.4). Low velocity (V_S < 215m/s) areas as deep as 25 metres have been interpreted based on the analysis, however this is limited to approximately the first 200 metres of the profile length. It appears based on the analysis that the eastern boundary of the Aerodrome site has low velocity material as Line 3 also displays low velocity material down to 10 metres depth. Both of these lines display an increase on velocity at shallow depths as the lines approach the western side of the site. Line 1 displayed a reduction in corrected shear-wave velocity at the northern extent of the Aerodrome, as it approached the current estuary. Localised “soft” spots (areas that do not reach more than 5 metres depth) are present throughout these profiles though they are not continuous across the site.

At Victoria Park Racecourse, much the same is observed based on the profile (Figure 5.5). Generally, the material displays a corrected shear-wave velocity greater than 215m/s, with localised “soft” spots in the upper 2 – 3 metres below the surface. There is a distinct low velocity layer at depths between ~7 – 10 metres for the last 170 metres of the profile however. This is likely due to the effect of the change in the direction of the array as it went from running parallel to running perpendicularly towards the historic estuary channel, with the last 40 metres of the profile showing this low velocity layer becoming thicker and extending to the surface.

The truck depot situated on Charles O’Connor Street clearly displays a continuous low velocity layer from ~5 – 10 metres depth across the array profile (Figure 5.6). This likely reflects the historical estuary channel with the fill material emplaced above it, showing higher velocities. This highlighted the possibility for fill land to fail during

earthquake event, where low velocity material below the fill can fail, resulting in failure of the overlying material (as was seen during the 1995 Kobe Earthquake [Soga, 1998]).

Based on Figure 5.3, the relationship between liquefaction susceptibility and CSR/CRR is outlined graphically based on case history data. This relationship signifies that as CSR or CRR increase, the upper limit for liquefaction occurring with regard to stress-corrected shear-wave velocity also increases exponentially. Applying this as an initial estimate to whether liquefaction will occur, it was interpreted that the areas displayed in blue colouration for the overburden stress-corrected shear-wave velocity profiles in Chapter 5 that liquefaction is possible, though this would be heavily dependent on the CRR/CSR obtained through the analysis, and analysis for the factor of safety (FoS) would state the potential for liquefaction to occur, as outlined below in Chapter 5.3.3.

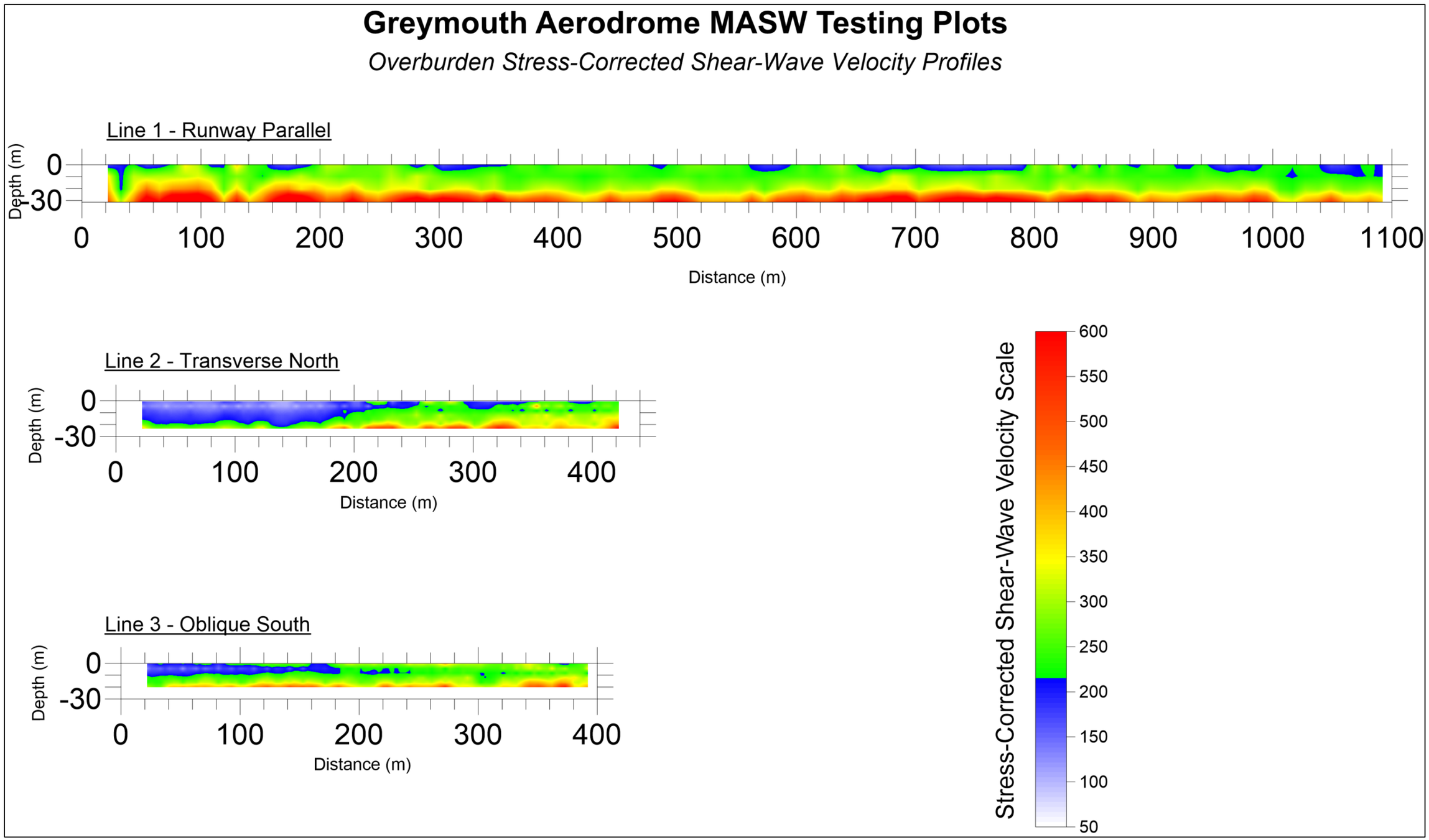

Figure 5.4 - Overburden Stress-Corrected Shear Wave Velocity Profiles for the testing based at the Greymouth Aerodrome

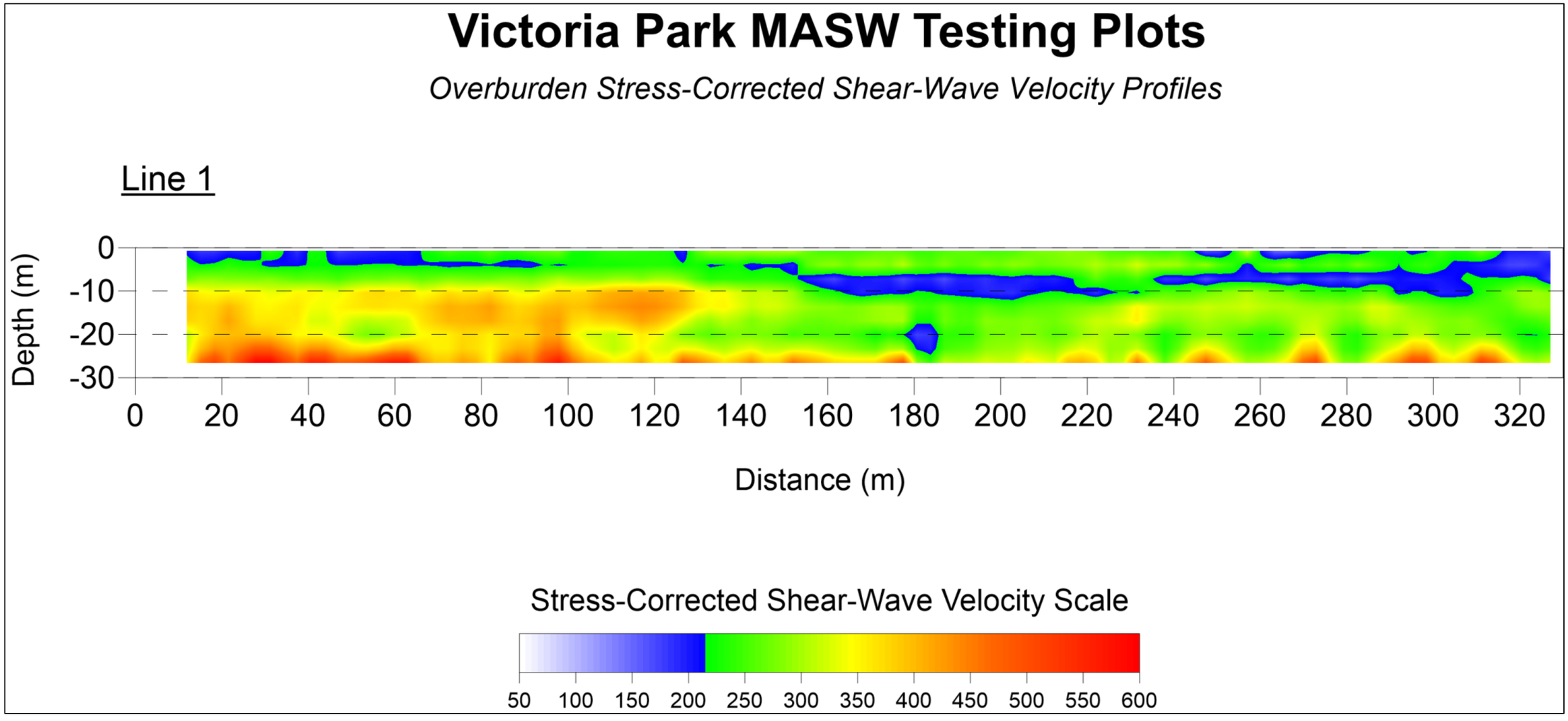

Figure 5.5 - Overburden Stress-Corrected Shear Wave Velocity Profile for the testing based at Victoria Park Racecourse

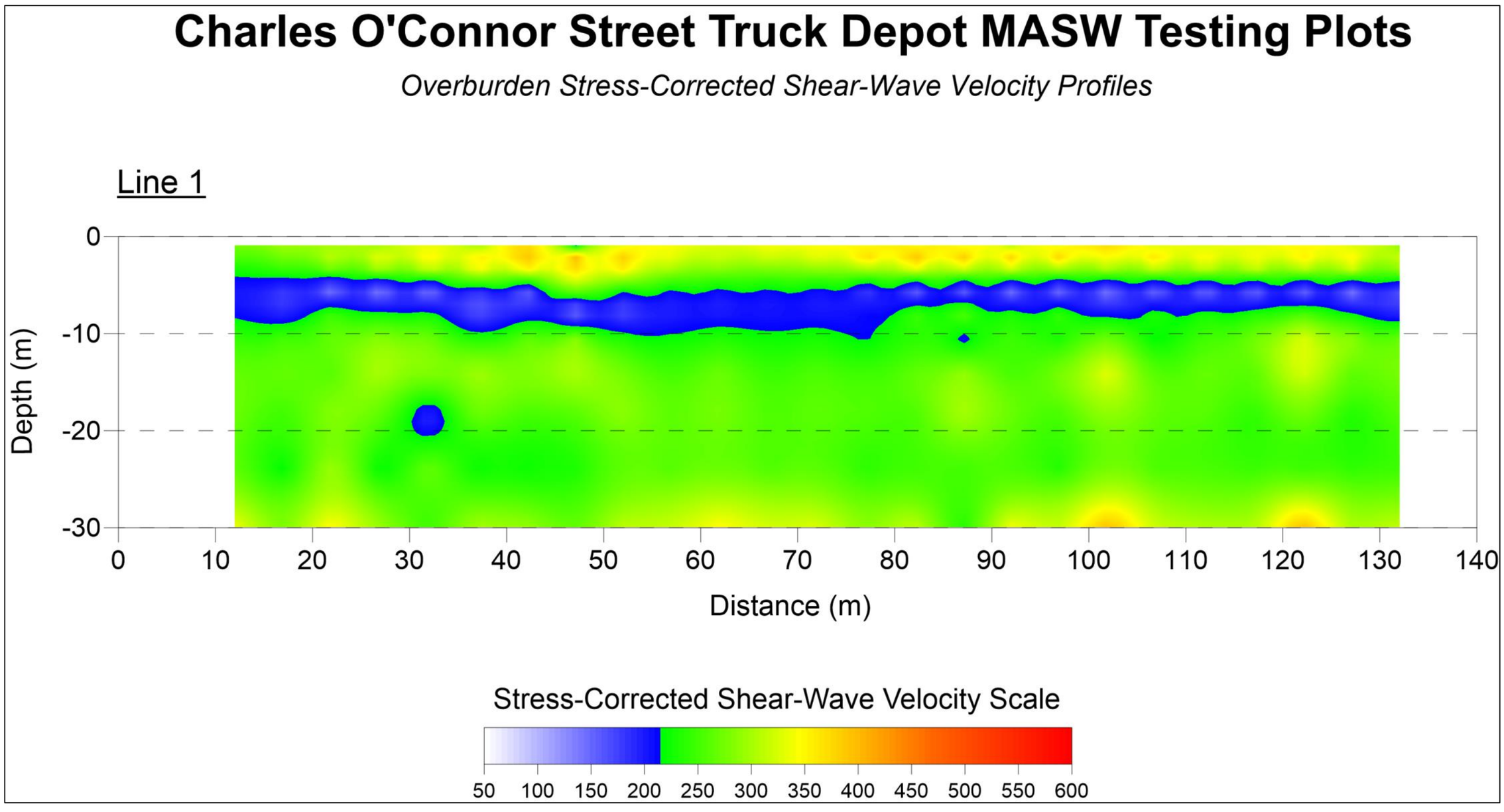

Figure 5.6 - Overburden Stress-Corrected Shear Wave Velocity Profiles for the testing based at the Truck Depot on Charles O'Connor Street

5.3.3 Factor of Safety

The profiles for Factor of Safety are shown below. Figures 5.7, 5.8 and 5.9 are based on the Greymouth Aerodrome for earthquakes of Mw 8.0, 6.5 and 5.5, respectively. Figure 5.10 shows the factor of safety for these events based on the Victoria Park profile, while Figure 5.11 shows the factor of safety for the 3 design earthquakes based on the work done at the Charles O'Connor Street Truck depot.

The analysis for CRR and CSR, with regard to the particular overburden stress-corrected velocities, provides a factor of safety profile, indicating the resistance of the soil to liquefy in the given design earthquake scenarios and parameters defined in Tables 5.1 and 5.2. As above, the clear contrast between blue (FoS≤1) and green (FoS>1) was used to define the boundary between possible liquefiable and non-liquefiable soils, respectively.

The profiles for the M_w8.0 Alpine Fault and M_w6.5 localised earthquake for the test lines based at the Greymouth Aerodrome are very similar (Figures 5.7 and 5.8). The area identified at the start of Line 2 which could be susceptible is very distinct again in the factor of safety profiles. Based on the analysis it is inferred that the top 10 metres of the north-eastern part of the site is potentially highly susceptible to liquefaction following an Alpine Fault or localised event similar to that which was experienced in Christchurch on February 22 2011. Localised areas at the surface also indicate liquefaction is possible though this would be dependent on what depth the water table is at the time of the event. The influence of the water table is discussed later in this chapter. The area of interest within Line 3, described in Section 6.2.1, indicates that liquefaction is unlikely to occur for both these events. It should be noted however, that the values appear to be close to the boundary between liquefaction and non-liquefaction values, meaning this designation could change with better constraint of the constants used in the analysis, such as fines content for individual layers. The M_w5.5 localised earthquake event (Figure 5.9) does not appear to indicate any potential liquefaction susceptibility in any of the test lines completed at the Aerodrome. Though, like was mentioned above, the area of possible liquefaction at the start of Line 2 following the larger events, this area appear to show values close to the boundary between potential liquefaction and non-

liquefaction. Further testing here would allow better constraint of the parameters used in the analysis, thus giving a more accurate prediction.

The factor of safety analysis carried out on the line at Victoria Park Racecourse indicates a similar pattern to that of the Aerodrome analysis. The Alpine Fault design earthquake and localised M_w6.5 design earthquake provide very similar profiles. The analysis completed indicates that liquefaction is unlikely to occur following these events however. The layer of low velocity material indicated in the stress-corrected velocity profiles is prevalent in the factor of safety profiles also. This layer, though considered non-liquefiable, has values represented that are again close to the boundary between liquefaction occurring and not occurring. As stated above with regard to Line 2 and 3 at the Aerodrome, sampling and penetration-based testing should allow better constraint of the parameters used in the analysis. Also similar to the Aerodrome analysis, the M_w5.5 local event does not appear to induce liquefaction due to all values having a factor of safety greater than 1. The values obtained for this event are much higher than the boundary so liquefaction can be interpreted to not occur at this site following an event similar to the design earthquake used in this analysis.

The Charles O'Connor Street Truck Stop mirrors the other two sites tested, in particular the Victoria Park site. The larger events (i.e. the Alpine Fault and local M_w6.5 events) show the soil here to be non-liquefiable, though the low velocity layer represented in the stress-corrected velocity profile is distinct. Again these values obtained are close to the boundary and following more testing the analysis applied here could better determine the material susceptibility during events similar to that used as part of the analysis. Like the other sites again, the M_w5.5 event does not appear to induce liquefaction and the factor of safety values are sufficiently high that the interpretation that liquefaction not occurring following an event similar to this can be stated with some confidence.

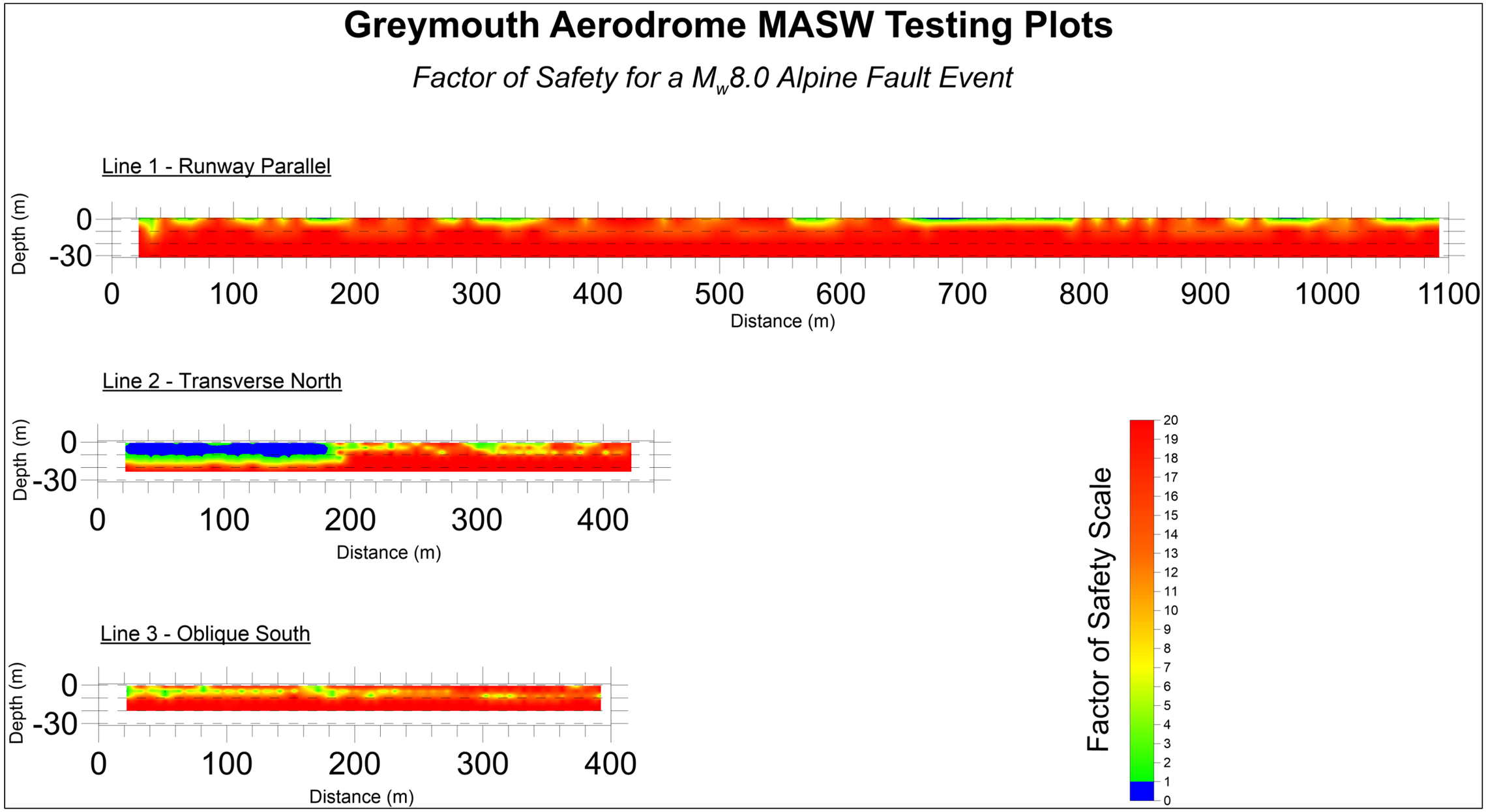

Figure 5.7 - Factor of Safety Profile based on a design Mw8.0 Alpine Fault Earthquake for the soils found at the Greymouth Aerodrome

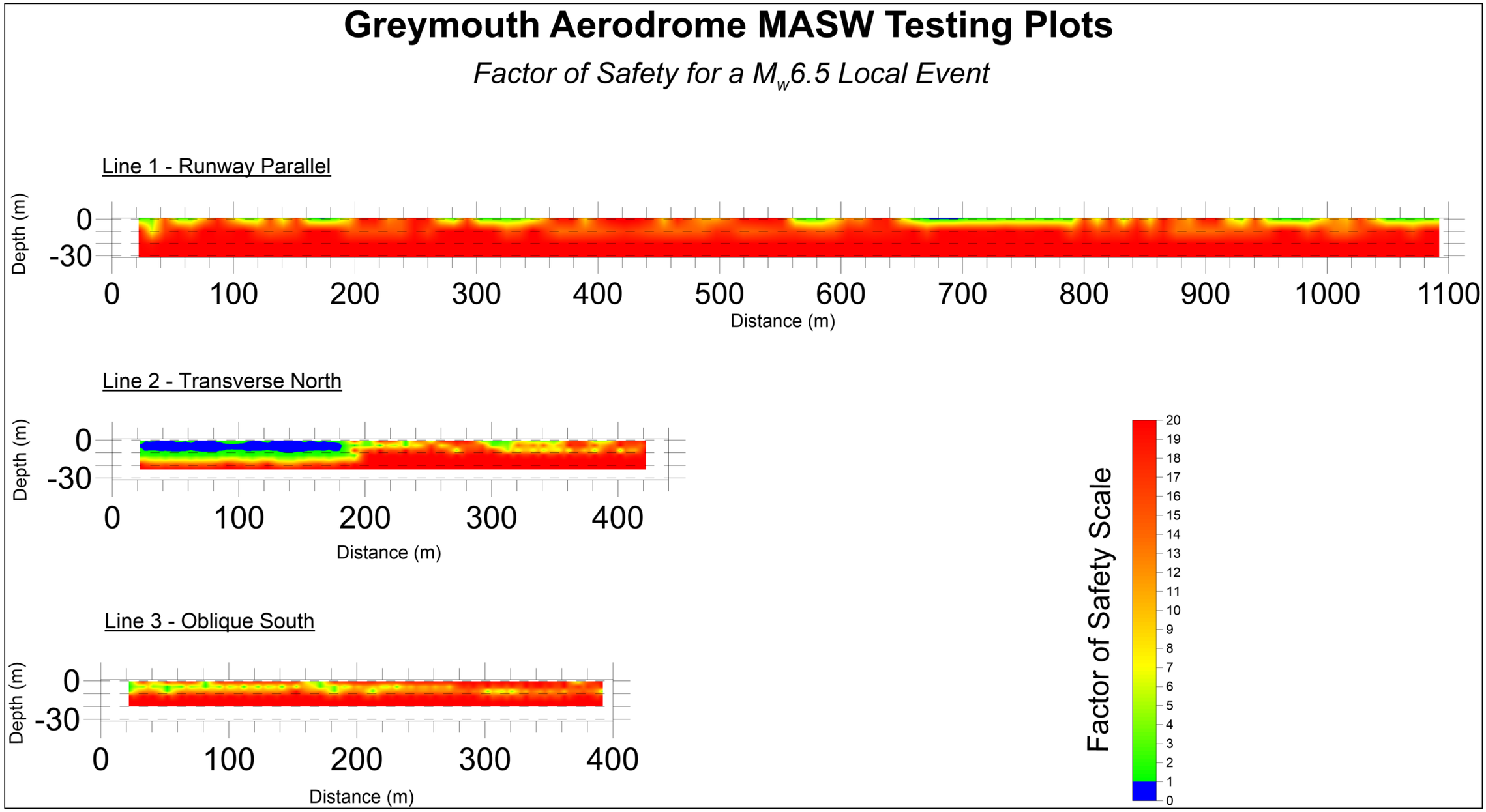

Figure 5.8 - Factor of Safety Profile based on a design Mw6.5 Localised Earthquake for the soils found at the Greymouth Aerodrome

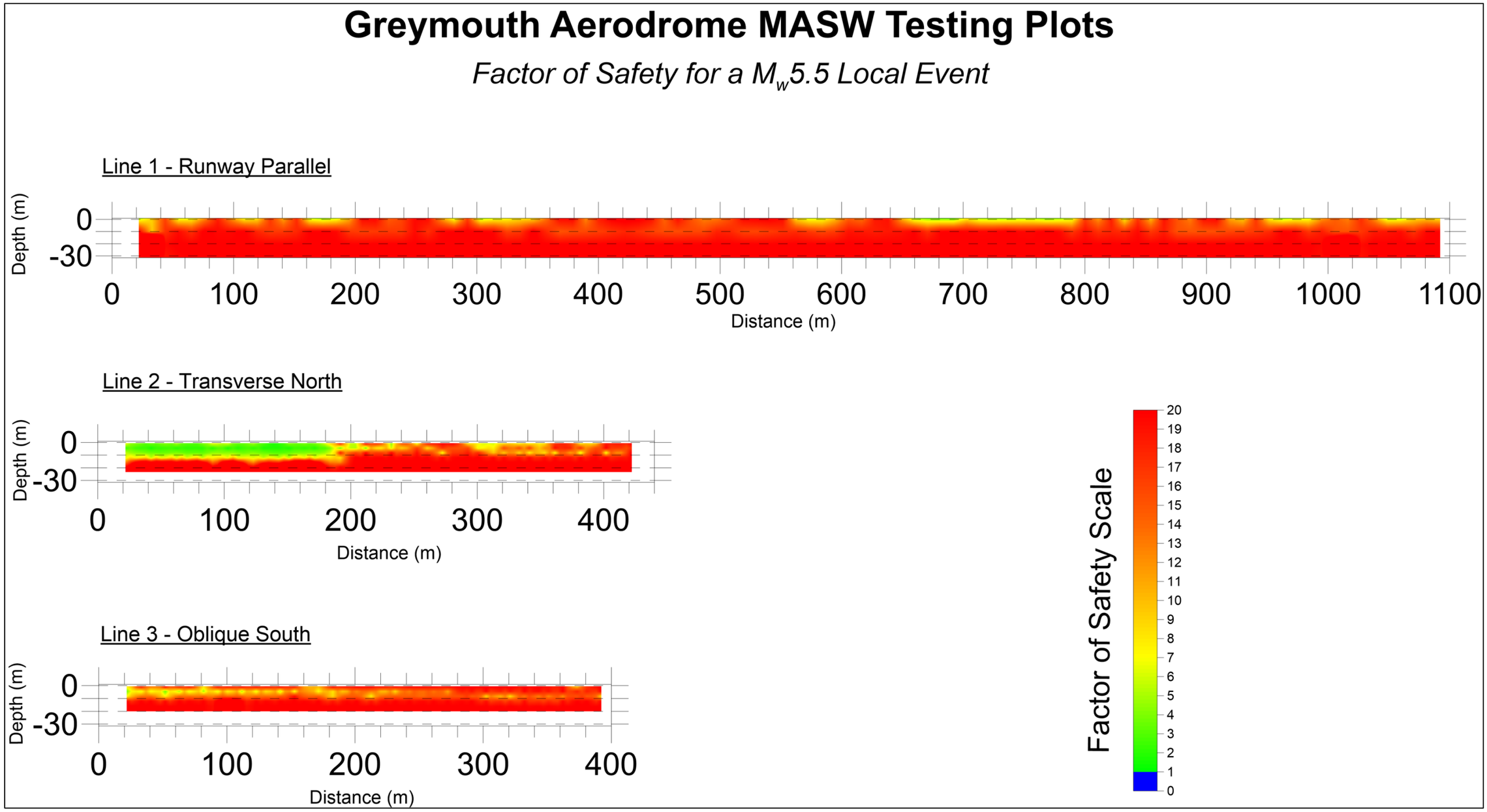

Figure 5.9 - Factor of Safety Profile based on a design Mw5.5 Localised Earthquake for the soils found at the Greymouth Aerodrome

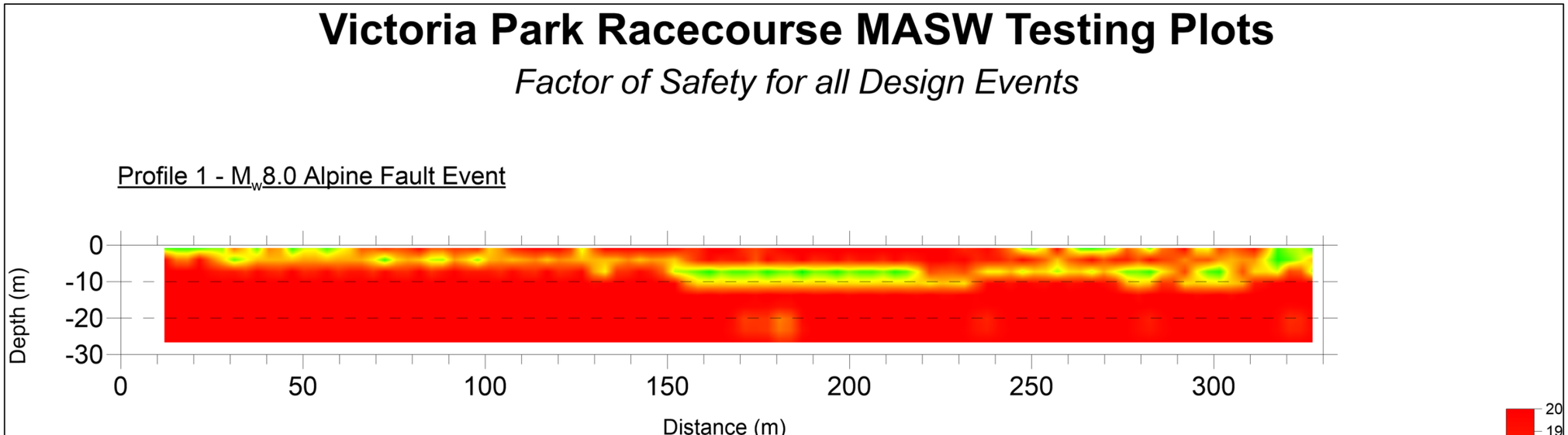

Figure 5.10 - Factor of Safety Profiles based on all design earthquakes for soils found at Victoria Park Racecourse

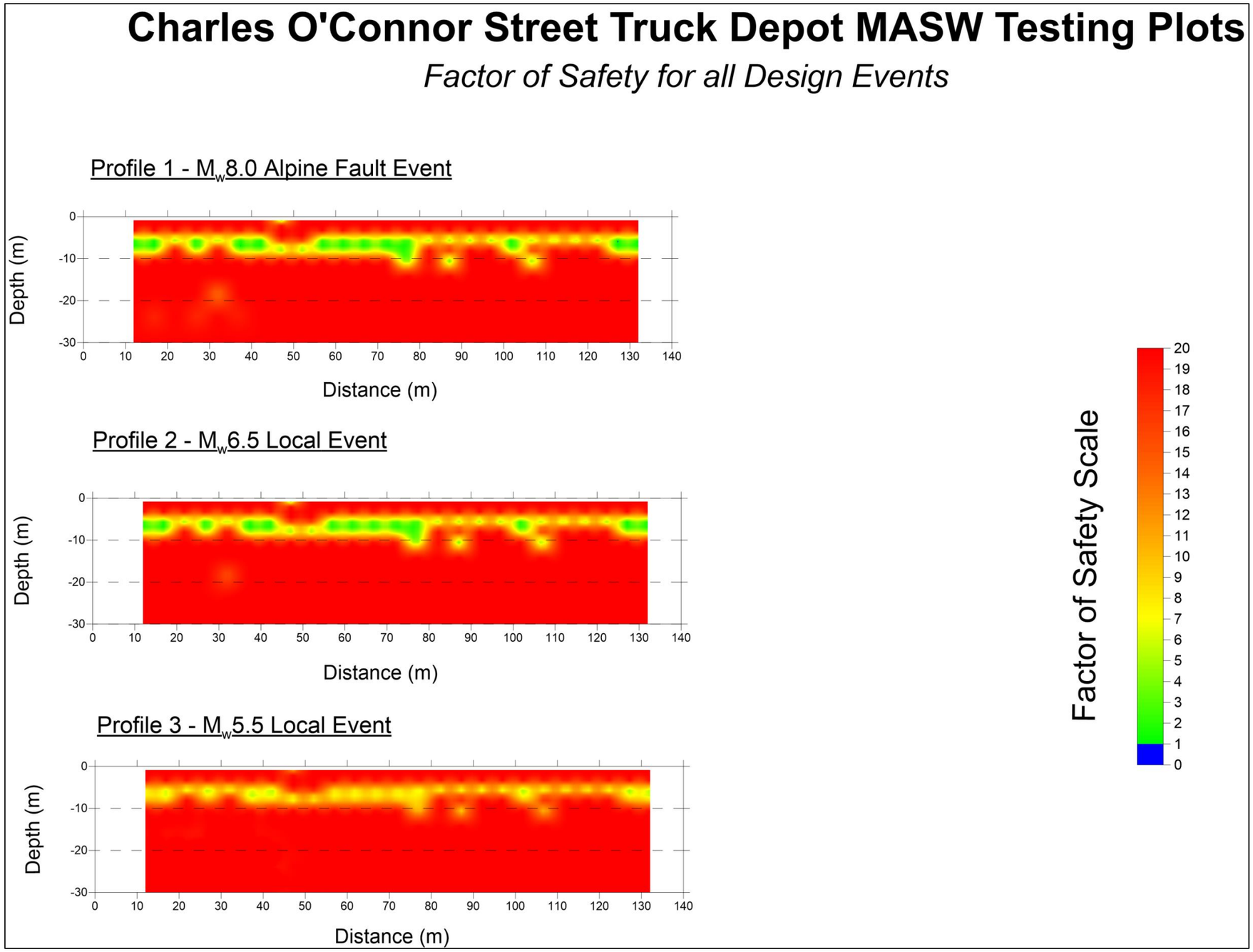

Figure 5.11 - Factor of Safety Profiles based on all design earthquakes for soils found at Charles O'Connor Street Truck Depot

6 Discussion

6.1 Introduction

Based on the results obtained as following the overburden stress-corrected shear wave velocity and factor of safety analysis completed in Chapter 5 it is observed that the majority of the areas tested as part of this study are likely to be highly resistant to liquefaction for the design earthquakes proposed. This chapter discusses the implications of the results obtained, with regard to the surficial geology and geomorphology, seismic hazard, and critical infrastructure. Particular comment with regard to areas of reclamation or fill that were assessed as part of this study is also discussed. The influences that factors such as seismicity and geology, have on the analysis are described.

Limitations of the results obtained will be discussed with regard to liquefaction susceptibility and potential future land use possibilities for the areas tested. Finally, recommendations for future work are outlined along with recommendations for supplementary work to better assess the analysis completed as part of this study.

6.2 Discussion of results of analysis

The aim of this study was to assess the use of shear-wave velocity as a proxy for liquefaction potential. This is reflected in the factor of safety analysis from Andrus and Stokoe (2000). Each analysis was undertaken for one of three different seismic events outlined below.

6.2.1 Alpine Fault M_w8.0 Earthquake

The results for liquefaction susceptibility obtained following the analysis of the M_w8.0 Alpine Fault were as to be expected. This event shows the largest areas of liquefaction susceptibility for the three earthquakes used, with the area on the north-eastern part of the Aerodrome appearing to be most likely to liquefy during this type of event. The upper 10m in this part of the site shows low factors of safety (FoS < 1). Small areas of the Aerodrome also appear to be liquefiable though this is restricted to the upper 1-2 metres. Of the other sites (Victoria Park and Charles O'Connor Street), no areas appear liquefiable though the values for factor of safety are close to

the boundary between liquefaction and non-liquefaction, predominantly in areas that historically could have been influenced by the estuary.

6.2.2 Local M_w6.5 Earthquake

A M_w6.5 local earthquake with accelerations similar to that of the February 2011 Christchurch earthquake was used as a basis for the next design earthquake. Based on the experiences of Christchurch, liquefaction could be expected following an event of this type. Similar to the Alpine Fault event, the north-eastern event shows a high potential for liquefaction, though the total area is slightly smaller. Overall the analysis of this event highlights areas of liquefaction susceptibility much the same areas to that of the Alpine Fault event. The other sites both again appear to be non-liquefiable, though some values were close to the boundary between liquefaction and non-liquefaction.

6.2.3 Local M_w5.5 Earthquake

The smallest of the proposed design earthquakes displays factors of safety much higher than those found in the two larger events. The areas of high liquefaction susceptibility at the Aerodrome are visible in the first two events, though the factors of safety are greater than 1 indicating non-liquefaction. Some values for the factor of safety analysis are close to the threshold between liquefaction and non-liquefaction however. This is also reflected at the other sites, where lower factor of safety values are represented, though the values are higher in general.

6.3 Implications of results with regard to geology and geomorphology

There are several implications with regard to the surficial geology and geomorphology that this analysis has identified.

Firstly, the more recent reclamation work (i.e. post-1979) appears to have been completed to a standard sufficient enough that liquefaction can be considered unlikely following events similar to that used as design events in this analysis. This is best represented by the Charles O'Connor Street testing, where the factor of safety analysis signified that the fill material and natural ground beneath the fill are at an acceptable level that renders failure due to liquefaction-induced causes unlikely. The older reclamation works, however, appear to not be to as liquefaction resistant. This

is best represented by the north-eastern part of the area of the Aerodrome site. This material was reclaimed and filled between 1873 and 1945 although this time-frame was unable to be constrained further. As observed in both the stress-corrected velocity and factor of safety profiles, this material appears to be highly susceptible to liquefaction, especially following events greater than M_w5.5. This site could potentially be deemed liquefiable following the smaller event if further penetration-based testing and analysis better constrain the parameters.

Secondly, the surficial geology appears to have distinct differences based on the stress-corrected profiles in particular. An overlay of the microzones map for Greymouth (Dowrick et al., 2003), on the aerial photo (Figure 6.1) shows that the Greymouth Aerodrome and Victoria Park Racecourse are located across an inferred boundary between different kinds of deposits. Based on the analysis completed during this study, it was interpreted that the "estuarine and lagoonal silt" (Dowrick et al., 2003) is of much lower shear-wave velocity than the other materials that were tested. A clear example of this is Line 2 at the Aerodrome. Based on Figure 6.1, the low velocity material is classified as this silt material, and the western part of the line, with increased shear-wave velocities is "beach sand and gravel". The difference in the material types is clearly defined in the shear-wave velocity profiles. Likewise, but to a lesser extent, the profile from Victoria Park showed the transition from the "sandy gravel and river gravel" material towards the "estuarine and lagoonal silt".

Based on these analyses, some inferences can be made about the nature of the material on which this part of Greymouth is built on, though the total area of tested is low and more extensive testing should be completed to confirm these inferences. Carr (2004) states that the sediments trapped in the Blaketown area (i.e. around the estuary) are thought to be fairly loose in comparison to sand dunes subject to wave action. This looser material is thought to be more susceptible to liquefaction. The interpretation as part of this study confirms this. Therefore the material that has been deposited in more energetic environments (i.e. the coastline and river) is inferred to be more consolidated than that in low energy environments (i.e. the estuary) and therefore more resistant to liquefaction. As mentioned earlier, this should be confirmed through further testing as only a small portion the material was tested during this study.

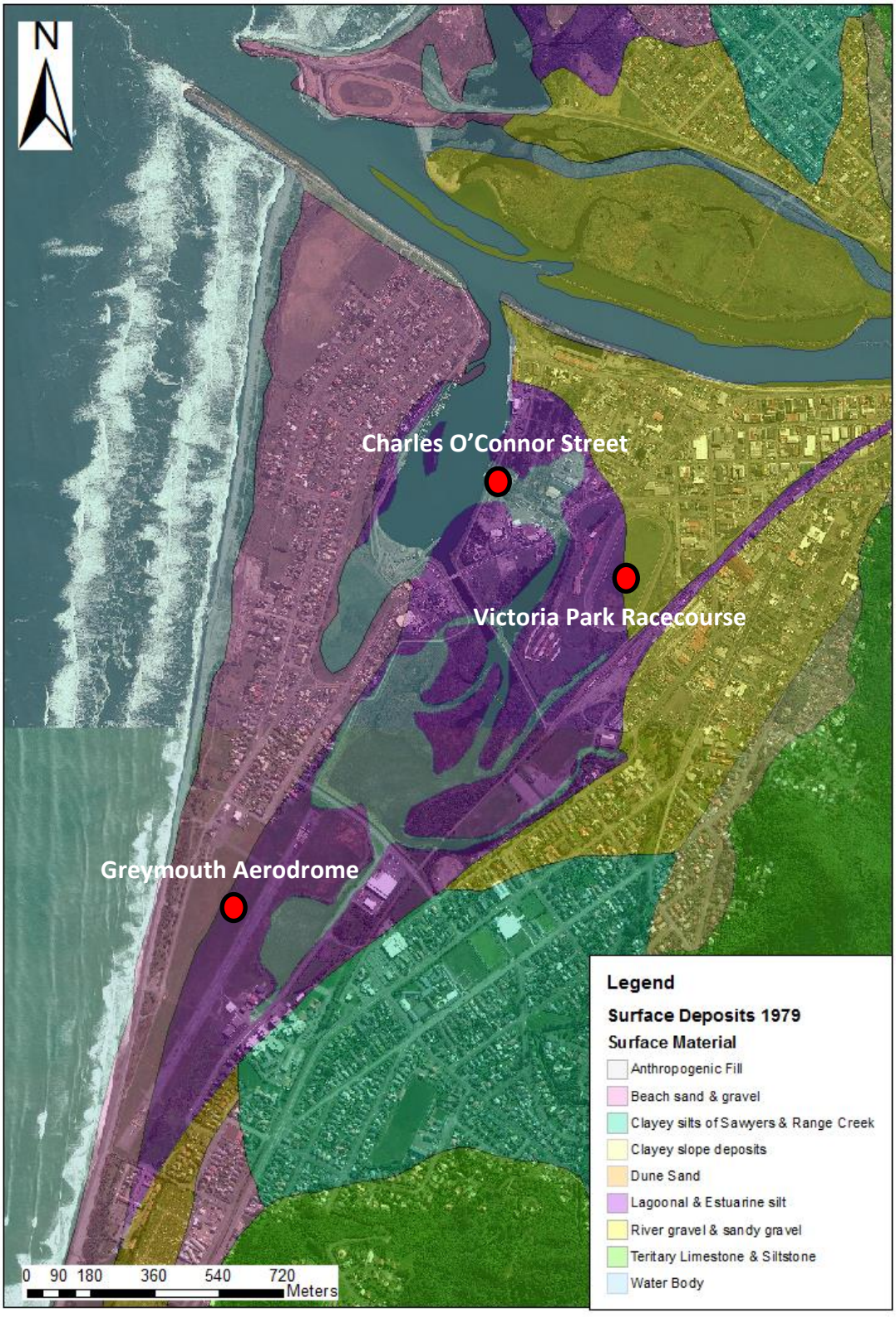

Figure 6.1 - Microzones of surficial sediment type and origin (Dowrick et al., 2004)

6.4 Implications of results with regard to the seismic hazard and infrastructure

Based on the analysis undertaken during this study, implications for seismic hazards to critical infrastructure have been identified.

The seismic hazard in associated with the Alpine Fault is high, with it being located approximately 30 kilometres east of Greymouth, and being capable of producing an earthquakes of M_w8.0+ (Robinson and Davies, 2013). These analyses have shown that generally the areas tested could be resilient enough to not liquefy during an event of this magnitude. There is an exception to this, where the north-eastern part of the Aerodrome site has been inferred to show a high potential for liquefaction, with a liquefiable layer possibly reaching 10 metres in depth. There are also small localised areas throughout all three test sites where the factor of safety values obtained to close to the threshold between liquefaction and non-liquefaction occurring, and it is still a possibility that these layers could fail following cyclic loading in an earthquake.

There are also several mapped local faults and several unmapped faults in the area around Greymouth. Given their dimension (typically ~10 – 12km long) it is entirely possible that these faults produce events similar to that experienced in the Canterbury Earthquake Sequence. The factor of safety analysis based on a Christchurch-type event produced similar results to that of the Alpine Fault scenario.

Based on this, it can be implied that these sites, as an initial estimation, will be generally resilient to liquefaction and liquefaction-based effects. Aside to this historical earthquakes have affected some of the areas tested. During the 1929 Murchison earthquake, Victoria Park sustained ground fracturing following the event. However, no liquefaction was observed with the ground cracking. This is consistent with the results obtained through the factor of safety analysis. Also, based on anecdotal evidence, a small area of the Aerodrome had sand boils occur on the site following the event. The sand boils were located near a flagpole which is currently located on the north-eastern part of the site, which again is consistent with the results of the analysis carried out as part of this study. This is important because

Quigley et al. (2013) state that old liquefaction structures can act reactivate and act as a conduit for future liquefaction-inducing seismic events, as observed following the Canterbury Earthquake Sequence.

Infrastructure, such as the St. John Building and Greymouth Aerodrome, are going to be critical assets in response to a large seismic event. Functionality of these assets following an event is of paramount importance to the civil response effort. McCahon et al. (2007) state that the Aerodrome is the primary way of getting resources into the community if access is limited after an earthquake, and initially based on this study, the Aerodrome should theoretically remain functional. Along with the Aerodrome, the St. John Ambulance Service needs to be functional. The St. John Ambulance Building is located next to the Aerodrome and part of the ambulance site was surveyed during the testing completed at the Aerodrome. The start of Line 3 runs parallel to the boundary between the Aerodrome and the St. John Building and as seen in Chapter 5, this ground can generally be considered resistant to liquefaction.

Currently no critical infrastructure is planned for the other sites tested during this survey, though any future developments on the sites may cause them to become important, for example, as a civil defence base. Future construction of critical sites should focus on un-filled locations, particularly avoiding old fill.

It should be noted that these implications are related to liquefaction-based effects only; other effects as a result of an earthquake (e.g. building damage) are not covered by the scope of this study.

6.5 Influence of factors on Analysis

A number of factors that are used as part of the simplified procedure can have an influence on the outcome of the analysis. Some of these factors are described below, and include but are not limited to: Seismic factors (i.e. moment magnitude and peak acceleration); geological factors (i.e. age of deposit and the effect of soil type); and hydrological factors (seasonal fluctuations in water table levels).

6.5.1 Seismic Factors

The application of the simplified procedure for the evaluation of liquefaction susceptibility requires estimates of two ground motion parameters – earthquake magnitude and peak horizontal ground acceleration. These factors characterise duration and intensity of ground shaking, respectively (Youd and Idriss, 2001).

6.5.1.1 Earthquake Magnitude

Though magnitude is the primary factor that characterises duration of shaking during an earthquake, this relationship is rather uncertain and factors other than magnitude also influence duration. An example of this is unilateral faulting, in which rupture begins at one end of the fault and propagates to the other, usually produces longer shaking duration for a given magnitude than bilateral faulting, in which slip begins near a midpoint on the fault and propagates in both directions simultaneously. Duration also generally increases with distance from the seismic source and may vary with site conditions and bedrock topography (basin effects), for example (Youd and Idriss, 2001).

Characteristics of coseismic slip and shaking duration are difficult to predict in advance of an earthquake event. These effects are not sufficiently predictable to be adequately accounted for in engineering practice. Therefore the conservative relationship between magnitude and duration is applied for the simplified procedure outlined by Seed and Idriss (1971) and summarised by Andrus and Stokoe (2000) and Youd and Idriss (2001).

Changes in the moment magnitude can tend to affect the results as it influences the magnitude scaling factor (MSF), which is applied directly to the CRR value. Thus influences the factor of safety to a greater extent than any other seismic factor. It should be noted that the MSF applied in the case of this study (Andrus and Stokoe, 2000) does tend to be at the upper end of range of magnitude scaling factors used in engineering practice, making it a conservative predictor of liquefaction.

6.5.1.2 Peak Ground Acceleration

The Peak Ground Acceleration (PGA) applied in the procedure is the peak acceleration that would occur at the ground surface in the absence of pore pressure increases or liquefaction.

A change in the peak acceleration is less likely to affect the overall factor of safety calculation, and thus liquefaction susceptibility, due to the acceleration being standardised against the acceleration due to gravity within the equation for CSR. This would give a small overall change and is likely to only influence this result when CRR and CSR are equal, the point between liquefaction and non-liquefaction.

6.5.2 Geological Factors

Geological factors can have an effect on the behaviour of the soil during a seismic event. Two of these factors (age of the deposit and sediment type) are discussed briefly below.

6.5.2.1 Age of deposit

Liquefaction resistance increases with age (Youd and Hoose, 1977; Youd and Perkins, 1978; Seed, 1979; Youd and Idriss, 2001).

Sediments deposited within the last few thousand years are generally much more susceptible to liquefaction than older Holocene sediments; Pleistocene sediments are even more resistant; and pre-Pleistocene sediments are generally immune to liquefaction.

Andrus and Stokoe (2000) provide a correction factor K_C to correct for high values of V_{S1} caused by cementation and aging. However this is generally based on penetration data. They do however provide a range of values from 0.6 - 1.0 that are representative of these differences. Selection of these values depends on knowledge of sediment age and penetration data. This correction is applied to the CRR equation which is very sensitive to the selected value. Lower values of K_C result in lower factors of safety.

6.5.2.2 Sediment Type

The type of sediment within the subsurface will have an effect on the susceptibility for liquefaction. More specifically the fines content (expressed as a percentage) can be accounted for, within the CRR equation. This is done by reducing the limiting upper value of V^*_{S1} to account for the increase in fines content of the soil as shown in Table 6.1 (Andrus and Stokoe, 2000).

Table 6.1 – The relationship between fines content and the limiting upper value for liquefaction (V_{S1}) (Andrus and Stokoe, 2000)

Fines Content (FC)	Limiting Upper Value (V^*_{S1}) based on FC
FC ≤ 5%	V^*_{S1} = 215 m/s
5% < FC < 35%	V^*_{S1} = 215 – 0.5(FC – 5) m/s
FC ≥ 35%	V^*_{S1} = 200 m/s

An increase in the fines content results on a reduction in the pore space between the individual grains. This in turn limits the amount of water in the pore space and thus larger pore-water pressure increases may not be possible in an earthquake. This would reduce liquefaction susceptibility, and this is reflected in the reduction of the upper limit of V_{S1} for liquefaction occurring. The effect that differing fine content has on the analysis can be significant. Due to no information being available for fines contents the largest value of V^*_{S1} is used, making it conservative, especially in areas that have greater fines content. Thus the potential susceptibility determined using this method is conservative.

Also in soils above the ground-water table, particularly silty soils, negative pore pressures can increase the effective stress and, hence, the value of V_S measured in seismic tests. This effect should be considered in the estimation of σ'_V for correcting V_S to V_{S1} and for computing CSR (Andrus and Stokoe, 2000).

6.5.3 Hydrological Factors

The predominant hydrological factor associated with this survey is the water table depth, and therefore the amount of saturated material. However, seasonal fluctuations in the water table can change liquefaction susceptibility.

6.5.3.1 Seasonal Water Table Fluctuations

Seasonal fluctuations in the water table can influence the stresses associated with overburden stress. The West Coast is known for its high annual precipitation, with up to 3000mm annually (NIWA, 2014). This is reflected in Figure 6.2 below.

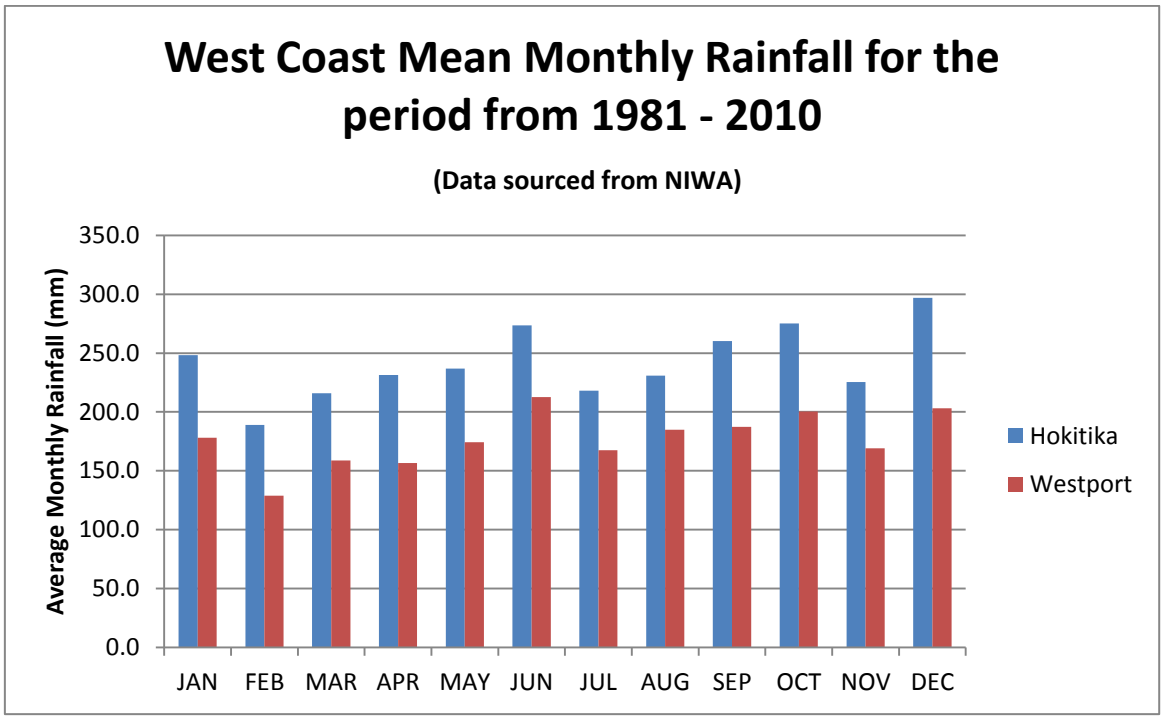

Figure 6.2 - Mean Monthly Rainfall for Hokitika and Westport from 1981 – 2010 [Note: no rainfall information was available for Greymouth] (NIWA)

These differences in rainfall can influence the depth to water table. This not only affects the effective hydrostatic pressure (and total effective pressure as a result), but also affects the material that can liquefy following an earthquake event. For example, an earthquake that occurred in December when rainfall is high could result in liquefaction being more likely to occur due to the higher rainfall reducing the depth

to the water table. This will increase the amount of the soil profile that is saturated, which is a requirement for liquefaction to occur.

6.6 Limitations of using Shear-Wave Velocity for Liquefaction Susceptibility Analysis

There are three concerns over the use of shear-wave velocity as an indicator of liquefaction susceptibility:

(1) No physical soil samples are obtained as part of seismic testing. This means that no soil classification and identification of non-liquefiable material can be conducted;

(2) Thin, low shear-wave velocity strata may not be detected if the measurement interval is too large. This could result in liquefiable material being missed during the analysis process, and thus giving an inaccurate estimate for liquefaction potential;

And, (3) seismic measurements are made at small strains, whereas pore-water pressure build-up and liquefaction are medium- to high-strain phenomena. This limitation can be significant for cemented soils, because small-strain measurements are highly sensitive to weak interparticle bonding that is eliminated at medium to high strains. It is also significant in silty soils above the water table where negative pore-water pressures can increase shear-wave velocity.

By conducting sufficient in-situ testing (i.e. penetration based testing) and drilling of boreholes, liquefiable weakly cemented soils and non-liquefiable clay-rich soils can be identified, and also thin liquefiable strata that may not have been observed following the seismic testing.

6.7 Conclusions

To conclude, the initial desk-based investigation into the geomorphology clearly identified areas of natural and reclamation fill land. These areas of reclamation material are distributed generally around the historic estuary boundary as a way to constrain the extent of the estuary and also to mitigate against flood hazards by the increase in elevation of the land surrounding the estuary.

Following the testing completed at the various sites chosen as part of this study, areas of low shear-wave velocity were able to be identified. Further analysis was based on the simplified procedure outlined by Andrus and Stokoe (2000), and using a range design earthquakes events. The analysis showed that much of the area tested was resistant to liquefaction effects following these design events. An area of historic, early 20th century fill, located in the north-east of the Aerodrome site showed high potential for liquefaction to occur following the Alpine Fault and local M_w6.5 design earthquakes. Areas of more modern fill, such as that tested on Charles O'Connor Street showed low potential for liquefaction, reflecting the improved methods of reclamation and fill emplacement.

Based on the analysis completed it can be stated with some confidence that these sites would generally be resistant to liquefaction effects based on the design events. However due to several assumptions made as part of the analysis these predictions should not be used as the sole indicator for liquefaction. Penetration-based in-situ testing and soil sampling should be conducted in the areas tested to allow for better constraint of the parameters used in the analysis. This more thorough testing is of particular importance to areas where critical infrastructure is located, such as the Aerodrome site. The importance of key buildings such as the St. John's Ambulance building to remain in working order following a potentially lethal earthquake event is paramount, though ground stability is only one factor related to a buildings ability to function after an earthquake. As an initial estimate it appears that this ground is resistant to liquefaction.

6.8 Future Work

Below are several suggestions for future supplementary work, as a result of this study:

- The multichannel analysis of surface wave (MASW) method is a cheap, effective way to obtain shear-wave velocity data and therefore can be used to make initial estimations of liquefaction susceptibility. Further MASW testing around the rest of the township, with particular attention to key infrastructure, such as the hospital, medical centres, police and fire stations etc. This could allow for detailed modelling of the Greymouth subsurface to determine the extents of potentially liquefiable material beneath the town.
- It is recommended that penetration-based (CPT and SPT) testing be carried out and boreholes be drilled to determine the stratigraphy. This will allow for parameters used in the simplified method to be better constrained leading to a better estimation of liquefaction susceptibility and also the identification of thin low velocity, potentially liquefiable layers that may not have been identified otherwise. The combination of seismic profiles with CPT and SPT data would allow an extensive and detailed analysis of the Greymouth subsurface to be carried out.
- This method of using MASW to provide initial estimates for liquefaction susceptibility in Greymouth makes it a useful tool for making estimates for this in other towns constructed on similar material, and that face similar seismic hazards, such as Hokitika and Westport.

7 References

Andrus, R.D., and Stokoe, K.H., 1996, Guidelines for evaluation of liquefaction resistance using shear wave velocity: Draft of paper presented at the NCEER Workshop on Evaluation of Liquefaction Resistance, Salt Lake City, UT, January 4-5.

--, 1997, Liquefaction resistance based on shear wave velocity: Proceedings from the NCEER Workshop on Evaluation of Liquefaction resistance of soils, Technical report NCEER-97-0022, National Centre for Earthquake Engineering Research, Buffalo, pp. 89-128.

--, 2000, Liquefaction resistance of soils from shear-wave velocity: Journal of Geotechnical and Geoenvironmental Engineering, v. 126, p.1015-1025.

Bannister, S & Gledhill, K 2012, 'Evolution of the 2010–2012 Canterbury earthquake sequence', New Zealand Journal of Geology and Geophysics, vol. 55, no. 3, pp. 295-304. DOI:10.1080/00288306.2012.680475

Brackley, H.L., 2012, Review of liquefaction hazard information in eastern Canterbury, including Christchurch City and parts of Selwyn, Waimakariri and Hurunui Districts: GNS Science Consultancy Report 2012/218. 99 pp.

Bradley, B.A. and Hughes, M., 2012a, Conditional peak ground accelerations in the Canterbury earthquakes for conventional liquefaction assessment: Technical report prepared for the Department of Building and Housing, 13 April 2012.

--, 2012b, Conditional peak ground accelerations in the Canterbury earthquakes for conventional liquefaction assessment Part 2: Technical report prepared for the Department of Building and Housing, 22 December 2012.

Brown, LJ & Weeber, JH 1992, 'Geology of the Christchurch urban area'. Institute of Geological and Nuclear Sciences Ltd., Lower Hutt, New Zealand, p. 1 map sheet + 104p.

Carr, K.M., 2004, Liquefaction Case Histories from the West Coast of the South Island, New Zealand; Unpublished Master's Thesis, University of Canterbury, Christchurch.

Cubrinovski, M, Green, RA, Allen, J, Ashford, S, Bowman, E, Bradley, B, Cox, B, Hutchinson, T, Kavazanjian, E, Orense, R, Pender, M, Quigley, MC & Wotherspoon, L 2010, 'Geotechnical reconnaissance of the 2010 Darfield (Canterbury) earthquake', Bulletin of the New Zealand Society for Earthquake Engineering, vol. 43, no. 4, pp. 243-320.

Dobry, R., 1989, Some basic aspects of soil liquefaction during earthquakes: Earthquake hazards and the design of constructed facilities in the eastern United States, Ann. Of the New York Academy of Science, K.H. Jacob and C.J. Turkstra, erds., New York, 558, pp.172-182.

Downes, G & Yetton, M 2012, 'Pre-2010 historical seismicity near Christchurch, New Zealand: the 1869 M W 4.7–4.9 Christchurch and 1870 M W 5.6–5.8 Lake Ellesmere earthquakes', New Zealand Journal of Geology and Geophysics, vol. 55, no. 3, pp. 199-205. DOI:10.1080/00288306.2012.690767

Dowrick, D.J., Rhoades, D.A., and Davenport, P.N., 2003, Effects of microzoning and foundations on damage ratio for domestic property in the magnitude 7.2 1968 Inangahua, New Zealand earthquake: Bulletin of the New Zealand Society for Earthquake Engineering, v. 36, No. 1.

Dowrick, D.J. and Sritharan, S., 1993, Attenuation of peak ground accelerations in some recent New Zealand earthquakes: Bulletin of the New Zealand National Society fro Earthquake Engineering, Vol. 26, No. 1.

Duffy, B.D., 2008, Development of Multi-channel Analysis of Surface Waves (MASW) for characterising the internal structure of active fault zones as a predictive method of identifying the distribution of ground deformation: Unpublished master's thesis, University of Canterbury, Christchurch, New Zealand.

Golesorkhi, R., 1989, Factors influencing the computational determination of earthquake-induced shear stresses in sandy soils: Unpublished doctoral dissertation, University of California, Berkeley, California.

Greene, M., Power, M., and Youd, T.L., 1994, Liquefaction - What it is and what to do about it: Earthquake Basics Brief, No. 1, 7p.

Grey District Council, 2014, Port of Greymouth, updated 25 June 2014, http://www.greydc.govt.nz/our-services/port/Pages/default.aspx

Hicks, M.A., 2011, Geotechnical Investigations of Wind Turbine Foundations using Multichannel Analysis of Surface Waves (MASW): Unpublished master's thesis, University of Canterbury, Christchurch, New Zealand.

Idriss, I.M., 1999, Presentation notes – An update to the Seed-Idriss simplified procedure for evaluating liquefaction potential: Proceedings from the TRB Workshop on New Approaches to Liquefaction Analysis, Publication No. FHWA-RD-99-165, Federal Highway Administration, Washington, D.C.

Idriss, I. M., and Boulanger, R. W., 2008, Soil liquefaction during earthquakes. Monograph MNO-12, Earthquake Engineering Research Institute, Oakland, CA, 261 pp.

-- , 2014, CPT and SPT Based Liquefaction Triggering Procedures: Report UCD/CGM-14/01, Department of Civil and Environmental Engineering, University of California, Davis, CA,136 pp.

Ishihara, K. and Koga, Y., 1981, Case Studies of Liquefaction in the 1964 Niigata Earthquake: Soils and Foundations, Vol. 21, No. 3, p. 35-52

Ivanov, J., Park, C.B., Miller, R.D., and Xia, J., 2005, Analyzing and filtering surface wave energy by muting shot gathers: Journal of Environmental and Engineering Geophysics, v. 10, p. 307-322.

Ivanov, J., Park, C.B., Miller, R.D., Xia, J., and Overton, R., 2001, Modal separation before dispersion curve extraction by MASW method, Proceedings of the SAGEEP: Denver, Colorado.

Kaiser, A, Dellow, G, Denys, P, Fielding, E, Fry, B, Gerstenberger, M, Langridge, R, Massey, C, Motagh, M, Pondard, N, McVerry, G, Holden, C, Ristau, J, Stirling, M, Thomas, J, Uma, SR, Zhao, J, Beavan, J, Beetham, D, Benites, R, Celentano, A, Collett, D, Cousins, J & Cubrinovski, M 2012, 'The M-w 6.2 Christchurch earthquake

of February 2011: preliminary report', New Zealand Journal of Geology & Geophysics, vol. 55, no. 1, pp. 67-90. DOI:10.1080/00288306.2011.641182

Kayen, R. E., Mitchell, J. K., Seed, R. B., Lodge, A., Nishio, S., and Coutinho, R., 1992, Evaluation of SPT-, CPT-, and shear wave-based methods for liquefaction potential assessment using Loma Prieta data: Proc., 4th Japan-U.S. Workshop on Earthquake Resistant Des. of Lifeline Fac. and Countermeasures for Soil Liquefaction, Tech. Rep. NCEER-92-0019, M. Hamada and T. D. O'Rourke, eds., Vol. 1, National Centre for Earthquake Engineering Research, Buffalo, pp. 177–204.

Marcuson, W.F., 1978, Definition of Terms Related to Liquefaction: Journal of the Geotechnical Engineering Division, Vol. 104, No. 9, pp. 1197-1200

Mew, G., 1980, Soils of Greymouth-Hokitika Region, South Island New Zealand and, Soil Mapping Unit Descriptions for Greymouth-Hokitika Region, South Island, New Zealand. Separate parts of: NZ Soil Survey Report 58, New Zealand Soil Bureau, Department of Scientific and Industrial Research, Wellington, New Zealand.

McCahon, I., Mackenzie, J., Dewhirst, R., and Elms, D., 2007, Grey District Lifelines study: Alpine fault earthquake scenario & lifelines vulnerability assessment, Grey District Council, 198 pp.

Metcalf, P.L., 1993, Landslide Investigation and Hazard zonation in the Greymouth Urban area: Unpublished Master's Thesis, University of Canterbury, Christchurch.

Nathan, S., 1974, Stratigraphic nomenclature for the Cretaceous-lower Quaternary rocks of Buller and North Westland, West Coast, South Island, New Zealand: New Zealand Journal of Geology and Geophysics, Vol. 17, No. 2, pp. 423-445.

Nathan, S., Rattenbury, M.S., and Suggate, R.P., 2002, Geology of the Greymouth Area: Institute of Geological & Nuclear Sciences Ltd., Lower Hutt, New Zealand.

O'Neill, A., and Matsuoka, T., 2005, Dominant higher surface-wave modes and possible inversion pitfalls: Journal of Environmental and Engineering Geophysics, v. 10, p. 185-201.

Park Seismic, n.d., Retrieved on 22 August 2014, from Multichannel Analysis of Surface Waves (MASW): http://www.masw.com/DataAcquisition.html

Park, C.B. and Brohammer, M., 2003, Surfseis Multichannel Analysis of Surface Waves - MASW User's Manual, Lawrence, Kansas Geological Survey.

Park, C.B., and Miller, R.D., 2006, Roadside passive MASW: Proceedings of the SAGEEP, April 2-6, 2006, Seattle, Washington.

Park, C.B., Miller, R.D., and Ivanov, J., 2002, Filtering surface waves, Proceedings of the SAGEEP 2002: Las Vegas, Nevada

Park, C.B., Miller, R.D., and Miura, H., 2005, Optimum Field Parameters of an MASW survey: http://www.kgs.ku.edu/Geophysics2/Pubs/Pubs/PAR-02-03.pdf, Kansas Geological Survey.

Park, C.B., Miller, R.D., and Xia, J., 1998, Imaging dispersion curves of surface waves on multi-channel record, 68th Annual International Meeting of the Society of Exploration Geophysicists, Expanded Abstracts, p. 1377-1380.

—, 1999, Multichannel analysis of surface waves: Geophysics, v. 64, p. 800-808.

Pettinga, JR, Yetton, MD, Van Dissen, RJ & Downes, G 2001, 'Earthquake source identification and characterisation for the Canterbury Region, South Island, New Zealand.', Bulletin of the New Zealand Society for Earthquake Engineering, vol. 34, no. 4, pp. 282-317.

Quigley, M, Bastin, S & Bradley, B., 2013, Recurrent liquefaction in Christchurch, New Zealand, during the Canterbury earthquake sequence, *Geology,* Vol. 41, No. 5, p. 614. DOI:10.1130/G33944.1

Quigley, MC, Van Dissen, R, Litchfield, N, Villamor, P, Duffy, B, Barrell, D, Furlong, K, Stahl, T, Bilderback, E and Noble, D, 2012, Surface rupture during the 2010 M_W 7.1 Darfield (Canterbury) earthquake: implications for fault rupture dynamics and seismic-hazard analysis', Geology, vol. 40, no. 1, pp. 55-8. DOI:10.1130/G32528.1

Quigley, MC, Villamor, P, Furlong, K, Beavan, J, Van Dissen, R, Litchfield, N, Stahl, T, Duffy, B, Bilderback, E, Noble, D, Barrell, D, Jongens, R & Cox, S, 2010, Previously unknown fault shakes New Zealand's South Island, EOS, vol. 91, no. 49, pp. 469-70.

Rauch, A.F., 1997, EPOLLS: An Empirical Method for Predicting Surface Displacements due to Liquefaction-Induced Lateral Spreading in Earthquakes: Unpublished doctoral dissertation, Virginia Polytechnic Institute and State University, Virginia, United States of America.

Richart, F. E., Jr., Woods, R. D., and Hall, J. R. Jr., 1970, Vibrations of Soils and Foundations: Prentice Hall, Englewood Cliffs, New Jersey, 414 pp.

Robertson, P.K., and Campanella, R.G., 1985, Liquefaction Potential of sands using the CPT: J. Geotech. Engrg., ASCE, Vol. 111, Vol. 3, p.384-403.

Robertson, P. K., Woeller, D. J., and Finn, W. D. L., 1992. Seismic cone penetration test for evaluating liquefaction potential under cyclic loading: Canadian Geotechnical Journal., Ottawa, Vol. 29, pp. 686–695.

Seed, H.B., and Idriss, I.M., (1971, Simplified procedure for evaluating soil liquefaction potential: J. Soil Mechanics and Foundations Div., ACSE, Vol. 97, No. 9, p. 1249-1273.

Seed, H.B., Idriss, I.M., and Arango, I., 1983, Evaluation of liquefaction potential using field performance data: Journal of Geotechnical Engineering, ASCE, Vol. 109, No. 3, pp. 458-482.

Sladen, J.A., D'Hollander, R.D., and Krahn, J., 1985, The liquefaction of sands, a collapse surface approach: Canadian Geotechnical Journal, Vol. 22, pp. 564-578.

Soga, K., 1998, Soil liquefaction effects observed in the Kobe earthquake of 1995: Proceedings of the ICE – Geotechnical Engineering, Vol. 1331, No. 1, pp 34-51.

Stewart, J.P., Seed, R.B., and Bray, J.D., 1996, Incidents of ground failure from the 1994 Northridge earthquake: Bulletin Seismological Society America, Vol. 86, No. 1B, pp. S300-S318.

Stokoe, K.H., Roesset, J.M., Bierschwale, J.G., and Aouad, M, 1988, Liquefaction potential of sands from shear-wave velocity: Proceedings from the 9th World Conference on Earthquake Engineering, Vol. 3, pp. 213-218.

Stokoe, K.H., Wright, G.W., James, A.B. and Jose, M.R., 1994, Characterisation of geotechnical sites by SASW method, in geophysical characterisation sites, ISSMFE Technical Committee #10, Oxford Publishers, New Delhi.

Suggate, R.P., 1965, Late Pleistocene geology of the northern part of the South Island, New Zealand: Bulletin of the NZ Geological Survey, Vol. 77.

Suggate, R.P., 1968, The Paringa Formation, Westland, New Zealand: NZ Journal of Geology and Geophysics, Vol. 13, pp. 742-750.

Suggate, R.P. and Moar, N.T., 1970, Revision of the chronology of the late Otira glacial: NZ Journal of Geology and Geophysics, Vol. 13, pp. 742-746

Tokimatsu, K. and Uchida, A., 1990, Correlation between liquefaction resistance and shear wave velocity: Soils and Foundations, Tokyo, Vol. 30, No. 2, pp. 33-42

Vincent, P.D., Tsoflias, G.P., Steeples, D.W., and Sloan, S.D., 2006, Fixed-source and fixed-receiver walkaway seismic noise tests: A field comparison: Geophysics, Vol. 71, p. W41-W44.

Wang, H.B., Sassa, K. and Xu, W.Y., 2004, Analysis of a spatial distribution of landslides triggered by the 2004 Chuetsu earthquakes of Niigata Prefecture, Japan: Natural Hazards, Vol. 41, No. 1, p. 43-60. DOI:10.1007/s11069-006-9009-x

Westfleet Seafood Ltd., date unknown, History of our wharf, http://www.westfleet.co.nz/about-westfleet/our-factory/

Xia, J., Miller, R.D., and Park, C.B., 1999, Estimation of near-surface shear-wave velocity by inversion of Rayleigh waves: Geophysics, v. 64, p. 691-700.

Youd, T. L., et al., 1997, Summary report. *Proc., NCEER Workshop on Evaluation of Liquefaction Resistance of Soils, Tech. Rep. NCEER-97-0022*, T. L. Youd and I. M. Idriss, eds., National Center for Earthquake Engineering Research, Buffalo, 1–40.

Youd, T.L., 1992, Liquefaction ground Failure and consequent damage during the 22 April 1991 Costa Rica Earthquake: Proceedings of the NSF/UCR U.S.-Costa Rica Workshop on the Costa Rica Earthquakes 1990-1991: Effects on soils and structures. Oakland, California, Earthquake Engineering Research Institute

Youd, T. L., and Hoose, S. N., 1977, Liquefaction susceptibility and geologic setting: *Proc., 6th World Conf. on Earthquake Engrg.*, Vol. 3, Prentice-Hall, Englewood Cliffs, N.J., pp. 2189–2194.

Youd, T.L., and Idriss, I.M., 2001, Liquefaction Resistance of Soils: Summary Report from the 1996 NCEER and 1998 NCEER/NSF Workshops on Evaluation of Liquefaction Resistance of Soils: Journal of Geotechnical and Geoenvironmental Engineering, Vol. 127, No. 4.

Youd, T. L., and Perkins, D. M., 1978, Mapping of liquefaction induced ground failure potential: *Journal of Geotech. Engrg. Div.*, ASCE, Vol. 104, No. 4, pp. 433–446.

Yuan, J., 2011, Field Studies comparing SASW, beamforming and MASW test methods and characterization of geotechnical materials based on Vs: Unpublished doctoral dissertation, University of Texas, Austin, TX, United State of America.

Zhang, S.X., and Chan, L.S., 2003, Possible effects of misidentified mode number on Rayleigh wave inversion: Journal of Applied Geophysics, v. 53, p. 17-29.

Appendices

A. Detailed Geological History (with Geological Map on CD-ROM)

B. Greymouth Argus Excerpt

C. Historical Maps and Drawings (on CD-ROM)

D. Historical and Site Testing Photos (on CD-ROM)

E. Field Data and Analysis Spreadsheets (on CD-ROM)

Appendix A: Geology

The following description relates to all bedrock units found within the wider Greymouth Area. It is based on the descriptions provided by Nathan et al. (2002). Geological Map and Full Stratigraphic Column are included on the CD-ROM.

Ordovician (490 to 443 Ma)

The oldest rocks to outcrop in the Greymouth area are the Greenland Group (Ɵg). This consists of interbedded light greenish grey muddy quartzose sandstone (greywacke) and shale (argillite), which has been hornfelsed locally near granitoid plutons. These have been interpreted as a proximal turbidite sequence deposited on a submarine fan. It contains abundant detrital quartz, minor sodic plagioclase and scattered volcanic and sedimentary rock fragments. The age of these rocks (Ordovician) is based on graptolites found at the Waitahu River.

The Greenland Group rocks make up much of the mountainous terrain in the north of Greymouth and are distributed from the coastline, inland. There are also smaller localised outcrops within the inland valleys of the Grey River and associated tributaries. The localised outcrops are also generally bounded by faults.

Early Cretaceous (142 to 98.9 Ma)

Following the Greenland Group rocks there was several other rock units deposited. However the next rock that outcrops in the area is the Pororari Group. The Pororari Group rocks are mainly coarse-grained, non-marine sedimentary rocks. These rocks are generally preserved in partly fault-bounded blocks in and around the Paparoa Ranges. These sedimentary rocks contain clasts of nearby basement lithologies, indicating local derivation. Pollen and spores show it is of late Early Cretaceous age.

The dominant lithology with the Pororari Group is the Hawks Crag Breccia (Koh). This unit consists of a poorly-sorted, matrix-supported breccia and breccia-conglomerate in a coarse-grained sandy matrix. The Hawks Crag Breccia is located on the southern edge of the Greenland Group contact, generally constrained by faults, in an area several kilometres north-northeast of Greymouth.

Late Cretaceous to Paleocene (98.9 to 54.8 Ma)

Overlying the Pororari Group is the Paparoa Coal Measures (Kpc). This consists of a non-marine assemblage of fluvial conglomerate and sandstone, lacustrine mudstone and lensoidal coal seams. This formation is subdivided into seven members; 3 coal units with 4 mudstone and sandstone units separating the coal units. Basalt flows and breccia are interbedded within the lower part of the Paparoa Coal Measures with these deposits being dated between 68 and 71 million years ago, and appear to part of an episode of latest Cretaceous basaltic volcanism that was widespread on the West Coast. Dating of pollen shows most of the Paparoa Coal Measures is latest Cretaceous in age, but the uppermost part is Early Paleocene. The Cretaceous-Tertiary boundary is recorded within a coal seam in the upper part of the Rewanui Member. The Paparoa Coal Measures outcrop north of the towns of Runanga and Dunollie, some 10 kilometres north-east of Greymouth, along with a limb that extends from the eastern edge, south towards the town of Taylorville.

Eocene (54.8 to 33.7 Ma)

Following a regional unconformity, the next lithology is the Brunner Coal Measures (Eb). The Brunner Coal Measures consists of quartz sandstone, conglomerate, carbonaceous shale and lensoidal coal seams, some up to 10 metres thick locally. The formation as a whole is quartzose, due to being largely derived from deeply weathered, granitoid basement rocks. The sandstone beds are commonly silica-cemented, due to be deeply buried in some areas, and therefore from characteristic bluffs and plateaus.

The Brunner Coal Measures are not extensive near Greymouth and are only present as small outcrops on the south side of the Paparoa Coal Measures.

Lying conformably on top of the Brunner Coal Measures are the Island Sandstone and the Kaiata Formation.

The Island Sandstone (Ers) consists of a shallow marine sandstone. However this unit is not widespread and is only observed in localised areas, and has a variety of local names, with the Island Sandstone being one of these varieties which outcrops near Greymouth.

The major overlying conformable unit above the Brunner Coal Measures is the Kaiata Formation (Erk). This is a massive, dark brown carbonaceous mudstone which contains interbedded mass-flow deposits (conglomerate debris-flow beds) near Greymouth. The Kaiata Formation is a shallow-water sedimentary rock, as well as the Island Sandstone, as a result of marine transgression though the Kaiata Formation is much more widespread including outcrops around Westport.

The Island Sandstone forms the hills east of the Runanga and Rapahoe townships, whereas the Kaiata Formation forms much of terrain south and east of Kaiata and is bounded by the Oligocene formations within the limbs of the Brunner Anticline.

Oligocene (33.7 to 23.8 Ma)

The continued marine transgression from the Eocene meant that terrigenous sediment dwindled and consequently the Oligocene sediments are calcareous and limestone units are widespread. The Nile Group (On) is a grouping of all calcareous sediments for much of the West Coast during the Oligocene. This Group is then divided into two major facies: Platform facies, consisting of shallow-water bioclastic limestone and muddy micaceous limestone formed on a relatively stable shelf; and Basinal facies, consisting of muddy limestone, massive calcareous mudstone and interbedded calcareous sandstone and mudstone formed in rapidly subsiding basins.

The Platform facies is not observed in the Greymouth area, and is generally confined to the northern part of the West Coast. However, the Basinal facies occurs mainly around Greymouth.

The Port Elizabeth Member (Onp) sits directly above the Kaiata Formation. This member consists of a grey-brown calcareous mudstone.

The Port Elizabeth Member grades upwards into the Cobden Limestone (Onc). The Cobden Limestone is a muddy micritic limestone, with thin layers of clay/mud infill between some beds, giving the outcrops a wavy appearance due to the less resistant mud layers being eroded quicker than the limestone beds.

The Nile Group outcrops in Greymouth as the hills directly behind Greymouth as part of the westward-dipping limb of the Brunner Anticline and also further inland as part of the eastward-dipping limb

Miocene (23.8 to 5.3 Ma)

The Blue Bottom Group was deposited above the Nile Group during the Miocene. This Group reflects another change in tectonic activity and uplift as another change from carbonate-rich to terrigenous muddy sediments. There are several members within the Blue Bottom Group, with some members being locally unconformable due to regional uplift and changing depocentres.

The Stillwater Mudstone (Mbs) is a grey calcareous mudstone that formed throughout the Early to Middle Miocene and sits conformably above the Cobden Limestone of the Nile Group.

During the Late Miocene the Eight Mile Formation (Mbe) formed above the Stillwater Mudstone. This formation has a dominant lithology of blue-grey muddy sandstone and yellow-brown fine-grained sandstone.

These formations outcrop as part of the eastward-dipping limb of the Brunner Anticline. They have been eroded extensively due to river incision and other processes during the Quaternary period. The Stillwater Mudstone is also present as the lesser hills behind the southern part of Greymouth, as part of the westward-dipping limb of the same anticline.

Pliocene (5.3 to 1.8 Ma)

The youngest sedimentary rocks in the area around Greymouth are the Old Man Group (Þo) and are Late Pliocene in age. This Group originated due to rapid uplift of the Southern Alps and is reflected by a flood of fluvial gravel and sand. The resulting conglomerate is dominated by clasts of greywacke and schist. Locally, glacial beds have been recorded. In some places the Eight Mile Formation grades upwards into the Old Man Group.

The Old Man Group is present in the stratigraphic record as a localised deposit near Stillwater, approximately 12 kilometres inland from Greymouth.

Appendix B: Greymouth Argus Excerpt

Excerpt from the Greymouth Argus, dated 11 August 1904, page 3

Greymouth Harbour

Mr Thompson's Report

Regarding the Greymouth harbour, Mr Thompson, engineer, reported to the Harbour Board yesterday as follows: — As instructed, I have now the honour to lay before you a report on the present state of the entrance. As the members may not be acquainted with what has taken place, I have given a short account of the works from the commencement.

In December, 1870, Sir John Coode sent plans and a report showing how the proposed harbour works were to be constructed. In the report he says: It is also impossible that the width (400ft) at low water may in some small degree be varied with advantage. Experience alone can determine with precision this, as well as the other points just named, but the width laid down in the drawing has been arrived at after calculation and careful consideration; based on the data, available for the purpose.

The work was actually set out to give a width of 450 feet at low water and the level of the stone on the South Breakwater was made up to the sleeper level on top of the staging, instead of being kept to about 3ft above high water, as shown on Sir John Coode's plans. The latter alteration, although it gave increased shelter, contracted the width of the sailing channel, as the stone went further into the river. Another cause of the narrowing of the channel was the use of too many small stones, which could not resist the heavy seas, and were flattened out, forming wide aprons along the river face of the South Mole. I found, on taking charge in 1893, that the above conditions existed, but that to assist the width no stone had been tipped for some time from the inner line of railway on the North Mole, thus improving matters to the extent of 25ft. The final results from measurements were that at the narrowest point the width at low water was 430 feet, and opposite the end of the North Mole it was 445 ft. The overlap of the South Breakwater at the time work stopped in 1895 was 530 feet.

In June, 1895, Messrs Hales and Napier Bell reported on the harbour, and recommended the extension of the North Breakwater, the line being slightly altered to give a width of 550 ft at low water. No action was taken.

Mr Napier Bell again reported on the harbour in June, 1900, and advised the Board to at once set about extending the southern one (breakwater) partly on account of the shelter it will give to the entrance, and partly because, as it must be done before long, it may as well be done now. He also had no doubt that before long the North Breakwater must also be extended to preserve the depth by confining the currents. He also advised that instead of extending the work on the lines of the present wall, it should be done by constructing a new breakwater parallel to the old, but 200 feet further up the beach, so as to give a width of entrance of 600 ft at low water mark. The report goes on to say that the width of 600ft at low water mark is no doubt too wide for a small river like this with such au insufficient tidal compartment, but this cannot be helped, as the present width of 400ft at low water, although more suitable for the size of the river, is dangerous for navigation. To assist the scour he advises the opening up of the lagoons, as was previously advised by Sir John Coode.

Plans for the extension of the breakwaters were prepared on these lines and submitted to Government for approval. The Marine Engineer, however, objected on account of the width being too great. He then came down and examined the site, and as a result plans were prepared for the extension of the South Mole on the present lines, but instead of adopting Mr Napier Bell's proposed new North Breakwater, it was proposed to extend the present one by continuing the two northerly rows of piles only. This would have given an additional 25ft, and as I proposed to keep the stone on the South Mole down to Sir John Coote's level, there would also be a gain of width on the south side. Altogether, at the outer and the low water width would have been above 475 feet.

These plans were approved, and work commenced lengthening the South Breakwater. Shortly afterwards permission to go on with the South Mole was withdrawn in order to reconsider the question of site and width. I then advised the Board to stop work on the south side till matters were settled, as we had already constructed an additional 150 feet making the overlap 700 feet, which was quite too great. The two designs were then sent to London for the opinion of Messrs Coode, Son and Mathews, who are chief engineers to the Admiralty for the new Dover Harbour, now being built by the Home Government.

Their report of September, 1902, states that there can be no question that the time has now arrived when further works of extension can with advantage be undertaken. Also, that after careful consideration, we are unable to recommend this (Mr Napier Bell's) project, mainly on grounds corresponding to those given in the report of the Marine. . . We are of opinion that 600ft would be a far greater width than could be effectively kept open by the scour, and as pointed out by the Marine Engineer…dredging in such an exposed position as the entrance

to the Grey River, where there is always a heavy swell, and frequently seas running, would be both a difficult and expensive work.

They recommended the extension of the South Breakwater 400ft and the North Breakwater 500 ft. The North Breakwater to start at the same point as shown on the Marine Engineer's plan, but to trend slightly to the north, so as to give a low water width of 500ft at its seaward end. They also recommended an overlap of 450 feet.

After consideration of the three plans, it was decided to carry out Mr Napier Bell's idea, and to extend the new breakwater to such a length that its outer end would be 400 feet seaward of the old North Mole. The work was put in hand at once. We are now within 50 feet of the terminal point.

Owing to dry weather and heavy seas the entrance has been in a very bad condition since the end of June. The average depth at H.W.O.S.T. in June was 20 feet 10 inches. In July it was only 16ft 10in, the least depth being 14ft on the 23rd. In August the depth has only been 14 and 15 feet. In addition, since the 21st July, the larger vessels have had to be towed in and out, and during the first week in August three coal-laden vessels had to discharge part of their cargoes to enable them to go to sea.

These facts show that although the new breakwater is in such an advanced condition, it has not had the slightest beneficial effect in regulating the current or increasing the depth on the bar. At the present time there is a bank commencing at the river face of the South Breakwater, and extending right across the river, overlapping the end of the old North Mole, with only a depth of seven feet at low water, or 16 foot at high water, in the line of entrance for shipping.

Recommendations — as it would be impracticable, now that so much of the new work had been built, to carry out either Messrs Hales or Coode’s plans, the only thing to do is the following: —As many be seen from the authorised plan, the greater portion of the new work is built in a straight line at an angle to the beach trending to the southwards. This is continued till the width of entrance is narrowed to 600 feet. The work then turns seaward, and the other portion is parallel to the South Breakwater. I would recommend the Board to go back on the work to where the straight portion ends, and continue this straight till the width is reduced to 500 feet at low water, and then turn seawards.

Regarding the amount of overlap, Sir John Coode reported the precise amount can only be determined by experience. His original plan scales 130 feet. The point where the alteration

recommended above meets a line 500 feet from and parallel to the south pier is about opposite to the beginning of the 150 feet addition lately built. Consequently, when we get to that point the overlap would the 150 feet, and if this was then found to be too small we have authority to extend the South Breakwater another 250 feet which would give an overlap of 400 feet if necessary.